Mariana Afonso Barata

Licenciada em Bioquímica

Understanding the impact of sporadic Alzheimer's disease mutations on BIN1

Dissertação para obtenção do Grau de Mestre em
Genética Molecular e Biomedicina

Orientador: Cláudia Guimas de Almeida,
Investigadora Principal, CEDOC, NMS

Júri:

Presidente: Prof. Doutora Margarida Castro Caldas Braga
Arguente: Prof. Doutor Hugo Vicente Miranda
Vogal: Prof. Doutora Cláudia Guimas de Almeida

FACULDADE DE CIÊNCIAS E TECNOLOGIA
UNIVERSIDADE NOVA DE LISBOA

Setembro, 2019

Mariana Afonso Barata

Licenciada em Bioquímica

Understanding the impact of sporadic Alzheimer's disease mutations on BIN1

Dissertação para obtenção do Grau de Mestre em
Genética Molecular e Biomedicina

Orientador: Cláudia Guimas de Almeida,
Investigadora Principal, CEDOC, NMS

Júri:

Presidente: Prof. Doutora Margarida Castro Caldas Braga
Arguente: Prof. Doutor Hugo Vicente Miranda
Vogal: Prof. Doutora Cláudia Guimas de Almeida

Setembro, 2019

Understanding the impact of sporadic Alzheimer's disease mutations on BIN1

Para o meu avô,
José Lopes Barata

Acknowledgments

Here, I express my sincere gratitude to everybody that gave me precious help during this last year in my master dissertation development, as well as the ones that have been there for me long before.

Como não podia deixar de ser, Cláudia, és tu a quem me refiro primeiro. Quero agradecer, desde já, por me teres aceite neste projeto e no teu laboratório. Tenho também de agradecer ao Dr. Jorge Dias pelas suas preciosas palavras de recomendação que te levaram a ver para além da minha forte timidez. Durante este último ano, tens sido uma formidável orientadora, professora e amiga. Com o teu vasto conhecimento do mundo celular e biológico ao mundo informático e tecnológico, trabalhar contigo tem me permitido uma excelente oportunidade de aprendizagem, um privilégio que espero continuar a usufruir. O teu enorme positivismo e entusiamo pela ciência têm sido uma fonte de inspiração para mim. E o teu apoio e encorajamento, todos os empurrões que me tens dado para sair mais um pouco da minha casca, e toda a confiança que depositaste em mim, levam-me a considerar-me capaz de seguir este árduo caminho que é a investigação.

Catarina, minha co-orientadora não oficial, quero te deixar um especial agradecimento por toda a tua orientação no terreno. Obrigada por todos os teus ensinamentos desde do trabalho com as linhas celulares à análise dos resultados, tens sido inalcançável em toda a tua ajuda desde o primeiro ao último dia. Obrigada por toda a tua paciência e atenção e todos os tempinhos que arranjaste para mim mesmo quando estavas atolada em trabalho. Ademais, encontrei em ti não só uma magnífica orientadora, mas também uma excelente amiga. Agradeço-te por todo o teu apoio e companheirismo, por todas as vezes que me fizeste sorrir e todas as Somersby oferecidas. A Rua de Portas de Santo Antão é demasiado pequena na tua companhia.

Tatiana, nunca conheci pessoa mais simpática e sempre disposta a ajudar como tu. És aquela que melhor conhece os cantos do laboratório e a nossa salvação em todas as questões do dia a dia. Obrigada por toda a ajuda que tão prontamente dispões, a esta tua minion, apesar do teu atarefado horário. És uma ótima colega e professora, uma investigadora autónoma e respeitável, e uma inspiração para mim.

Inês, obrigada pela tua orientação no trabalho com as linhas celulares, algo completamente novo para mim, mas também pela alegria e vivacidade que sempre trazes contigo e me contagias.

Farzaneh please continue to share all your cultural knowledge with us, it's been incredibly interesting and fun. متشكرم

To all Neuronal Trafficking in Aging Lab, Luís included, thank you for all of your support, companionship and numerous laughs.

We thank Dr. Rune Matthiesen and Dr. Ana Carvalho (CEDOC) for outstanding help and expertise in mass spectrometry.

Agradeço ao Dr. Hugo Miranda pelas valiosas discussões e ajuda no design e setup de experiências.

Agradeço aos meus colegas do CEDOC, com especial carinho a Alexandra, Liliana, Rita, Andreia e Daniela. Um muito obrigado a Ana pelo apoio e amizade e boa disposição.

À minha família do Taekwondo um muito obrigado. Conciliar a tese com os treinos e atividades nem sempre foi fácil, mas permitiram-me crescer como pessoa e aprender que posso alcançar qualquer objetivo.

A Cláudia, Marta, Carolina, Catarina, Guilherme e David obrigada pela vossa amizade desde a licenciatura. Os melhores de BQ. Cláudia e Marta agradeço-vos pelos momentos inesquecíveis e cheios de risos. Carolina, tens sido o meu principal ponto de apoio durante o mestrado, obrigada por toda a companhia, gargalhadas e cusquices.

A toda família agradeço a preocupação, mas também o apoio e motivação em todas as etapas da minha vida. Henrique, és um verdadeiro irmão mais velho, obrigada pelo teu apoio e todas as tolices e brincadeiras. Aos meus pais agradeço-vos todo o apoio, confiança e muita paciência. Pai obrigada por todos os conselhos, as boleias e saborosa comida. Mãe obrigada por todo o carinho e amor incondicional, conselhos e sobretudo imensa paciência. Palavras não conseguem descrever o que significam para mim.

Abstract

Amyloid β (Aβ) accumulation plays an early role in Alzheimer's disease (AD), leading to neuronal and synaptic dysfunction, cell death and dementia. Aβ production occurs by the cleavage of APP, by BACE1 and γ-secretase, mainly in endosomes, and is regulated by the differential trafficking of BACE1 and APP. The late-onset form of AD (LOAD) is a multifactorial disease, whose cause still needs to be elucidated. Bridging Integrator 1 (BIN1), a strong candidate for a genetic risk factor that might increase susceptibility to LOAD, is implicated in intracellular trafficking, including BACE1 recycling. This work will focus on investigating the molecular mechanisms by which BIN1 controls Aβ production and the impact of *BIN1* variants, rs754834233 and rs138047593, genetically associated with LOAD.

Using the N2a cell line, and immunofluorescence and immunoblotting methods, we found that BIN1 BAR domain is important to regulate $A\beta_{42}$ levels. Importantly, we discovered that sporadic AD mutations in BIN1 likely cause BIN1 loss of function in Aβ production since they did not rescue augmented $A\beta_{42}$ levels induced by BIN1 loss, while neuronal BIN1 wild-type did, and at least one of the mutants increased APP processing. Both mutants rescued early endosomes enlargement caused by BIN1 knockdown, indicating that they do not affect early endosomes morphology. BIN1 wild-type and mutant's interaction with BACE1 was observed by co-immunoprecipitation, and allied to mass spectrometry, their differential interactome started to be investigated.

In conclusion, BIN1 mutants impact Aβ accumulation and the causative mechanisms could involve BIN1 structure and conformation, important for BIN1 self-regulation. The dysregulation of interactions by the mutations will be investigated upon identification of lost or gained partners, through mass spectrometry, to elucidate the specific mechanisms whereby the mutations contribute to BIN1 loss of function. Thus, genetic variants in AD may contribute to trigger AD pathogenesis via increasing Aβ production.

Keywords: Late-onset Alzheimer's Disease, BIN1, amyloid β, BACE1, intracellular trafficking

Resumo

A acumulação de Aβ desempenha um papel precoce na Doença de Alzheimer (AD), levando à disfunção neuronal e sináptica, morte celular e demência. A produção de Aβ ocorre pela clivagem de APP por BACE1 e γ-secretase, principalmente nos endossomas, e é regulada pelo tráfego diferencial de BACE1 e APP. A forma de início de tardio de AD (LOAD) é uma doença multifactorial, cuja causa ainda não foi elucidada. Bridging Integrator 1 (BIN1), um forte candidato para factor de risco genético que pode aumentar a susceptibilidade para LOAD, está implicado no tráfego intracellular, incluindo reciclagem de BACE1. Este trabalho se focará em investigar os mecanismos moleculares pelos quais BIN1 controla a produção de Aβ e o impacto de variantes de *BIN1*, rs754834233 e rs138047593, geneticamente associadas à forma esporádica de AD.

Utilizando células N2a e métodos de imunoflourescência e imunotransferência, verificámos que o domínio BAR de BIN1 é importante para regular os níveis de $A\beta_{42}$. Ademais, descobrimos que mutações de AD esporádica no BIN1, provavelmente, levam a perda de função de BIN1 na produção de Aβ, porque não resgataram o aumento de $A\beta_{42}$ induzido pela perda de BIN1, enquanto que BIN1 neuronal wild-type o fez, e pelo menos uma das mutações aumentou o processamento de APP. Ambos os mutantes resgatam o alargamento de endosomas precoces, indicando que não afetam a morfologia dos endossomas precoces. A interação de BIN1 wild-type e mutantes com BACE1 foi observada por co-imunoprecipitação, e aliada a espectrometria de massa, os seus diferentes interactomas começaram a ser investigados.

Concluindo, observámos o impacto de variantes de BIN1 na acumulação de Aβ e os mecanimos causativos podem envolver a estrutura e conformação de BIN1, importante para a sua auto-regulação. Desregulação de interações pelas mutações será investigada após identificação da perda ou ganho de parceiros, através de espectrometria de massa, para elucidar os mecanimos específicos pelos quais as mutações podem contribuir para a perda de função de BIN1. Assim, variantes genéticas de AD podem contribuir para desencadear a patogénese de AD pelo aumento da produção de Aβ.

Termos Chave: Doença de Alzheimer de início tardio, BIN1, β-amiloíde, BACE1, Tráfego intracelular.

Contents

List of Figures

List of Tables

Abbreviations

4HNE	4-hydroxynonenal
ABCA7	ATP-binding cassette sub-family A member 7
Ac	acidic domain
AChE	acetylcholinesterase
AD	Alzheimer's disease
ADAM	a disintegrin and metalloproteinase
ADL	activities of daily living
AICD / γCTF	APP intracellular domain / γ carboxyl terminal fragment
AMPH	amphiphysin
AP-2	adaptor protein complex 2
Aph-1	anterior pharynx defective-1
APL1	amphiphysin-like protein 1
APOE	Apolipoprotein E
APP	amyloid precursor protein
APS	Ammonium Persulphate
ARF6	ADP-ribosylation factor 6
Aβ	amyloid β
BACE	β-site APP-cleaving enzyme 1 or β-secretase 1
BAR	BIN1/amphiphysin/RVS167 domain
BIN1	Bridging integrator 1 / Myc box-dependent-interacting protein 1
BLAST	Basic local alignment search tool
BSA	bovine serum albumin
C83 / αCTF	carboxyl-terminal fragment (83 residues)
C99 / βCTF	carboxyl-terminal fragment (99 residues)
CAA	cerebral amyloid angiopathy
CBD	corticobasal degeneration
CD2AP	CD2-associated protein
cDNA	complementary DNA
CDR	Clinical Dementia Rating
CLAP	clathrin and AP2 binding domain
CLU	Clusterin
CME	clathrin-mediated endocytosis
CO-IP	Co-Immunoprecipitation
CR1	Complement receptor type 1
CSF	cerebrospinal fluid
CuBD	copper binding domain
DMEM	Dulbecco's Modified Eagle Medium
DMSO	Dimetly sulfoxide
DOC	sodium deoxycholate
ECL	enhanced chemiluminescence
EDTA	Ethylenediamine tetraacetic acid
EEA1	Anti-Early endosome antigen 1
EGTA	Ethylene Glycol Tetraacetic Acid
eNFTs	extracellular "ghost" NFTs
EPHA1	ephrin type-A receptor 1
ESI	electrospray ionization
FAD /EOAD	familiar Alzheimer's disease / early onset Alzheimer's disease
FBS	fetal bovine serum
FDG	fluorodeoxyglucose
FTDP-17	frontal temporal dementia with parkinsonism linked to chromosome 17
GDP	Guanisine 5'-diphosphate
GTP	Guanisine 5'-triiphosphate
GVD	granulovacuolar degeneration
GWAS	genome-wide association studies

HBD	heparin-binding domain
HCD	high energy collision dissociation
HRP	Horseradish peroxidase
ILVs	intraluminal vesicles
iNFTs	intraneuronal NFTs
IPSC	high energy collision dissociation
KPI	Kunitz-type protease inhibitor domain
LB	Luria-Bertani
LC-MS/MS	Liquid chromatography coupled to tandem mass spectrometry
LDL	low-density lipoprotein
LDS	Lithium dodecyl sulfate
LOAD	late-onset Alzheimer's disease
MAF	minor allele frequency
MALDI	matrix-assisted laser desorption-ionization
MBD	Myc-binding domain
MMSE	Mini-Mental State Examination
MRI	structural magnetic resonance imaging
MVB	multivesicular bodies
N2a	Neuro-2a
Nct	nicastrin
NFTs	neurofibrillary tangles
NMDAR	*N*-methyl-D-aspartate receptor
NMR	nuclear magnetic resonance
NS	not significant
N-Wasp	Neural Wiskott-Aldrich syndrome protein
P3	amyloid β-peptide$_{17–40/42}$
PBS	phosphate buffered saline
PBS-T	phosphate buffered saline with Tween 20
Pen-2	PSEN enhancer-2
PET	positive positron-emission tomography
PI	phosphoinositide (PI)-binding motif
PI(3)P, PI(4)P, PI(5)P	phosphatidylinositol 3/4/5-phosphate
PI(4,5)P_2	phosphatidylinositol 4,5-biphosphate
PIC	Protease Inhibitor Cocktail
PICALM	phosphatidylinositol-binding clathrin assembly protein
PRD	proline-rich motif
PS	proline-serine rich domain
PSEN	presenilins
PSEN1	presenilin-1
PSEN2	presenilin-2
PSP	progressive supranuclear palsy
RIPA	Radio-Immunoprecipitation Assay
RNAi	RNA interference
RT	Room temperature
RVS167	Reduced viability upon starvation protein 167
sAPPα	secreted amyloid precursor protein-α
sAPPβ	secreted amyloid precursor protein-*β*
SDM	Site Directed Mutator
SDS	sodium dodecyl sulfate
SDS-PAGE	SDS-polyacrylamide gel eletrophoresis
SEM	standard error of mean
SH3	Src homology 3 domain
siRNA	small interfering RNA
SNPs	single nucleotide polymorphisms
SORL1	sortilin-related receptor
TACE	tumour necrosis factor alpha-converting enzyme
TEMED	*N, N, N′, N′-tetramethylethylenediamine*
TGN	trans-Golgi network

TREM2	Triggering receptor expressed on myeloid cells 2
VDCC	voltage-dependent chloride channel

Chapter 1

Introduction

1.1 Alzheimer's Disease

More than 100 years ago, in 1901, Alois Alzheimer, a German psychiatrist and neuroanatomist (Hippius and Neundörfer, 2003), first met Auguste Deter, who had been admitted to a mental asylum the day before. She presented changes in behaviour, memory loss, spatial and temporal disorientation and psychosocial impairment. After her death, 5 years later, Alzheimer examined Auguste D.'s brain that showed massive loss of neurons and the presence of amyloid plaques and neurofibrillary tangles (Figure 1.1), the histological features that are today associated with Alzheimer's disease. However, it was not until 1910, that Emil Kraepelin first introduced the term "Alzheimer's disease", distinguishing this new disease from senile dementia, a decline in mental ability due to aging (Cipriani et al., 2011). In 1970, is clarified that senile (late-onset) and pre-senile (early-onset) dementia are a part of the same disease (Cipriani et al., 2011; S. A. Small and Gandy, 2006).

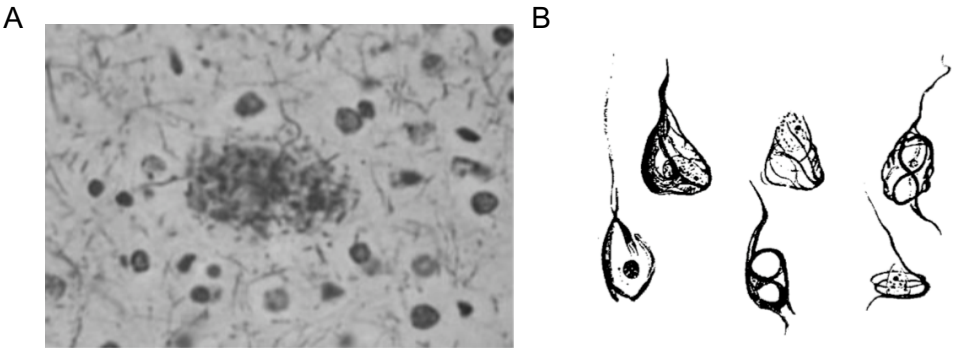

Figure 1.1: **Neuropathology features of Alzheimer's disease.** A. Tissue section of the patient Auguste D.'s brain shows amyloid plaques with Bielschowsky staining. Retrieved from Graeber and Mehraein, 1999. B. Sketch published by Alois Alzheimer in 1911 of neurofibrillary tangles found in Auguste D.'s brain.

Currently, Alzheimer's disease (AD) accounts for 60 to 80% of cases of dementia (World Health Organization, 2017), being the most common neurodegenerative disorder at any age worldwide (Burns and Lliffe, 2009; Caselli et al., 2017). In 2005, a Delphi study (Ferri et al., 2005), guided by an international panel of dementia experts, predicted that, in 2020, there would be 42.3 million people with dementia in the world and 81.1 million by 2040. According to Alzheimer's Disease International (ADI), however, in 2018 there was already 50 million people living with

dementia and this number is predicted to rise to 82 million in 2030 and 152 million by 2050, predicting a new case of dementia every 3 seconds. In 2016, it was reported to be the 5th leading cause of death (Global Health Estimates, 2016), as severe dementia causes life-threatening complications (Alzheimer's Association, 2019), and the total estimated worldwide cost of dementia in 2018 was US$1 trillion (ADI, 2018). These numbers highlight the urgency to find novel therapies to target early mechanisms of the disease and the need to research such mechanisms.

1.2 Pathology of Alzheimer's Disease

Neuropathologically, Alzheimer's disease is characterized by two hallmark proteinaceous aggregates, amyloid plaques and neurofibrillary tangles (LaFerla and Oddo, 2005) that will be addressed separately.

1.2.1 Amyloid plaques

Amyloid, or senile, plaques are compact, spherical extracellular deposits formed by the abnormal accumulation of the small protein amyloid β-peptide (Aβ) (LaFerla and Oddo, 2005; Haass and Selkoe, 2007). Amyloid plaques are initially found in neocortical regions, affecting largely the association multimodal areas (Caselli et al., 2017; Serrano-Pozo et al., 2011), which are involved in visuospatial localization, language, attention, motor planning, judgment, emotion and memory functions (Kandel et al. 2000). Amyloid plaques distribution further progress to involve allocortical and limbic structures, and in a later stage, subcortical structures including the diencephalon, and eventually the brainstem and cerebellum (Figure 1.2) (Caselli et al., 2017; Serrano-Pozo et al., 2011).

Amyloid plaques are described as either diffuse or dense-core plaques, based on their negative or positive staining for β-sheet conformation, respectively, using the dyes Thioflavin-S or Congo Red. Dense-core plaques are composed of fibrillar amyloid deposits with a compact core and are generally associated with the presence of cognitive impairment, since they are typically surrounded by dystrophic neurites, reactive astrocytes and activated microglial cells, and associated with synaptic loss. On the other hand, diffuse plaques, composed of amorphous amyloid deposits with ill-defined contours, are usually non-neuritic and not associated with glial responses or synaptic loss. Since this plaque type is commonly present in the brains of cognitively intact elderly people is not considered for the pathological diagnosis of AD (Serrano-Pozo et al., 2011).

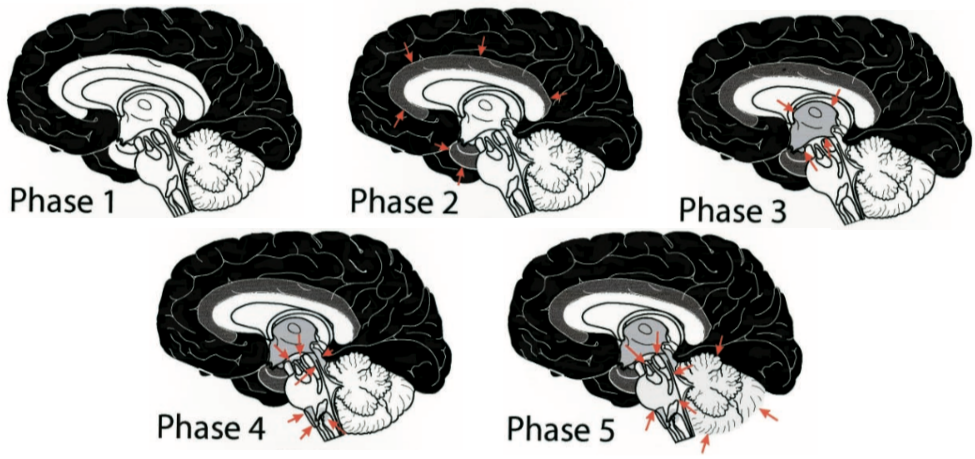

Figure 1.2: **Pattern of amyloid plaque deposition.** Phase 1 is characterized by neocortical Aβ deposits (neocortical regions in black). In phase 2, Aβ deposits progress to allocortical regions (red arrows), and in phase 3 to the subcortical regions, including the diencephalon (red arrows). In phase 4, additional Aβ deposits appear in distinct brainstem nuclei (red arrows), and phase 5 in the cerebellum and additional brainstem nuclei (red arrows) (Caselli et al., 2017; Serrano-Pozo et al., 2011; Thal et al., 2002). Retrieved from Thal et al., 2002

Amyloid β-peptides, with 39 to 43 amino acids, are a product of the sequential cleavage of the amyloid precursor protein (APP) by the β-secretase enzyme and the γ-secretase enzyme complex (Citron et al., 1996; U. C. Müller and Zheng, 2012; Serrano-Pozo et al., 2011)

APP is an integral type I transmembrane protein that is expressed ubiquitously, and particularly enriched in neurons, as multiple alternate transcripts (Hardy, 1997; U. C. Müller and Zheng, 2012). APP with 695 amino acid residues is the major brain isoform. APP has a large ectodomain that comprises the E1 extracellular domain, divided into the heparin-binding domain (HBD) and the copper binding domain (CuBD), an acidic domain (AcD), an E2 extracellular domain, and a short cytoplasmic domain with a YENPTY motif (Dawkins and Small, 2014; U. C. Müller and Zheng, 2012) (Figue 1.3. A).

The functions of APP have not yet been defined (Hardy, 1997), but it may have a role in cell proliferation and cell adhesion (Dawkins and Small, 2014; U. C. Müller and Zheng, 2012; Rajendran and Annaert, 2012) and the intracellular domain (AICD), generated by the proteolytic cleavage of APP, can be transported to the nucleus, where it might function as a modulator of gene expression (Dawkins and Small, 2014; T. Müller et al., 2008). In addition, APP might form a complex with heterotrimeric GTP-binding proteins to contribute to signal transduction (Sisodia et al., 2002) and act as receptor for kinesin 1 during the fast axoplasmic transport of vesicles that contain APP, β-secretase, also known as β-site APP-cleaving enzyme 1 (BACE1), and presenilin-1 (PSEN1), component of the γ-secretase complex (Kamal et al., 2001; Sisodia et al., 2002).

1.2.1.1 APP processing

APP can be processed by different pathways. In the non-amyloidogenic pathway, APP is cleaved by the α-secretase that includes members of the ADAM (a disintegrin and metalloproteinase) family, ADAM10, ADAM9 and the tumour necrosis factor alpha-converting enzyme (TACE)/ADAM17. This cleavage releases a soluble fragment, sAPPα, and a carboxyl-terminal fragment consisting of 83 residues (C83; αCTF). C83 might undergo further processing by γ-secretase to release the P3 peptide and the APP intracellular domain (AICD/γCTF) (Caselli et al., 2017; LaFerla and Oddo, 2005; Mattson, 2004; J. Z Tan and Gleeson, 2019). The γ-secretase is a

multiprotein complex formed by the presenilins (PSEN1 and PSEN2) and three other proteins, anterior pharynx defective-1 (Aph-1), PSEN enhancer-2 (Pen-2), and nicastrin (Nct), all necessary for full proteolytic activity (De Strooper, 2003; Mattson, 2004). However, additional proteins might be involved, such as the armadillo-repeat proteins, δ-catenin and β-catenin (Sisodia et al., 2002). The presenilins, an aspartyl protease, encode the active site of the γ-secretase complex (Caselli et al., 2017; Mattson, 2004).

In the amyloidogenic pathway, APP is first cleaved by BACE1, a type I transmembrane aspartyl protease (Rajendran and Annaert, 2012), releasing the ectodomain sAPPβ. The remaining membrane-associated carboxyl-terminal fragment (C99 or C89; βCTF) is subsequently cleaved by γ-secretase at multiple sites, releasing the insoluble Aβ peptides and γCTFs (Figure 1.3) (Caselli et al., 2017; LaFerla and Oddo, 2005; Mattson, 2004).

Cleavage by γ-secretase starts ~10 amino acids downstream of Aβ generation sites (referred to as ε-cleavage), releasing the γCTFs. The remaining fragments are then sequentially cleaved at every three residues to generate Aβ. Thus, $A\beta_{49}$, with 49 amino acids, is processed to $A\beta_{46}$ (ζ-cleavage), $A\beta_{43}$ and $A\beta_{40}$ (γ-cleavage) subsequently, where processing of $A\beta_{48}$ originates $A\beta_{45}$, $A\beta_{42}$ and $A\beta_{39}$ (Morishima-Kawashima, 2014; Wolfe, 2007; Zhao et al., 2005).

Between the Aβ peptides, $A\beta_{40}$ accounts for 90% of the total Aβ secreted. On the other hand, $A\beta_{42}$, while accounting for only 10% of the Aβ released, aggregates more readily into insoluble amyloid fibrils, playing a key role in plaque formation (Ballard et al., 2011; Citron et al., 1996).

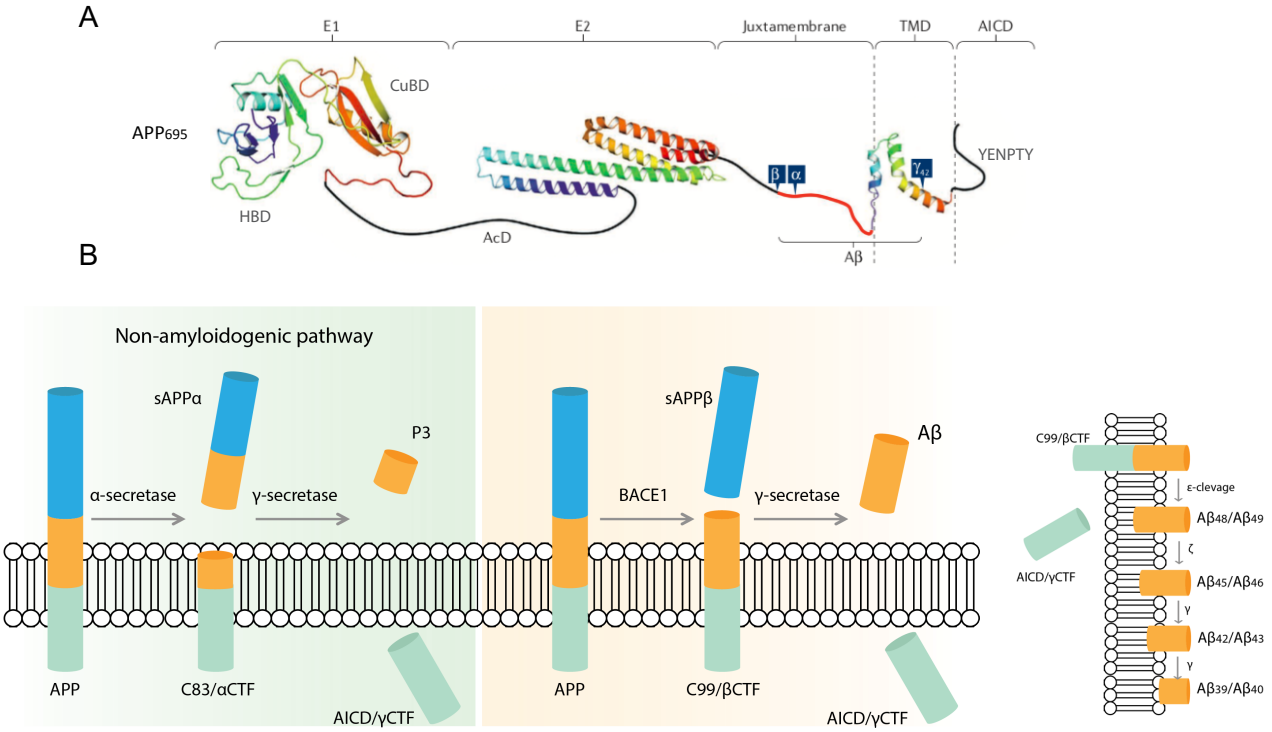

Figure 1.3: **APP processing pathways.** A. Structure of the brain APP isoform (APP_{695}). Adapted from U. C. Müller et al., 2017. In the large ectodomain, APP has an E1 and E2 extracellular domains and an acidic domain (AcD). In the cytoplasmic domain, APP has a YENPTY motif. HBD, heparin-binding domain; CuBD, Copper binding domain. B. In the non-amyloidogenic pathway, APP is cleaved by α-secretase, releasing sAPPα and the carboxyl-terminal fragment, C83. C83 is, in turn, cleaved by γ-secretase, releasing P3 peptide and APP intracellular domain, CTFγ. In the amyloidogenic pathway, APP is cleaved by BACE1, generating sAPPβ and the carboxyl-terminal fragment, C99, which is subsequently cleaved by γ-secretase, releasing the insoluble Aβ peptides and CTFγ. Cleavage by γ-secretase starts at the ε-cleavage, and then the remaining fragments are sequentially cleaved at every three residues. $A\beta_{49}$ is processed to $A\beta_{46}$ (ζ-cleavage), $A\beta_{43}$ and $A\beta_{40}$ (γ-cleavage), where processing of $A\beta_{48}$ originates $A\beta_{45}$, $A\beta_{42}$ and finally $A\beta_{39}$.

Physiologically, Aβ may have a role in synaptic activity depression, participating in normal negative feedback mechanism to control neuronal activity (Kamenetz et al., 2003). As well, sAPPα has shown synaptotrophic and neuroprotective functions (U. C. Müller and Zheng, 2012) and, together with sAPPβ, stimulate neural stem cell proliferation and differentiation (Caselli et al., 2017; Chasseigneaux and Allinquant, 2012).

1.2.1.2 Intracellular Aβ accumulation

In neurons, an important site for Aβ production is in the endocytic pathway. Aβ production requires the internalization of BACE1 and APP, present at the cell surface, and sorting through the endocytic pathway (S. A. Small and Gandy, 2006; J. Z. Tan and Gleeson, 2019). At the plasma membrane, BACE1 is mainly present in microdomains rich in cholesterol and flotillin, termed lipid rafts, whereas APP is mainly present in non-rafts domains (Almeida et al., 2018; Rajendran and Annaert, 2012). Outside the lipid rafts, APP undergoes cleavage by α-secretase, following the non-amyloidogenic pathway. Interestingly, increase in cholesterol promotes the relocalization of APP to lipid raft domains that increases Aβ generation (Di Paolo and Kim, 2011; Marquer et al., 2011).

Upon synaptic activity-induction, APP and BACE1 are endocytosed independently, through a clathrin-dependent mechanism and, in the case of BACE1, also through a clathrin-independent mechanism regulated by a small GTPase ADP-ribosylation factor 6 (ARF6) (Chia et al., 2013; Cirrito et al., 2008; Almeida et al., 2018; Sannerud et al., 2011). APP internalization can be stimulated by the cholesterol/flotillin-dependent clustering of APP (Rajendran and Annaert, 2012). After endocytosis, APP and BACE1 reach the early endosomes, where endosomal acidification, required for optimal BACE1 activity, triggers APP processing (Das et al., 2013; Almeida et al., 2018; J. Z. Tan and Gleeson, 2019). To avoid this, BACE1 is rapidly sorted into endosomal tubules to be recycled to the plasma membrane and APP is sorted into intraluminal vesicles (ILVs) during multivesicular bodies (MVB) biogenesis for the degradative pathway or is recycled to the trans-Golgi network and, posteriorly, to the plasma membrane (Figure 1.4) (Chia et al., 2013; Almeida et al., 2018).

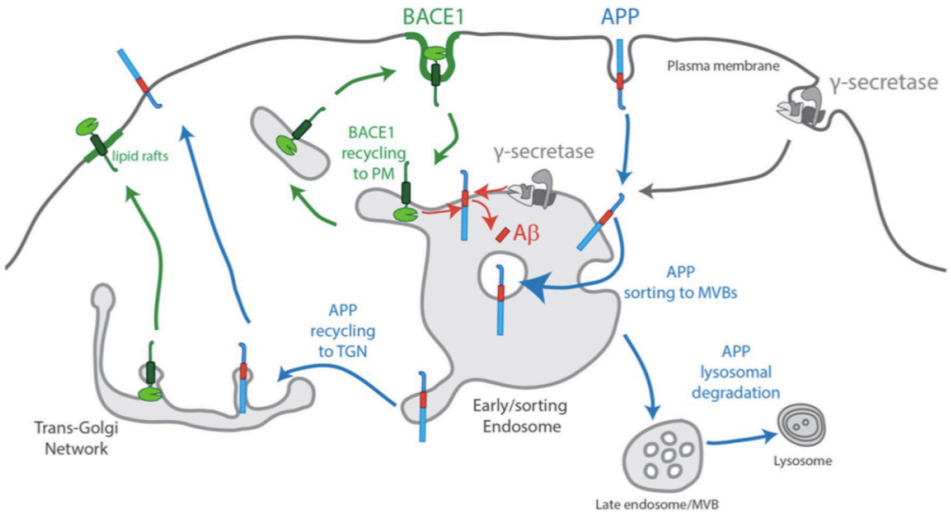

Figure 1.4: **Intracellular trafficking pathways in Aβ production.** APP and BACE1 are separately transported from the trans-Golgi network (TGN), to the plasma membrane (PM), where BACE1 prefers lipid rafts. After endocytosis, APP processing by BACE1 can occur upon acidification of the early endosome. BACE1 is, quickly, recycled to the plasma membrane and APP is sorted into intraluminal vesicles (ILVs) in multivesicular bodies (MVB) to be degraded in the lysosomes. APP can also be recycled to the TGN and, posteriorly, to the plasma membrane. Retrieved from Almeida et al., 2018.

The amyloid cascade hypothesis proposes the sequence of pathogenic events leading to progressive neuronal and synaptic dysfunction, which results in neuronal cell death, mostly apoptotic, and dementia (Hardy and Selkoe, 2002). The increased $A\beta_{42}$ production and accumulation result in the production of small oligomers of Aβ (small aggregates of 2 to 12 peptides), known to be more toxic than mature fibrils (Ballard et al., 2011). These Aβ oligomers accumulate within neurons (Gouras et al., 2000; Mochizuki et al., 2002), where they are thought to play an early and crucial role in AD pathogenesis (Tampellini and Gouras, 2010). Indeed, cognitive impairment (Moechars et al., 1999), as well as, increased oxidative damage (Praticò et al., 2001) was found in AD transgenic mice before Aβ plaques formation, and in human AD brains, soluble Aβ levels, but not insoluble, correlate with severity of the disease, namely neurofibrillary changes and age at death (McLean et al., 1999).

$A\beta_{42}$ accumulation in neurons occurs in the outer limiting membrane of MVBs within presynaptic (axon terminals) and especially postsynaptic (distal dendrites) compartments, where it is associated with abnormal synaptic morphology (Almeida et al., 2006; Takahashi et al., 2002), that likely leads to synaptic dysfunction (Takahashi et al., 2004). Furthermore, cultured primary neurons from the Tg2576 transgenic mice harboring the human APP gene with the familial AD Swedish mutation, showed decreased levels of the postsynaptic density protein PSD-95 (Almeida et al., 2005), a member of the membrane associated guanylate kinases (MAGUKs) family that drives α-amino-3-hydroxy-5-methyl-4-isoxazolepropionic acid (AMPA) receptors incorporation in the postsynaptic density, particularly receptors containing the subunit GluR1 (Ehrlich and Malinow, 2004). In agreement, decreased surface expression of GluR1 was also observed (Almeida et al., 2005).

In point of fact, the best pathological correlation with cognitive impairment in Alzheimer's disease is synaptic loss (Tampellini and Gouras, 2010), identified with immunohistochemical studies using antibodies against pre- or postsynaptic proteins and with electron microscopy studies. Synaptic loss can exceed the existing neuronal cell death, indicating that synapse loss predates neuronal loss (Serrano-Pozo et al., 2011). Neurons in layer II of the entorhinal cortex and hippocampal CA1 neurons, particularly glutamatergic neurons, are the most vulnerable (Holtzman et al., 2011; Mattson, 2004) and the increased size of the remaining surviving synapses, measured by the length of the postsynaptic density, has been interpreted as a compensatory response (Serrano-Pozo et al., 2011).

In addition, Aβ appears to be an important instigator of neuronal oxidative damage. Aβ oligomers, by interacting with Fe^{2+} or Cu^{+}, generate reactive oxygen species and, consequently through lipid peroxidation at the membrane, 4-hydroxynonenal (4HNE), that covalently modifies proteins, including membrane transporters (ion-motive ATPases, glucose and glutamate transporters), receptors, GTP-binding proteins and ion channels (VDCC, voltage-dependent chloride channel; NMDAR, N-methyl-D-aspartate receptor) (Mattson, 2004). Aβ-induced oxidative stress also leads to mitochondrial oxidative stress and dysregulation of calcium homeostasis. Aβ also triggers microglial and astrocytic activation, resulting in an inflammatory response that can contribute to the neurodegenerative process (González-Reyes et al., 2017; Hardy and Selkoe, 2002; Mattson, 2004).

1.2.2 Neurofibrillary tangles

Neurofibrillary tangles (NFTs) are intraneuronal aggregates of the microtubule-associated protein tau (Mattson, 2004) that accumulate in selective neurons in the brains of individuals with AD, but also occur in other neurodegenerative disorders, commonly known as 'tauopathies', such as frontal temporal dementia with Parkinsonism linked to chromosome 17 (FTDP-17), Pick's disease, progressive supranuclear palsy (PSP) and corticobasal degeneration

(CBD) (Holtzman et al., 2011; V. Lee et al., 2001).

NFTs, present in neuronal cell bodies (Holtzman et al., 2011), are primarily made of paired helical filaments (PHFs) with a β-sheet pleated structure. NFTs can be shown by silver impregnation methods, considering that they are argyrophilic, by staining with fluorescent dyes, such as Thioflavin-S, or by immunostaining with anti-tau antibodies. NFTs can be distinguished by three morphological stages, pre-NFTs, mature or fibrillar intraneuronal NFTs (iNFTs) and extracellular "ghost" NFTs (eNFTs). Pre-NFTs or diffuse NFTs are defined by a diffuse tau staining within the cytoplasm of otherwise normal neurons, with well-preserved dendrites and a centered nucleus. iNFTs consist of filamentous aggregates of tau that displace the nucleus toward the periphery of the soma and often extend to distorted-appearing dendrites and to the proximal segment of the axon. eNFTs result from the death of the tangle-bearing neurons and are identifiable by the absence of nucleus and stainable cytoplasm. Invariably accompanying NFTs are the neuropil threads, axonal and dendritic segments containing aggregated and hyperphosphorylated tau (Serrano-Pozo et al., 2011).

The neurofibrillary degeneration starts in the allocortex of the medial temporal lobe (entorhinal cortex and hippocampus), explaining the initial impairment of episodic memory characteristic of AD. Next, NFTs spread to neocortical multimodal association regions, relatively sparing the primary sensory, motor, and visual areas, but leading to the progressive impairment of additional cognitive domains, including executive dysfunction, apraxias, visuospatial navigation deficits, visuoperceptive deficits, and semantic memory. NFT pathological changes can be organized into six stages (Braak and Braak, 1995), referred to as Braak staging, and can be summarized in three: entorhinal, limbic, and neocortical (Figure 1.5) (Serrano-Pozo et al., 2011; Tam and Pasternak, 2017). Nonetheless, whether NFT formation leads to the neuronal death in AD or is a protective response of damaged neurons against toxic tau species is still disputable (Serrano-Pozo et al., 2011).

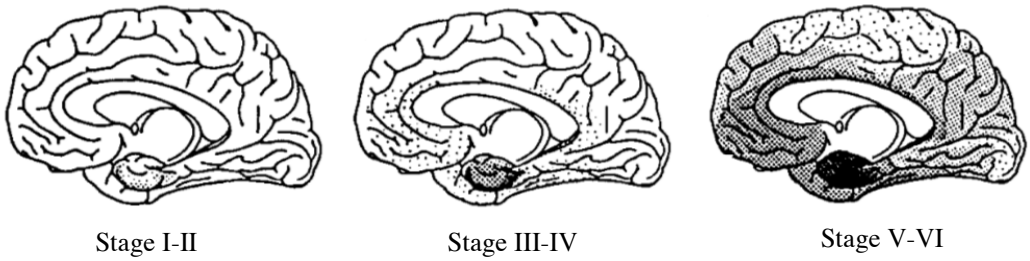

Figure 1.5: **NFT pathological changes are organized by Braak staging.** NFTs first appear in the transentorhinal and entorhinal regions of the medial temporal lobe (stage I and II). Next, NFTs develop and accumulate in limbic structures such as the subiculum of the hippocampal formation and the amygdala, thalamus, and claustrum (stage III and IV). Finally, NFTs spread to all neocortical areas (stage V and VI) (Serrano-Pozo et al., 2011; Tam and Pasternak, 2017). Increasing density of shading proportional to the severity of neurofibrillary changes (Braak and Braak, 1995). Retrieved from Braak and Braak, 1995.

In its normal state, tau is a soluble protein normally located to the axon, where it promotes microtubule assembly and stabilization by being dynamically phosphorylated and dephosphorylated at multiple serine and threonine residues. However, pathological tau protein becomes abnormally hyperphosphorylated leading to its dissociation from microtubules, misfolding and aggregation, giving rise to neurofibrillary tangles and neuropil threads (Figure 1.6) (Brunden et al., 2009; Holtzman et al., 2011; Serrano-Pozo et al., 2011).

Tau phosphorylation can be enhanced by protein kinase and/or phosphatase activities and additional post-translational modifications may also contribute to tau dysfunction, for example a decreased in tau serine–threonine O-glycosylation increase the extent of tau phosphorylation.

Proteolytic cleavage, by calpain and caspases, may produce tau fragments with a faster rate of fibrillization than the full-length protein and so facilitate tau aggregation. Further, the presence of anionic cofactors such as heparin, RNA or negatively charged lipids may facilitate tau deposition (Brunden et al., 2009; Serrano-Pozo et al., 2011).

Abnormalities in tau disturb the structure and function of the neuron by the disruption of microtubule stability (Caselli et al., 2017; Mattson, 2004). This instability leads to deficits in the axonal transport of synaptic vesicles and mitochondria (Mattson, 2004; Kins and Beyreuther, 2006) and impair the neurons ability to maintain extensive dendritic and axonal arborizations, ultimately leading to loss of synaptic connectivity and neuronal death (Caselli et al., 2017).

According to the amyloid cascade hypothesis, the earliest stages of AD are characterized by amyloid deposition that is followed later by tau pathology, triggered by toxic concentrations of Aβ (Ballard et al., 2011; Caselli et al., 2017). Indeed, FAD mutations induced extracellular deposition of Aβ, in a human neural stem-cell-derived 3D culture model, that triggered the aggregation of phosphorylated tau (Choi et al., 2014). Extracellular amyloid deposits and intracellular Aβ protein may activate caspases, leading to a caspase-cleaved form of tau with more propensities to aggregate (Dickson, 2004). In addition, the oxidative stress induced by Aβ can promote oxidative modifications of tau, for example by 4HNE, and thereby induce its aggregation and the formation of neurofibrillary tangles (Mattson, 2004). Nonetheless, there is also likely tau-related brain damage in AD that is independent of Aβ, since tau mutations were discovered in other tauopathies, with no Aβ pathology, establishing that changes in tau structure and/or function are sufficient to cause neurodegeneration and a non-AD dementing disorder (Holtzman et al., 2011; Kins and Beyreuther, 2006). However, neuronal loss can exceed the number of neurofibrillary tangles, suggesting that there is a mechanism of neuronal death in AD affecting tangle-free neurons, where neurons die without forming tangles (Mattson, 2004; Serrano-Pozo et al., 2011).

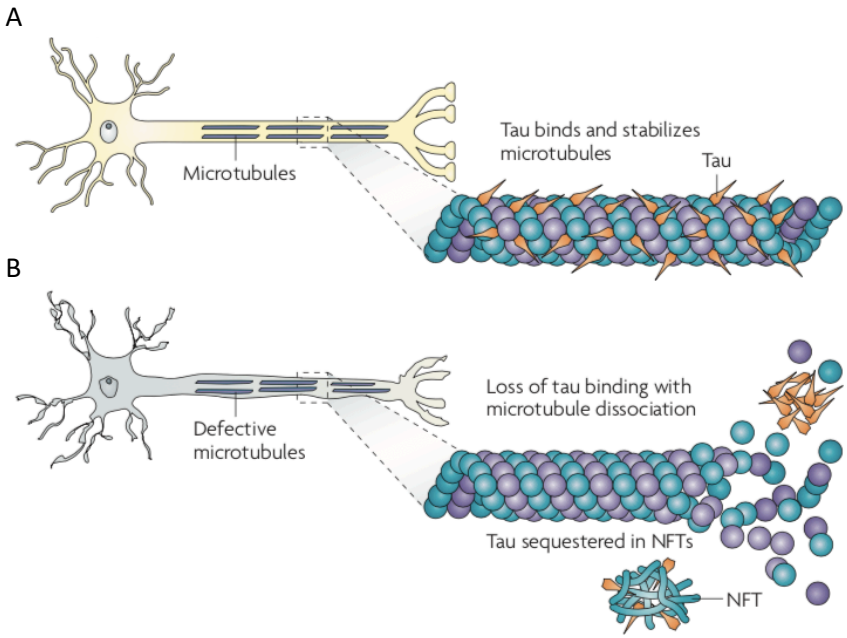

Figure 1.6: **Tau pathology in Alzheimer's disease.** A. In healthy neurons, tau binds microtubules and promotes their stabilization. B. In AD and other taupathies, tau is hyperphosphorylated, which reduces the binding to microtubules and leads to the sequestration of tau into neurofibrillary tangles (NFTs). Retrieved from Brunden et al., 2009.

1.2.3 Other features

In 80% of AD patients, Aβ not only deposits in the form of amyloid plaques but also in vessel walls in the form of cerebral amyloid angiopathy (CAA), being the $A\beta_{40}$ peptide the major constituent of CAA (Serrano-Pozo et al., 2011).

Granulovacuolar degeneration (GVD) and Hirano bodies are two lesions detected in hippocampal pyramidal neurons that are present in cognitively intact elderly people but are more severe and frequent in AD patients (Serrano-Pozo et al., 2011). GVD is characterized by the intraneuronal accumulation of large double-membrane bodies and composed of a variety of proteins, including tau and tau kinases, and those related to autophagy, diverse signal transduction pathways, cell stress and apoptosis (Serrano-Pozo et al., 2011; Köhler, 2016). Hirano bodies are eosinophilic cytoplasmic inclusions that contain epitopes of actin, actin-associated proteins, tau, neurofilaments proteins, advanced glycation end products and the carboxy-terminal fragments of APP (Hirano, 1994; Serrano-Pozo et al., 2011)

1.3 Clinical features of AD

Alzheimer's disease can be characterized by three groups of symptoms: (1) cognitive dysfunction, including memory loss, language difficulties, and executive dysfunction, (2) psychiatric symptoms and behavioral disturbances, such as depression, hallucinations, delusions and agitation, and (3) difficulties in performing activities of daily living, be it a complex activity, such as driving and shopping, or a more basic activity like dressing and eating unaided (Burns and Lliffe, 2009). These symptoms progress from a subclinical, pre-dementia stage, to mild, moderate and severe dementia stage (Figure 1.7) (Förstl and Kurz, 1999).

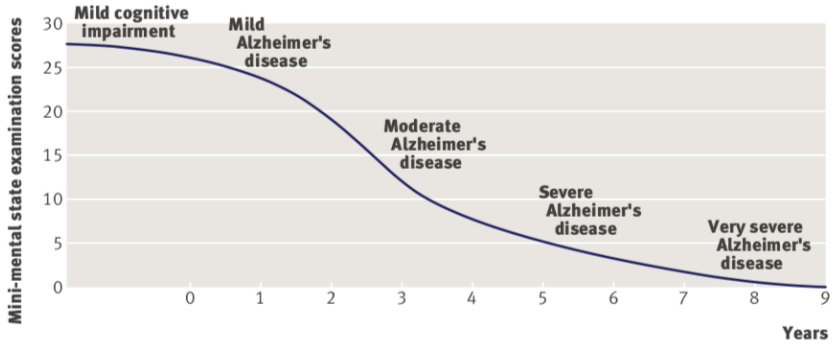

Figure 1.7: **Progression of Alzheimer's disease.** Mini-mental state examination scores (MMSE) according to the years after clinical diagnosis of AD. Alzheimer's disease progresses from the pre-dementia stage, characterized by mild cognitive impairment, to mild, moderate, severe and very severe dementia stages. Retrieved from Burns and Lliffe, 2009.

The pre-dementia stage, that can occur 5 years before the clinical diagnosis, corresponds to a phase of mild cognitive impairment. In this phase, individuals have difficulties in acquiring new memories, and in other cognitive tasks, including the ability to plan or to access the semantic memory store. In addition, the performance of complex work tasks may be reduced, and individuals tend to avoid difficult challenges and downplay or dissimulate their problems. It may also be present non-cognitive alterations of behavior, including social withdrawal and depressive dysphoria. Nonetheless, individuals do not show a significant deterioration in Activities of Daily

Living (ADL) and at this phase, it is still not yet possible to differentiate between incipient AD and a reversible condition or benign, non-progressive memory impairment (Burns and Lliffe, 2009; Förstl and Kurz, 1999).

In the mild dementia stage, there is a significant impairment of learning and memory, in particular declarative recent memory. This memory impairment usually plays a key role in the patient's difficulties with ADL. The affected individual has reduced ability in planning, judgment and organization, and also presents constructional apraxia and spatial disorientation. The patient may present symptoms of depression (Förstl and Kurz, 1999).

The moderate dementia stage, lasting 2 to 4 years, is characterized by a progression of cognitive deficits and the loss of the ability to operate independently in the community (Förstl and Kurz, 1999; Holtzman et al., 2011). Language difficulties become more obvious, further impairment of ADL occurs, and cortical visual agnosia is often present and can include prosopagnosia, the inability to recognize familiar faces. At this stage, one third of AD patients develop illusionary misidentifications and other delusional symptoms and up to 20% of the patients develop hallucinations. Patients, also, develop restlessness, physical or verbal aggression, disorientation, and incontinence (Burns and Lliffe, 2009; Förstl and Kurz, 1999).

In the severe stage of Alzheimer dementia, individuals are totally dependent on caregivers and, in advanced disease, often become mute, bedridden, and unable to swallow or control bladder and bowel function (Holtzman et al., 2011). Patients often misinterpret nursing interventions leading to aggressive reactions. A large proportion of patients show extreme apathy and exhaustion. Myoclonus and epileptic seizures can be observed in a smaller proportion of patients with severe AD. A long persistence of symptoms, the severity of illness, old age, male sex, and physical disease are major risk factors for mortality in AD. Pneumonia, myocardial infarction and septicaemia are the most frequent causes of death in AD. The average duration of survival of AD patients is 5 to 8 years after clinical diagnosis (Förstl and Kurz, 1999).

1.3.1 Diagnosis

Alzheimer's disease can only be definitively diagnosed post mortem (Ballard et al., 2011). Clinically, individuals are classified with probable AD dementia, possible AD dementia, and probable or possible AD dementia with evidence of the AD pathophysiological process (McKhann et al., 2011). Firstly, cognitive impairment is assessed through a detailed history of the type and course of symptoms taken from the patient and a reliable informant, and through mental status examination or a neuropsychological assessment. The cognitive or behavioral impairment involves a minimum of two of the following domains: memory, executive, visuospatial, language, personality and behaviour (Table 1.1) (Caselli et al., 2017; McKhann et al., 2011). The differentiation of dementia from MCI rests on the determination of whether or not there is significant interference in the ADL (McKhann et al., 2011).

Table 1.1: **10 early signs and symptoms of Alzheimer's disease** (Alzheimer's Association, 2017).

1	Memory loss that disrupts daily life
2	Challenges in planning or solving problems
3	Difficulty completing familiar tasks at home, at work or at leisure
4	Confusion with time and place
5	Trouble understanding visual images and spatial relationships
6	New problems with words in speaking or writing
7	Misplacing things and losing the ability to retrace steps
8	Decreased or poor judgment
9	Withdrawal from work or social activities
10	Changes in mood and personality

Probable AD dementia is diagnosed when the patient meets criteria for dementia and in addition, has a gradual onset over months to years, worsening of cognition and the initial and most prominent deficits are in memory, language, and visuospatial and executive domains. The level of certainty that the condition is caused by AD phatology increases with the evidence of progressive cognitive decline and evidence of a causative AD genetic mutation. The criteria for possible AD dementia include the presence of an atypical course, such as a sudden onset, or etiologically mixed features of other diseases. Probable or possible AD dementia with evidence of the AD pathophysiological process is based in the detection of two types of biomarkers. Biomarkers of brain amyloid plaques include reduced levels in cerebrospinal fluid (CSF) of Aβ peptide $A\beta_{42}$ and positive positron-emission tomography (PET) amyloid imaging. Furthermore, biomarkers of the downstream neuronal degeneration or injury include elevated levels in CSF of tau, decreased glucose metabolism, evaluated through a fluorodeoxyglucose (FDG) PET scan, and brain atrophy through a structural magnetic resonance imaging (MRI) (Caselli et al., 2017; McKhann et al., 2011).

However, the research for a biomarker that allows the diagnosis of AD with high accuracy and in very early stages, and the monitorization of treatment efficacy is still a challenge (Mueller et al., 2005).

1.3.2 Current therapies

Currently, there is no cure for Alzheimer's disease. Indeed, the principle of therapy of AD is maximizing the quality of life trough symptom management. That management is accomplished through palliative drugs, such as acetylcholinesterase (AChE) inhibitors (Donepezil, Rivastigmine and Galantamine), in patients with mild to moderate stages of AD, and non-competitive NMDA-receptor antagonists (Memantine), in patients with moderate to late stages of AD (Caselli et al., 2017; González-Reyes et al., 2017). As well as drugs that ameliorate behavioral disturbances (Atri, 2019; Hardy and Selkoe, 2002).

Acetylcholinesterase is responsible for the breakdown of the neurotransmitter acetylcholine, so AChE inhibitors will increase the endogenous acetylcholine concentration available to stimulate cholinoceptors on the postsynaptic neuron and, consequently, counter the dysfunction of the cholinergic system in AD patients. This results in a modest increase in cognitive ability. Excessive NMDA-receptors activity, stimulated by the neurotransmitter glutamate, can lead to excitotoxicity, postulated to contribute to the pathology of AD. As so, Memantine is an "open channel blocker" that acts by blocking the current flow through channels of NMDA-receptors only after being opened. It prevents excessive synaptic NMDA-receptor activity, but still preserves physiological activity for neuronal transmission (Johnson and Kotermanski, 2006; Katzung et al., 2012; Tam and Pasternak, 2017). However, these drugs do not prevent the progression of the disease (Holtzman et al., 2011), remaining the need to pursue novel therapeutic targets.

The development of new therapies focuses on targeting specific sites in the amyloid cascade hypothesis. Since the generation of Aβ appears to be a pivotal and early event in AD pathogenesis, drugs that block β- or γ-secretase are, currently, being considered as a possible efficient treatment of AD. Although, side effects from this blockage has to be taken into account, since these compounds might interfere with the signaling by Notch proteins and other cell surface receptors (Ballard et al., 2011; Mattson, 2004).

Other approaches to reduce Aβ accumulation include chelators of copper and iron, considering their involvement in delaying the formation of the less toxic aggregates of amyloid-β and in the generation of oxidative stress in neurons (Ibrahim and Gabr, 2019; Mattson, 2004), and

the use of active or passive immunization to accelerate Aβ clearance. However, all clinical trials have failed due to autoimmune responses by the patients (Mattson, 2004; Cao et al., 2018).

Other strategies being tested include anti-inflammatory agents, based on the observation that the progressive accumulation of Aβ induces a cellular inflammatory response that amplifies neuronal damage, and modulation of cholesterol homeostasis by cholesterol-lowering drugs, such as the statins (Mattson, 2004; Hardy and Selkoe, 2002).

The failures of several AD clinical trials due to the irreversible neurodegeneration as AD progresses (Cao et al., 2018) demonstrate the importance of targeting early events of the disease.

1.4 Familial and sporadic AD

Familial early-onset AD and sporadic late-onset AD are two different, but neuropathologically indistinguishable (Weggen and Beher, 2012), forms of Alzheimer's disease.

Familial AD (FAD/EOAD) accounts for only a minor portion (<1%) of all AD cases and has an early onset before the age of 65 and, in some cases, as early as age 30 (Holztman et al., 2011; J. Z. Tan and Gleeson, 2019). FAD is a dominantly inherited form of AD that develops as a result of genetic mutations found in genes related to the production of Aβ (Caselli et al., 2017; Holztman et al., 2011). However, in the majority of AD cases the symptoms become apparent after the age of 65 and are referred to as late-onset AD (LOAD). This sporadic AD form is a multifactorial disease that develops from a combination of lifestyle, age and genetic risk factors (J. Z. Tan and Gleeson, 2019).

Through genetic linkage studies, causative genes of familial AD, β-amyloid precursor protein (APP), presenilin 1 (PSEN1) and presenilin 2 (PSEN2), were identified (Levy-Lahad et al., 1995; Schellenberg et al., 1992; Shao et al., 2017; St George-Hyslop et al., 1987). In the APP gene, missense mutations often occur around the sites of proteolytic processing by BACE1 and γ-secretase, leading to either an increase in the release of Aβ peptides or an increase in the $A\beta_{42}/A\beta_{40}$ ratio, shifting towards the production of the toxic Aβ peptides (Holztman et al., 2011; Shao et al., 2017; Weggen and Beher, 2012). Increased Aβ production was also found in individuals carrying a small duplication in the chromosome 21 of the region that encompasses the APP gene and also in individuals with Down's syndrome, since they carry a duplication of chromosome 21 (Caselli et al., 2017; Holztman et al., 2011; Rovelet-Lecrux et al., 2005). The majority of PSEN mutations also lead to an increase in the $A\beta_{42}/A\beta_{40}$ ratio (Shao et al., 2017).

In the sporadic AD, age is the highest risk factor, with the incidence of AD increasing exponentially with age (J. Z. Tan and Gleeson, 2019), taking only 5,5 years to double AD incidence rates (Ziegler-Graham et al., 2008). Higher levels of education and cognitive stimulating activities contribute to a cognitive reserve capacity, lowering the risk of developing Alzheimer's disease (James and Bennet, 2018; Stern et al., 1994). Likewise, physical activity, exercise and a healthy diet have been linked to a reduce risk of AD. This is accomplished through a range of mechanisms that include building cognitive reserve and reducing cardiovascular diseases (James and Bennet, 2018). Indeed, medical conditions, such as stroke, diabetes, midlife hypertension and hypercholesterolaemia, are associated with an increased risk of AD (Ballard et al., 2011; Burns and Lliffe, 2009; James and Bennet, 2018). In addition, head trauma has been linked to elevated risk of dementia (Jellinger, 2004).

1.4.1 Genetic rick factors of LOAD

The most firmly established genetic risk factor is Apolipoprotein E (APOE) – ε4 gene. ApoE, found associated to senile plaques and neurofibrillary tangles in 1991 by Namba, regulates lipid homeostasis by mediating lipid transport in the peripheral tissues and in the central nervous system. In the brain, apoE, mainly secreted by astrocytes, is responsible for the transport of cholesterol to neurons via apoE receptors, members of the low-density lipoprotein (LDL) receptor family (Liu et al., 2013; Saunders et al., 1993; Yamazaki et al., 2016). In the neurons, cholesterol is an essential component for axonal growth, synaptic formation and remodelling, events crucial for learning, memory formation and neuronal repair (Liu et al., 2013).

Two single nucleotide polymorphisms (SNPs) generate three allelic variants of the human APOE gene, ε2, ε3 and ε4 that affect the structure of the apoE protein, as well as, the binding to lipids, receptors and Aβ (Liu et al., 2013; Yamazaki et al., 2016). Worldwide, APOE ε3 is the most common allele, with a prevalence of 77,9%. Contrarily, ε2 allele is the less prevalent, with a worldwide frequency of 8,4%. The ε4 allele, with a frequency of 13,7%, has been linked to an increase risk of AD of 2 to 3-fold higher in people with only one ε4 allele and 12-fold higher in people with ε4/ε4 genotype (Farrer et al., 1997; Michaelson, 2014).

ApoE4 is associated with an increased production of Aβ, aggregation and deposition, by binding Aβ and stimulating APP transcription more effectively than apoE ε3 isoform (Christensen et al., 2010; Huang et al., 2017; Strittmatter et al., 1993). Indeed, apoE4 is found present in amyloid plaques in the brains of AD patients (Namba et al., 1991). Further, apoE4 seems to be less efficient in mediating Aβ clearance (Castellano et al., 2011; Verghese et al., 2013), by slowing Aβ removal from the brain to the systemic circulation through the blood–brain barrier (Liu et al., 2013). The three isoforms also regulate cholesterol levels differentially, being ApoE4 less efficient in transporting cholesterol (Michikawa et al., 200; Rapp et al., 2006). In addition, ApoE4 is preferential degraded (Riddell et al., 2008), which further reduces the capacity of neuronal delivery of cholesterol. Moreover, ApoE4 seems to induce neuroinflammation (Lynch et al., 2003; Ringman et al., 2012), which can exacerbate AD pathology (Bales et al., 2000). In opposition, the ε2 allele, negatively associated with the risk of developing AD (Corder et al., 1994; West et al., 1994), has shown to have protective effects against AD, being neuroprotective and reducing Aβ brain levels (Hudry et al., 2013; Shinohara et al., 2016).

Due to the increased risk of AD in APOE ε4 carriers, therapeutic strategies targeting apoE are being explored (Liu et al., 2013). However, no therapeutic approaches have been successfully implemented (Yamazaki et al., 2016). Furthermore, although APOE ε4 is expressed in more than 50% of AD patients (Rebeck et al., 1993; Ward et al., 2012), it does not account for the entirety of the genetic susceptibility (Stocker et al., 2018).

The search for the remaining AD susceptibility genes led to the execution of genome-wide association studies (GWAS). These studies allow the identification of the genetic variants associated with a trait, that is, the variants present at higher frequency in individuals with the trait compared with controls (Bush and Moore, 2012). Numerous GWAS prompted the identification of CLU, PICALM and CR1 (Harold et al., 2009; Lambert et al., 2009), CD33, MS4A4A/MS4A4E/MS4A6E locus, ABCA7, CD2AP and EPHA1, (Hollingworth et al., 2011; Naj, et al., 2011) and BIN1 gene (Seshadri et al., 2010) as susceptibility loci. These GWAS also further affirmed APOEε4 as the most significant risk factor and confirmed two genes SORL1 and TREM2, already identified by early genetic studies (Shen and Jia, 2016; Tosto and Reitz, 2013).

Several genes seem to mediate AD pathology through implications in the clearance of Aβ or through another immune-related function, such as CR1, CD33, MS4A genes, EPHA1, TREM2, CLU and ABCA7 (Guerreiro et al., 2013; Tosto and Reitz, 2013), the last two being also involved in lipid metabolism (Tosto and Reitz, 2013), which is thought to influence Aβ processing, aggregation and clearance (Di Paolo and Kim, 2011). In addition, endocytosis/intracellular trafficking is another pathway implicated in AD, as seen by the discovery of SORL1, PICALM, CD2AP and BIN1 as

genetic risk factors (Almeida et al., 2018; Tosto and Reitz, 2013). SORL1, sortilin-related receptor, is implicated in the sorting of APP to recycling endosomes to be transported to the TGN (Fjorback et al., 2012). Absence of SORL1 directs APP into early endosomes, where the amyloidogenic pathway takes course (Fjorback and Anderson, 2012; Willnow and Andersen, 2013). PICALM encodes for, phosphatidylinositol-binding clathrin assembly protein, involved in clathrin-mediated endocytosis. It recruits clathrin and adaptor protein complex 2 (AP-2) to promote the formation of endocytic vesicles (Meyerholz et al., 2005; Tebar et al., 1999), required for APP internalization and therefore Aβ production (Xiao et al., 2012). Further, is involved in synaptic vesicle protein retrieval (Meyerholz et al., 2005). Some studies suggest a deleterious effect of PICALM, while others propose a protective role (Almeida et al., 2018). CD2AP, CD2-associated protein, is a membrane-associated scaffolding protein that interacts directly with the actin cytoskeleton (Lehtonen et al., 2002). This interaction with actin favors a role of CD2AP in the intracellular trafficking (Gauthier et al., 2007). Indeed, decrease CD2AP expression results in an accumulation of APP at early endosomes limiting membrane (Ubelmann, Burrinha, Salavessa et al., 2017). This impairment in the sorting to multivesicular bodies leads to prevention of APP degradation by lysosomes, indulging Aβ production.

Amphiphysin II/BIN1 is considered the second most frequent susceptibility locus after APOE4 (Bertram et al., 2007). However, the mechanisms whereby BIN1 contributes to AD pathogenesis are still not fully understood (M. S. Tan et al., 2014). The current work will focus on investigating the role of BIN1 in AD development.

1.5 Bridging Integrator 1 (BIN1)/ Amphiphysin II

1.5.1 BIN1 gene and tissue-specific expression

BIN1, Bridging integrator 1 or box-dependent myc-interacting protein 1, also know as amphiphysin II, was firstly identified as a tumor suppressor as it interacts with the transcription factor Myc and inhibits its oncogenic activity (Sakamuro et al., 1996). Structural similarity between the N-terminal regions of BIN1, amphiphysin and RVS167 protein lead to this region been termed BAR (BIN1/amphiphysin/RVS167) domain (Sakamuro et al., 1996). Members of the BAR superfamily have been implicated in dynamic membrane remodelling by the promotion of membrane curvature and regulation of the actin cytoskeleton, playing diverse roles in intracellular trafficking, cell division, cell migration, organelle biogenesis and, also, apoptosis (Rao and Haucke, 2011; Ren et al., 2006). BIN1 further belongs to the amphiphysin subfamily (Leprince et al., 1997) due to its homology to the previously reported amphiphysin I (Lichte et al., 1992).

BIN1, mapped to chromosome 2q14.3 (Negorev et al., 1996), encodes a ubiquitously expressed protein, with highest expression in brain and skeletal muscle (Butler et al., 1997; Sakamuro et al., 1996). In skeletal muscle, BIN1 is concentrated around transverse (T) tubules. In the brain, BIN1 localizes to the axon initial segments and nodes of Ranvier (Butler et al., 1997). BIN1 undergoes alternative splicing (Tsutsui et al., 1997), originating at least 16 transcripts spliced in a tissue-specific manner (Gene, NCBI). Isoforms 9 and 10 are ubiquitously expressed, whereas isoforms 1-7 are expressed only in the brain and isoform 8 is a muscle-specific isoform (M. S. Tan et al., 2014; Tsutsui et al., 1997; WechslerReya et al., 1997). Neuronal-specific isoform 1 is the longest with 593 amino-acid residues (Ramjaun, et al., 1997; referred to as amphiphysin II).

All BIN1 isoforms contain a N-BAR domain, a Myc-binding domain (MBD; exons 17 and 18) (Sakamuro et al., 1996) and a C-terminal Src homology 3 (SH3) domain (Leprince et al., 1997). An additional domain, clathrin and AP2 binding (CLAP) domain, also known as clathrin-

associated protein-binding region, encoded by exons 13 to 16, is present in the longest isoform, the neuronal-specific isoform (isoform 1) (Ramjaun et al., 1997; Ramjaun and McPherson, 1998). In addition, a phosphoinositide (PI)-binding motif, encoded by exon 11, is only present in a few BIN1 isoforms, including the muscle-specific isoform (E. Lee et al., 2002) (Figure 1.8).

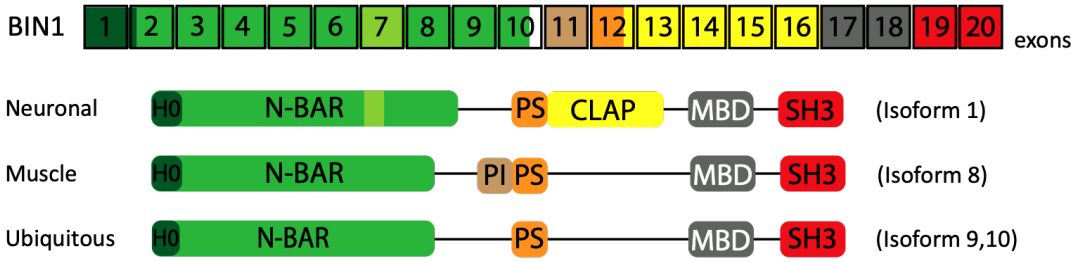

Figure 1.8: **BIN1 domain structure and tissue-specific isoforms.** Common BIN1 domains to neuronal (isoform 1), muscle (isoform 8) and ubiquitous isoforms (isoforms 9 and 10) include the BAR domain (exon 2 to 10), a proline-serine rich (PS) region (exon 12), a Myc-binding domain (MBD) (exon 17 to 18) and the C-terminal Src homology 3 (SH3) domain (exon 19 and 20). Neuronal isoform also contains a clathrin and AP2 binding (CLAP) domain (exon 13 to 16), and the alternatively spliced exon 7. A phosphoinositide (PI)-binding motif (exon 11) is present in the muscle isoform. BIN1 gene organization is based from NCBI database. H0, Helix-0.

1.5.2 BIN1 known functions

BIN1 has been implicated in intracellular endosome trafficking, specifically clathrin-mediated endocytosis, through membrane remodeling and ability to interact with endocytic and cytoskeleton proteins, in neuronal and non-neuronal cells. A role in DNA repair, cell cycle regulation and apoptosis as also been reported (Prokic et al., 2014).

BIN1 function in membrane and cytoskeleton remodeling

Through the presence of a BAR domain that forms crescent-shaped homo or hetero dimers (with amphiphysin I (Wigge et al., 1997)) with a positively charged concave face, BIN1 binds negatively charged phospholipid membranes (Casal et al., 2006; Peter et al., 2004). The concave face acts as a membrane-curvature sensing module (Peter et al., 2004). In addition, BIN1 N-terminus includes an unstructured residue extension predicted to form an amphipathic helix (Helix-0) upon membrane binding. The amphipathic helix penetrates into the membrane bilayer, displacing phospholipids and enhancing curvature. This enables the N-BAR domain to actively induce membrane curvature and further stabilize it (Löw et al., 2008; Peter et al., 2004).

In the skeletal muscle, BIN1 gene encodes a nuclear localization signal and a phosphoinositide (PI) binding motif (exon 11) that interacts with the phosphatidylinositol 4,5-biphosphate, $PI(4,5)P_2$, present in the plasma membrane, and the phosphatidylinositol phosphates PI(3)P, PI(4)P and PI(5)P (E. Lee et al., 2002; Fugier et al., 2010). PI(3)P is found in late endosomes and multivesicular bodies, PI(4)P is associated with the TGN and secretory vesicles and PI(5)P localizes to the nucleus, plasma membrane and early endosomes, and as been suggested to play crucial roles in the remodeling of actin cytoskeleton, endocytosis and nuclear signaling (Hasegawa et al., 2017; Falkenburger et al., 2010). Through this interaction, BIN1, in the skeletal muscle, induces plasma membrane invaginations to form T-tubules that propagate action potentials and trigger muscle contraction (excitation-contraction coupling) (E. Lee et al., 2002;

Razzaq et al., 2001). Furthermore, it was described a role in skeletal muscle maturation through the interaction of the C-terminal SH3 domain with sarcomeric actin and myosin filaments and the kinase Cdk5 (Fernando et al., 2009), and the actin nucleation-promoting factor N-WASP (Falcone et al., 2014). Another role in cytoskeleton regulation is suggested by the discovery of the interaction of the SH3 domain of APL1 (amphiphysin-like protein 1), a BIN1 splice variant (Ren et al., 2006), with proto-oncogene tyrosine kinase c-Abl, thought to have a role in cytoskeleton organization (Kadlec and Pendergast, 1997).

BIN1 function in intracellular trafficking

The presence of a CLAP domain allows neuronal BIN1 interaction with the endocytic proteins clathrin and adaptor protein complex 2 (AP2) (Ramjaun and McPherson, 1998), involved in the formation of clathrin-coated vesicles at the TGN and plasma membrane (Figure 1.9). The major constituent of this vesicle type is clathrin, a multi-subunit protein with a triskelion structure. Several triskelions further assemble to form a polyhedral, cage/lattice-like network that attaches to the membrane via an adaptor protein (AP) complex forming a coated pit (Kaksonen and Roux, 2018; McClure and Robinson, 1996). AP1 recruits and binds clathrin coats in the TGN, while AP2 participates in the assembly of clathrin-coated pits at the plasma membrane (Boehm and Bonifacino, 2001). By also binding cargo receptors, adaptor proteins appear to be responsible for the recognition of the appropriate cargo molecules (Kaksonen and Roux, 2018). In contrast to the neuronal isoform, muscle and ubiquitous isoforms (isoform 9 and 10) lack this domain suggesting a specific role of BIN1 in clathrin-mediated endocytosis (CME) in neurons.

In addition, several isoforms, like the neuronal isoform, include, in the BAR domain, an insertion of 31 residues, encoded by the alternatively spliced exon 7. This insertion promotes interaction with the GTPase dynamin II (Ellis et al., 2012), a ubiquitously expressed dynamin (Sontag et al., 1994), involved in the fission of clathrin-coated vesicles to free the nascent vesicle (Kaksonen and Roux, 2018). Equally, the SH3 domain mediate interactions with the proline-rich motif (PRD), sequence PSRPNR, of dynamin (Owen et al., 1998), as well as, a variety of endocytic and cytoskeleton proteins.

In mammalians, dynamin genes encode dynamin I, abundant in neurons and particularly concentrated in presynaptic nerve terminals, dynamin II, expressed ubiquitously, and dynamin III, restricted to testis, brain, and lung (Sontag et al., 1994; Urrutia et al., 1997). Dynamin I is involved in rapid synaptic vesicle retrieval/recycling from the plasma membrane following synaptic transmission, whereas dynamin II is predict to participate in a more ubiquitous process, such as clathrin-mediated endocytosis (McClure and Robinson, 1996; Urrutia et al., 1997).

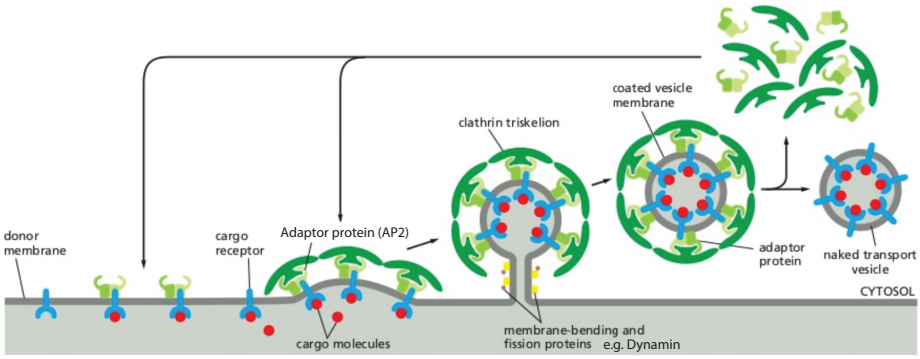

Figure 19: **Clathrin-coated vesicle formation.** Adaptor proteins, such as adaptor protein complex 2 (AP2) at the plasma membrane, recruit and bind clathrin triskelions, to assemble a lattice-like clathrin-coated bud. Dynamin is also recruited to form a ring at the neck of the bud and, through GTP hydrolysis, drives membrane fission of the nascent vesicle. Induction of membrane curvature and interaction with clathrin, AP2 and dynamin implicate BIN1 in clathrin-mediated endocytosis. Adapted from Alberts et al., 2015.

In CME, adaptor proteins and SH3-domain-containing proteins, recruit dynamin to clathrin-coated buds where, after forming a self-assembled ring at the neck of the bud, a GTP hydrolysis-dependent conformational change drives membrane fission to free the coated vesicle (Antonny et al., 2016; Kaksonen and Roux, 2018). It has been demonstrated that BIN1 SH3 domain regulates dynamin ring self-assembly, and, indeed, overexpression of SH3 domain alone inhibits endocytosis (Owen et al., 1998). This is the result of the presence of an insertion of acidic residues in the n-Src loop of SH3 domain of amphiphysins absent in other SH3 domain-containing proteins (Figure 10). The n-Src together with the RT loop form an unusual large region of negative electrostatic potential that explains the specific target site on the PRD of dynamin, which contains two arginine residues, which might lead to the obstruction of Dynamin GTPase domain and so, dynamin–dynamin interactions essential for dynamin ring formation (Owen et al., 1998).

BIN1 function in synapses

Synaptic vesicle recycling, the retrieval of vesicular membrane and its associated proteins by endocytosis, is essential to maintain a functional synaptic vesicle pool that sustains neurotransmitter release at synapses (Cremona and Camilli, 1997; Di Paolo et al., 2002). A major pathway of synaptic vesicle recycling is the clathrin-mediated endocytosis (Cremona and Camilli, 1997). Interestingly, BIN1 SH3 domain binds synaptojanin (Ramjaun et al., 1997), important for the clathrin uncoating of synaptic vesicles after retrieval from the plasma membrane (Cremona et al., 1999), and endophilin, a member of the BAR superfamily, also implicated in synaptic vesicle recycling (Micheva et al., 1997). In addition, deletion of amphiphysin I, predominately expressed in the brain, lead to the loss of both amphiphysin and BIN1 in the brain and synaptic vesicle recycling defects (Di Paolo et al., 2002). In a more recent study (Yao et al., 2010), BIN1 binding to the synaptic vesicle protein SV2, involved in the transport of neurotransmitters into synaptic vesicles (Feany et al., 1992), was also observed.

BIN1 specific function and localization in synaptic compartements is still controvertial, however recent data (Schürmann et al., 2018) provided new insights for BIN1 role in postsynaptic compartments, including dendritic spines. In the spines, BIN1 was reported to modulate trafficking of AMPA receptor subunit GluA1 (or GluR1) from recycling endosomes to the cell surface (Schurmann et al., 2018) and BIN1 loss was reported to alter synaptic morphology (Glennon et al.,

2019).

BIN1 function in tumorigenesis

BIN1 interacts with the N terminus of the Myc oncoprotein, through its Myc-binding domain, and leads to the inhibition of neoplastic transformation by MYC. In addition, BIN1 expression levels were found greatly reduced in tumor cell lines and absent in primary breast tumors (Sakamuro et al., 1996). Also, co-expression of the BIN1 slice variant APL1 and c-Abl resulted in morphological transformation of NIH 3T3 cells (Kadlec and Pendergast, 1997). As a result, there has been a growing interest in the establishment of BIN1 as a novel prognostic marker and therapeutic target through the characterization of BIN1 functional role in tumorigenesis.

1.5.3 BIN1 self-regulation

BIN1 interactions through the SH3 domain are reported to be regulated by the intramolecular binding to exon 11, in the muscle-specific isoform, (Kojima et al., 2004; Wu and Baumgart, 2014) and to CLAP domain (Malki et al., 2017) in the neuronal-specific isoform. Indeed, exon 11, the phosphoinositide (PI) binding motif, binds SH3 domain, blocking interaction with other proteins, and the presence of phosphoinositides allows the opening of BIN1 conformation (Kojima et al., 2004). This autoinhibition mechanism can also happen through the presence of the CLAP domain in neuronal isoform (Figure 1.10). As a result of the binding of CLAP and SH3 domain the neuronal isoform presents a closer conformation opposite to the open conformation of the ubiquitous isoforms (Malki et al., 2017).

Interestingly, dephosphorylation by the calcium-dependent phosphatase calcineurin of dynamin, amphiphysin I and II, and synapotjanin, triggered by calcium influx after nerve terminals depolarization, is thought to regulate synaptic vesicle retrieval (Marks and McMahon, 1998). Having in mind the role of BIN1 in preventing dynamin self-assembly, we can speculate that dephosphorylation of BIN1 allows the intramolecular interaction between CLAP and SH3 domain, and, consequently, the release of dynamin from BIN1 complex. Indeed, inhibition of the dephosphorylation by cyclosporin A promotes the open conformation of BIN1 (Sartori et al., 2018) and inhibits synaptic vesicle recycling (Marks and McMahon, 1998).

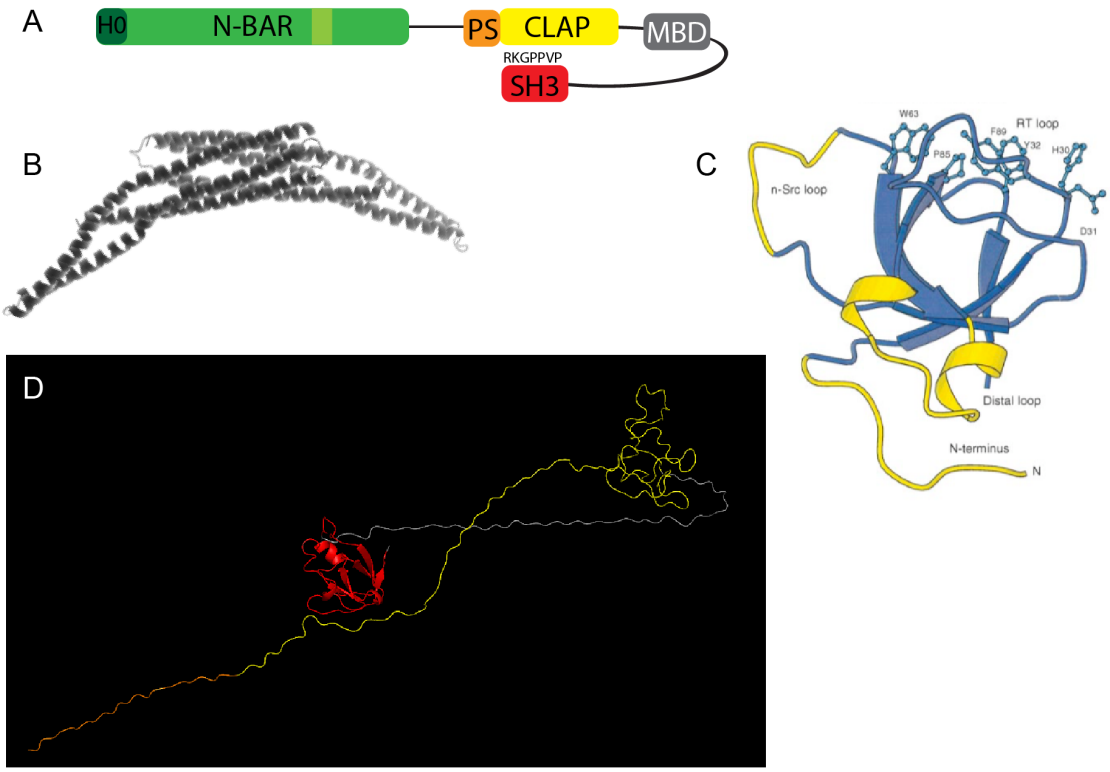

Figure 1.10: **BIN1 autoinhibition.** A. Close conformation of neuronal BIN1 isoform due to intramolecular interactions between SH3 domain and the proline rich-motif, sequence RKGPPVP, of CLAP domain. B. Structure of BIN1 BAR domain, visualized in PyMol (RCSB Protein Data Base (PDB) entry 2fic.1.B (Casal et al., 2006)). C. Structure of BIN1 SH3 domain. Hydrophobic residues involved in binding PRDs, pale blue. Novel inserts not found in others SH3 domains, yellow. (Owen et al., 1998). D. Structure of BIN1 residues 301-593 aa, visualized in PyMol (PDB entry 1mv3.1.A (Pineda-Lucena et al., 2005)). SH3 domain, red; CLAP domain, yellow; proline rich motif, orange.

1.5.4 BIN1 in AD

Although BIN1 is the second most frequent susceptibility locus for LOAD, it remains unclear if an increase or a decrease of BIN1 occurs in AD. In AD human brains, BIN1 transcription was found to be increased (Chapuis et al., 2013) and an aberrant accumulation of BIN1 adjacent to amyloid deposits were observed in mice and rat models (De Rossi et al., 2018). In contrast, a decrease in BIN1 protein levels in sporadic AD human brains was also described (Glennon et al., 2013). Subsequently, separate analysis of two isoforms of BIN1, a neuronal and a ubiquitous isoform, indicated that neuronal BIN1 was reduced in AD human brains, while ubiquitous BIN1 was increased (Holler et al., 2014; De Rossi et al., 2016).

BIN1 is found implicated in the two pathological hallmarks of Alzheimer's disease. BIN1 was shown to interact with the proline-rich domain of tau through its SH3 domain. And in fact, decrease expression of Drosophila melanogaster BIN1 homolog AMPH was found to suppress tau-induced neurotoxicity (Chapuis et al., 2013). In contrast, another study reported that loss of neuronal BIN1 isoform promotes tau pathology propagation due to an increase in endocytosis (Calafate et al., 2016). As so, the role of this interaction, and its potential contribution to Alzheimer's disease development, is not yet fully understood.

Importantly, BIN1 is also associated with Aβ pathology, thought to be the initial trigger of the disease. BIN1 depletion in mice primary cortical neurons led to increased BACE1 protein

levels, as well as, sAPPβ, $A\beta_{40}$ and $A\beta_{42}$ secretion levels. BACE1 activity was found increased in BIN1 knockdown Neuro2a (N2a) cells, a murine neuroblastoma cell line, and in HeLa cells, a human epithelial cell line, BIN1 knockdown resulted in the increase localization of BACE1 with EEA1-positive early endosomes in the perinuclear region. In addition, the interaction between BACE1 and BIN1 was proven by a GST pull-down assay, where the BIN1 BAR domain was essential for the interaction (Miyagawa et al., 2016). These results indicate a function of BIN1 in the regulation of the intracellular trafficking of BACE1. In point of fact, in previous work from our lab, BIN1 downregulation in mice primary cortical neurons increased intracellular $A\beta_{42}$, notedly in the axons. This was due to an increase in APP processing showed by the raise of APP-CTFs. Recycling of BACE1 to plasma membrane was demonstrated to be affected by its intracellular retention in BIN1-depleted neurons, and in N2a cells this phenotype was rescued by the expression of neuronal BIN1. Further, this retention was a result of the inhibition of the scission of tubular carriers required for BACE1 exit from early endosomes (Figure1.11) (Ubelmann, Burrinha, Salavessa et al., 2017).

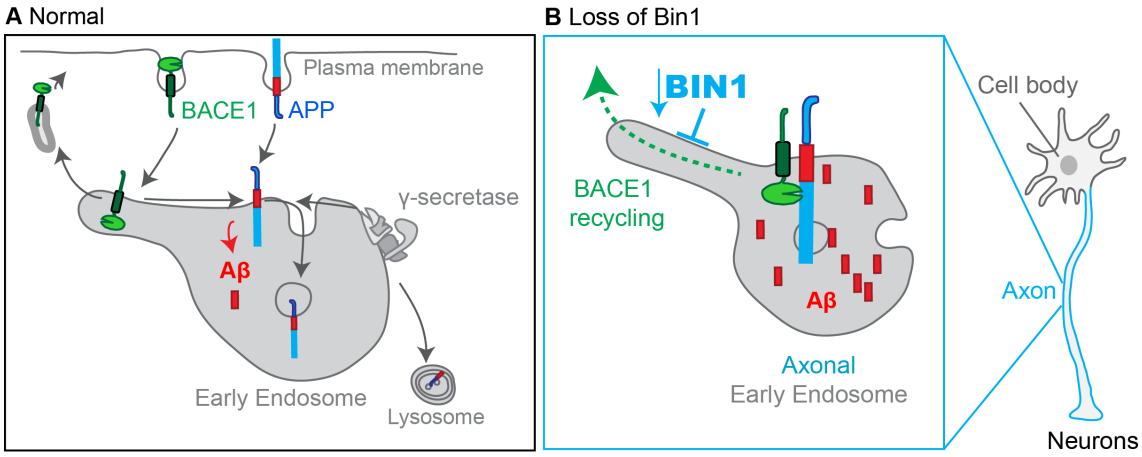

Figure 1.11: **Loss of BIN1 affects BACE1 exit from early endosomes.** A. In normal conditions, BIN1 is involved in tubule scission for BACE1 exit from early endosomes. This regulation leads to less BACE1 and APP encounter in the early endosomes and controls Aβ production. B. The loss of BIN1 in neurons inhibits tubule scission leading to BACE1 accumulation in axonal early endosomes increasing Aβ production. Adapted from Ublemann, Burrinha, Salavessa et al., 2017.

1.6 Aim of the current study

In the lab, previous work has been done to understand BIN1 role in sporadic AD cellular mechanisms, namely in Aβ production. In N2a cells and murine primary cortical neurons, intracellular $A\beta_{42}$ was found increased with BIN1 knockdown, and consistent with the observed increase in APP processing (Burrinha, 2014; Ubelmann, Burrinha, Salavessa et al., 2017).

To better understand the impact of BIN1 in sporadic AD, two rare coding variants, rs754834233 and rs138047593, identified by GWAS (M. S. Tan et al., 2014; Vardarajan et al., 2015), are now a major goal of research in the lab. The rs754834233 variant consists in a missense mutation that results in the exchange of a proline to a leucine (PL), p.Pro318Leu in the neuronal BIN1 isoform (NP_647593.1), whereas rs138047593 corresponds to a missense mutation of a lysine to an arginine (KR), p.Lys542Arg in the neuronal isoform (Figure 1.12). The PL mutation localizes to the proline-serine rich domain and the KR mutation to the RT loop of SH3 domain.

The rs754834233 (PL) variant in BIN1 was firstly found associated with LOAD in Han Chinese individuals. This rare coding variant (MAF in AD patients=0,01) was found more

frequently in LOAD patients than healthy controls ($p = 0,004$) and it was predicted in silico to be harmful for BIN1 protein structure and function (M. S. Tan et al., 2014). Indeed, this mutation is predicted to reduce BIN1 protein stability by the SDM server (Pandurangan et al., 2017) and to be deleterious for BIN1 function using the PredicSNP server (Bendl et al., 2014) and probably damaging using the PolyPhen-2 tool (Adzhubei et al., 2010). Although considered a conservative replacement, being both non-polar amino acids, the change of proline to leucine is predicted to alter BIN1 structure considering the involvement of prolines in the introduction of kinks, sharp twists, that result in tight turns in the protein structure (Barnes and Gray, 2003).

The rs138047593 (KR) variant in BIN1 was found significantly enriched in LOAD cases in the Caribbean Hispanic population compared with healthy controls (Vardarajan et al., 2015). Also, a conservative replacement between two positively charged amino acids, this variant is predicted to increase protein stability using the SDM server and to be possibly damaging using the PolyPhen-2 tool. Although lysines are frequently involved in protein binding sites, it only contains a single amino group, where arginines are able to form a greater number and more stable electrostatic interactions (Sokalingam et al., 2012). It is possible that this mutation, located in the SH3 domain, affects BIN1 interactions with other proteins but also favor BIN1 auto-inhibition regulated by the interaction of SH3 and CLAP domain. Moreover, ubiquitination occurs primarily on lysine residues of the target proteins (Piper et al., 2014), thus the substitution to arginine could lead to the disruption of BIN1 protein degradation. Indeed, since ubiquitin and PRDs-containing proteins compete for binding to SH3 domain (Stamenova et al., 2007), the KR mutation could favor interactions with proline-rich ligands rather than ubiquitin. Importantly, ubiquitination is an important step in clathrin-mediated endocytosis by serving as an internalization signal from the plasma membrane (Piper et al., 2014) and several endocytic proteins are able to bind ubiquitin, including amphiphysin I and BIN1 (Stamenova et al., 2007).

The aim of the current work was to, firstly, understand the molecular mechanisms by which BIN1 controls Aβ production and this was accomplished by investigating which BIN1 domains are pivotal for $A\beta_{42}$ production (1). Next, the involvement of BIN1 PL and KR variants in the development of sporadic Alzheimer's Disease was studied. In a previous master thesis (Marques, 2018) it was described that overexpression of BIN1 mutants increases $A\beta_{42}$ accumulation than BIN1 wild-type. Here, I aimed at confirming the involvement of these two BIN1 variants in AD pathology by assessing $A\beta_{42}$ production (2), in rescue experiments upon BIN1 knockdwon, and APP processing, by overexpression studies (3). In addition, considering the importance of early endosomes as a major site for Aβ production, alterations in their size and density by the impact of the two mutants in this pathway was investigated (4). Considering BIN1 involvement in the recycling of BACE1 from early endosomes to the plasma membrane, the impact of the two mutations in the interaction with BACE1 was assessed by co-immunoprecipitation (5). In addition to BACE1, BIN1 interactions with other relevant proteins may also be affected by the mutations, so I have initiated the protocol to identify the differential BIN1 wild-type and mutants interactome by mass spectrometry (6).

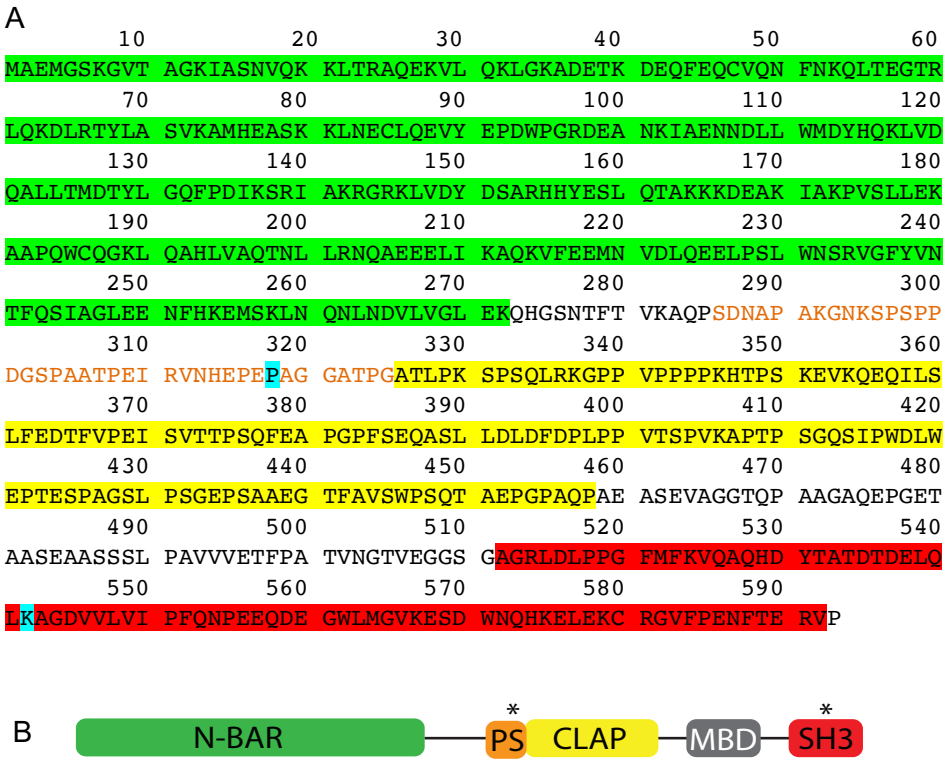

Figure 1.12: **Rare coding variants in Neuronal BIN1 isoform.** Amino-acid sequence of the neuronal BIN1 isoform with 593 aa residues (NP_647593.1, NCBI). p.Pro318Leu and p.Lys542Arg mutations (blue (A) or asterisks (B)) occur in the proline-serine rich domain (orange) and in the SH3 domain (red), respectively. N-BAR domain, green; CLAP domain, yellow.

Chapter 2

Materials and methods

2.1 Cell culture

Neuro-2a (N2a) is a *Mus musculus* brain neuroblastoma cell line established by R.J. Klebe and F.H. Ruddle (Klebe and Ruddle, 1969). N2a cells are derived from neural crest mouse cells, being neuroblast like, with neuronal and amoeboid stem cell morphology. These cells have the ability to suffer neuronal differentiation, and so, they have been used to study neuronal differentiation, neurite outgrowth, synaptogenesis, cytotoxicity, and signaling pathways (Salto et al., 2015, Tremblay et al., 2010). Human and mouse BIN1 coding sequences have 95% protein sequence homology (see Annex), allowing the study of BIN1 functions in mouse neuronal cells (Prokic et al., 2014).

N2a cells (ATCC® CCL-131™), gifted from Zsolt Lenkei (ESPCI-ParisTech), were cultured in Dulbecco's Modified Eagle Medium (DMEM) (DMEM, GlutaMAX™ Supplement, Gibco™, ThermoFisher Scientific) supplemented with 10% fetal bovine serum (FBS) (Fetal Bovine Serum, Research Grade, Sigma-Aldrich) (complete media), in a humidified incubator at 37°C and 5% CO_2. First, stored cells (1ml) were thawed quickly inside the water bath and diluted in 9ml of media. After centrifugation at 200x g, 5min at room temperature (RT), to remove Dimethyl sulfoxide (DMSO), a cryoprotectant agent, toxic at RT (Best, 2015), cells were resuspended in 5ml of media and plated in a T-flask (25 cm^2). To maintain cell culture, once the cells reached 90% confluence, the medium was discarded and the cells were rinse with phosphate buffered saline (PBS) (PBS pH 7.4, 1X, Gibco™, ThermoFisher Scientific) to remove all traces of serum that contains trypsin inhibitor. The cells were, then, trypsinized (1ml, T-25 cm^2 flask or 2ml, T-75 cm^2) (Trypsin-EDTA (0,25%), phenol red, Gibco™, ThermoFisher Scientific) for 2 min at 37°C in 5% CO_2 that inactivates adhesion molecules and integrins allowing the detachment of the cells (Kallas-Kivi et al., 2018). Trypsin activity was inhibited by addition of new complete media (total volume of 5ml (T-25) or 10ml (T-75)). Suspended cells were split in 1:5 every other day or 1:10 every two days or subsequently counted to plate for experiments (Table 2.1). For co-immunoprecipitations and mass spectrometry experiments, cells were split in 1:5 to a T-75 and allowed to reach 80-90% confluency before plating. To count cells, a Neubauer Chamber (Counting Chamber Neubauer 0.1mm no clamp, VWR, Marienfeld) was used and cells were diluted in Trypan blue (Trypan Blue Solution, 0.4%, Amresco®), a vital dye as it only penetrates non-viable cells (Strober, 2001). Number of cells per ml was determined by the mean number of viable cells counted in the 8 corner squares, and considering the dilution factor and conversion factor for neubauer, 10^4 (=1/ $volume_{corner\ square}$ = 1/ 1 mm^2 (surface area) x 0.1 mm (chamber depth) = 1/0.1 mm^3, or 10^4 ml) (Ausubel et al., 2003).

$$\text{Number of cells per ml} = \frac{number\ of\ viable\ cells}{Counted\ squares\ volume \times diluition\ factor} = \frac{number\ of\ viable\ cells}{squares\ counted} \times \frac{1}{diluition\ factor} \times 10^4$$

For immunofluorescence experiments, 30×10^3 N2a cells were plated per well, in 500 µL of complete media, of a 24-well plate in 13mm circular glass coverslips (VWR, Marienfeld), previously autoclaved, pre-washed with 40% ethanol/60% HCl (96% (v/v) pure Ethyl Alcohol 96, Manuel Viera & C[a] (Irmão) Sucrs, Lda; hydrochloride acid, 37%, Certified AR for Analysis, d=1.18, Fisher Scientific) 1 h at RT and washed 15 min 4 times with Milli-Q water at RT as described in Ubelmann, Burrinha, Almeida (2017). For immunoblotting experiments, 200×10^3 cells were plated per well in a 6-well plate and cultured with 1.5ml of compete media. In co-immunoprecipitations, 3.2×10^6 cells were plated in a 10 cm^2 dish or T-75 with 10 ml of compete media and for mass spectrometry twice the density was plated (Table 2.1). After 24 hours, the cell confluence reached about 80-90% and cells were treated with cDNA or small interfering RNA (siRNA), for overexpression and rescue studies.

To cryopreserve cells, media was removed by centrifugation 300x g, 5min, at RT, when the culture reached 75-80% confluence, and replaced by DMEM, 20% FBS and 10% DMSO. Cells were gradually stored at -20ºC, -80ºC and, finally, -150ºC.

Table 2.1: Plated cell density

Experiment	Method	Plates	Cell Density per well (x10^3)
Rescue	Immunofluorescence	24-well plate	30
Overexpression	Western Blot	6-well plate	200
	Co-immunoprecipitation	10 cm^2 or T-75	3200
	Mass spectrometry	10 cm^2 or T-75	6400

2.2 cDNA and siRNA transfection

Plasmid DNA preparation

For DNA amplification, DH5α competent E. coli cells (Invitrogen™) were transformed with the necessary DNA plasmids. DNA (0.5 µg) was added to 50 µl of slowly thawed bacteria cells and incubated 30 minutes on ice. Transformation was carried out by heat shock at 42°C for 45 seconds, which alters membrane fluidity creating pores in the plasma membrane from which the DNA plasmid can enter (Rahimzadeh et al., 2016). Incubation in ice 2 min allows the reclosing of the pores. Cells were put to growth in LB (Luria-Bertani) medium (LB Broth, Miller, Fisher BioReagents™, ThermoFisher Scientific), 1h at 37°C at 225 rpm in an orbital shaker. The medium with bacteria was spread on two 10cm LB agar (LB agar, NZYTech) plates containing the appropriate antibodies. Depending on the antibiotic resistance of the plasmid used, 100 µg/ml of ampicillin or Kanamycin (Ampicilin (sodium salt); Kanamycin (monosulphate), NZYTech) were added. Plates were incubated 16h at 37°C.

Using a sterile pipette tip, a single colony of transformed bacteria grown in LB agar plate, or from a glycerol stock, was selected and put to grow in 50ml of LB medium with the appropriate antibody added beforehand (100 µg/ml). Bacterial culture was incubated at 37°C, 16h, with 225 rpm. After incubation, the growth of bacteria cells was confirmed by the presence of a cloudy haze in the media. DNA purification was preformed using the NZYTech NZYMidiprep/NZYMiniprep kit, following the NZYTech protocol. It is based on the alkaline lysis of bacterial cells followed by

selective adsorption of DNA onto silica-based anion-exchange resin in the presence of high salt. Elution of pure DNA is carried out by a pH and ionic strength increase. After precipitation, DNA was eluted in elution buffer (Buffer EB, Qiagen) and its concentration was determined using the NanoDrop 2000 spectrophotometer (ThermoFisher Scientific™) and absorbance at 260 nm (A_{260}). DNA purity was assessed by A_{260}/A_{230} ratio and A_{260}/A_{280} ratio (Ausubel et al., 2003). For long-term storage of plasmids, a glycerol stock can be created from the grown bacterial culture, by adding equal volume of bacteria to 50% glycerol (Glycerol for molecular biology, Sigma-Aldrich), a cryoprotectant agent (Day and Stacey, 2007) and stored at -80°C.

Transient DNA transfection

For expression of cDNA, N2a cells were transiently transfected with 0.5 µg of cDNA for 24-well with Lipofectamine 2000 (Lipofectamine™ 2000 Transfection Reagent, Invitrogen™, ThermoFisher Scientific). First, DNA and Lipofectamine 2000 were diluted, separately, in 12.5 µl of Opti-MEM medium (Opti-MEM™ |Reduced Serium Medium, Gibco™, ThermoFisher Scientific). For 6-well plate, T-75 and 10cm^2 dish volumes used were proportional to surface area.

After 5min of incubation at room temperature (RT), the DNA mix was added to the diluted Lipofectamine (1:1 ratio) and incubated for 20min. The final DNA-lipid complex was added to the plated cells. This method uses the positive surface charge of the liposomes to mediate the interaction between the nuclei acid and the cell membrane, allowing endocytosis of the DNA-lipid complex. Cells were incubated at 37°C and 5% CO2 and analyzed 24h after treatment.

Cells were transfected with the following cDNA: Neuronal (brain amphiphysin II (BRAMP2); isoform 1; NP_033798.1) and ubiquitous (isoform 2; NP_001076803.1) mouse amphiphysin II constructs in the expressing vector pRK5-myc (from C. Leprince, University of Toulouse) and with five silent mutations introduced by site-directed mutagenesis in the siRNA target sequence (primers: 5'CCGGCTGCAGAAGGACCTCCGGACGTACCTTGCTTCTGTTA AAGCG3' and 5'CGCTTTAACAGAAGCAAGGTACGTCCGGAGGTCCTTCTGCAGCCGG3') that give resistance to siRNA; empty vector pCS2 with Myc was a gift from A. Gautreau (LEBS, Gif-sur-Yvette, France); mouse brain amphiphysin II P318L mutant (rs754834233) and K542R mutant (rs138047593) generated by site-directed mutagenesis from pRK5-myc-BRAMP2-5M; C-terminal domain of BRAMP2 deleted for its BAR domain, SH3 domain of BRAMP2 and BIN1 ubiquitous isoform deleted for its SH3 domain generated from pRK5-myc-BRAMP2-5M. BACE1-GFP was a gift from S. Miserey-Lenkei (Institut Curie); Rab5-GFP was a gift from M. Arpin (Institut Curie).

siRNA transfection

For small interfering RNA (siRNA) treatment, N2a cells plated in 24-well plates were transiently transfected with 5pmole of specific siRNA for BIN1 (BIN1 siRNA, ID 65598, Ambion™, ThermoFisher Scientific) or a non-targeting control siRNA (5' UUC UCC GAA CGU GUC ACG UTT ACG UGA CAC GUU CGG AGA ATT 3') (GeneCust) with Lipofectamine RNAiMax (Lipofectamine™ RNAiMAX Transfection Reagent, Invitrogen™, ThermoFisher Scientific). Similarly, to DNA transfection, siRNA and Lipofectamine RNAiMax (0,8 µl) were diluted, separately, in 25 µl of Opti-MEM medium (Opti-MEM™ |Reduced Serium Medium, Gibco™, ThermoFisher Scientific). After 5min of incubation at RT, the siRNA mix was added to the diluted Lipofectamine (1:1 ratio) and incubated for 20min. The cell culture media was removed to add 450 µl of complete media and the final siRNA-lipid complex was added to the plated cells. For rescue experiments, 48h after siRNA treatment, cDNA was transfected as described above. Cells were analyzed after 24h of DNA transfection.

2.3 Immunofluorescence labelling

For immunofluorescence labelling, N2a cells were washed 2x in PBS: 137 mM NaCl (Sodium Chloride for analysis, PanReac), 10 mM Na_2HPO_4 (Sodium phosphate dibasic, Sigma-Aldrich), 1.8 mM KH_2PO_4 (Potassium Dihydrogen Orthophosphate, Certified AR for Analysis, Fisher Chemical, Fisher Scientific), 2.7 mM KCl (Potassium chloride for analysis, PanReac), pH 7.4, and fixed with 4% (v/v) paraformaldehyde (paraformaldehyde, reagent grade, crystiline, Sigma-Aldrich) in PBS for 20 min at RT. Cells were then washed 2x in PBS and permeabilized and blocked in 0,1% Saponin (Saponin for molecular biology, Sigma-Aldrich), 1% bovine serum albumin (BSA) (Albumine bovine fraction V, NZYTech) and 2% FBS (blocking buffer) in PBS for 1 h at RT.

Immunofluorescence labelling was achieved by the use of primary antibodies against overexpressed proteins and secondary antibodies conjugated with Alexa Fluor dyes. Cells were incubated 1 h at RT with primary antibodies diluted in blocking buffer, washed 2x in PBS and incubated 1h, in the dark, with the secondary antibodies (Table 2.2). For each incubation, a humid chamber was prepared by overlaying, in a flat lid, wet paper and parafilm. In this chamber, the coverslips were overlaid onto a 25 µl drop of the diluted antibodies (cells facing the antibody solution) and covered to avoid evaporation. After incubation with the secondary antibodies, coverslips were mounted in an 8 µl drop of Fluoromount-G (Southern Biotech) in glass slides (Microscope Slides, Cut, SuperFrost™, Fisher Scientific).

Table 2.2: Immunofluorescence and Immunoblotting labeling

Antibodies	Raised In	Recognizes	IF dilution	WB dilution	Supplier
Primary Antibodies					
$A\beta_{42}$ (H31L21)	Rabbit	Mouse, Human, Rat	1: 150	-	ThermoFisher Scientific
Anti-APP (Y188)	Rabbit	Mouse, Human	-	1:1000	Genetex
Anti-c-Myc (9E10)	Mouse	Mouse, Human, etc	1:500	1:2500	ThermoFisher Scientific
Anti-Bace1 (PA1-757)	Rabbit	Human, Mouse			ThermoFisher Scientific
Anti-GFP	Rabbit	Mouse, Human	-	1:2500	M. Arpin
Anti-α-Tubulin (clone B-5-1-2, ascites fluid)	Mouse	Mouse, Human, etc	-	1:10 000	Sigma-Aldrich
IgG isotype control	Rabbit	-	-	-	GeneTex
Secondary Antibodies					
Anti-Rabbit IgG (H+L), Alexa Fluor™ 647	Chicken	Rabbit	1:250	-	ThermoFisher Scientific
Anti-Mouse IgG (H+L), Alexa Fluor™ 555	Goat	Mouse	1:250	-	ThermoFisher Scientific
Anti-Mouse IgG (H+L), Alexa Fluor™ 555	Donkey	Mouse	1:250	-	ThermoFisher Scientific
Anti-Mouse IgG (H+L), Alexa Fluor™ 488	Donkey	Mouse	1:250	-	ThermoFisher Scientific
Anti-Mouse IgG (H+L) HRP conjugate	Goat	Mouse	-	1:5000	Bio-Rad
Anti-Rabbit IgG (H+L) HRP conjugate	Goat	Rabbit	-	1:5000	Bio-Rad
Probes					
DAPI (for nucleic acid staining)	-	-	1:100	-	Sigma-Aldrich
Alexa Fluor™ 488/ 555/ 647 Phalloidin	-	-	1:250	-	ThermoFisher Scientific

Image acquisition

Immunofluorescence was examined on a widefield upright microscope Axio Imager.Z2 (Zeiss, Oberkochen, Germany), equipped with an AxioCam 506 mono camera (Zeiss), using the 63x 1.4 numerical aperture (NA) oil immersion plan-Apochromat objective and using the Zen Pro 2012 software. For direct comparison, samples were imaged using identical acquisition parameters.

Quantitative analysis

Image analyses were carried out using Icy (http://icy.bioimageanalysis.org). For fluorescence $A\beta_{42}$ intensity quantification (Figure 2.1 A-D), the cell boundary, based on Myc, was outlined (region of interest, ROI) by using the "polygon" tool in 2D ROI menu (Figure 2.1 A-B). A small region of the background was selected using the "rectangle" tool in the same menu (Figure 2.1 C) and was used for background fluorescence subtraction. The Mean $A\beta_{42}$ fluorescence per region was calculated as percentage of the indicated control. For Rab5 puncta analysis, quantification of the number and size of Rab5–positive endosomes was done using the "Spot Detector" in the detection menu (Figure 2.1 E-K). After the cell was outlined (Figure 2.1 E), Rab5-positive endosomes were selected using "Spot Detector" (Figure 2.1 F-H). In "Spot Detector" settings, the Rab5 channel was selected (Figure 2.1 I) and the same scale (scale 2; 3 pixels) was chosen and used throughout all conditions, as well as, the sensitivity, chosen to detect the largest number of true endosomes (Figure 2.1 J). Area in pixel was converted in μm^2 considering the objective (63x) and the CCD camera resolution pixel size of 0.072 x 0,072 μm^2.

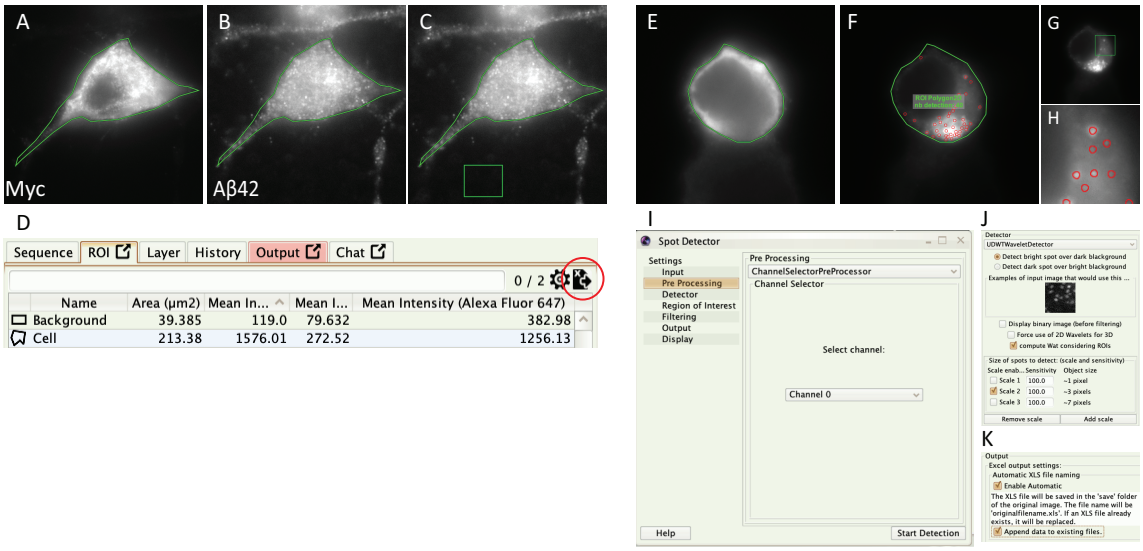

Figure 2.1: **Immunoflourescence quantitive analysis.** A-D. $A\beta_{42}$ mean intensity fluorescence quantification. A,B. The cell boundary was outlined using the "polygon" tool in 2D ROI menu, creating the region of interest, ROI. C. A region of the background was selected using the "rectangle" tool in the same menu, and was used for background fluorescence subtraction. D. Mean intensities of ROIs selected were exported to an excel file (red circle). E-K. Rab5 puncta analysis. E. Cell boundary was outlined. F-H. Using the "Spot Detector" in the detection menu, Rab5 positive endosomes were selected. I-K. "Spot Detector" settings. Channel of Rab5 was selected (I; "Pre Processing"), then scale and sensitivity were chosen to detect the largest number of true endosomes (J; "Detector") and finally results were exported to an excel file (K; "Output").

2.4 Immunoblotting

For protein quantification, immunoblotting can be performed. N2a cell lysates were prepared using a modified Radio-Immunoprecipitation Assay (RIPA) lysis buffer, 50 mM Tris-HCL pH 7.4 (Tris base, NZYTech), 150 mM NaCl, 1% NP-40 (Igepal CA-630, Sigma-Aldrich), 0.25% sodium deoxycholate (DOC) (≥97.0%, Sigma-Aldrich), 1mM EGTA (for molecular biology, ≥97.0%, Sigma-Aldrich), 0,1%-1% SDS (Sodium Dodecyl Sulfate, White Powder, Eletrophoresis, Fisher Scientific) and Protease Inhibitor Cocktail (PIC) 1X (stock 25X) (cOmplete, EDTA-free Protease Inhibitor Cocktail, Sigma-Aldrich) added fresh. On ice, cell culture media was removed, and cells were washed once with ice-cold PBS. After 5 min of incubation with lysis buffer (100 µl), cells were scraped off using a plastic cell scraper and, then, the cell suspension was gently transferred into a pre-cooled tube and stayed on ice for 15 min. Cell suspension was centrifuged 17 000x g, 15min, 4°C. Supernatants were stored at -80°C for posterior western blot assay.

Sonication was performed with the settings: 3 cycles of 1s on and 45ms off (pulse; total time of 30s) at 10% amplitude (SFX 150 Sonifier, Branson). To the cell lysates, 4X LDS Sample buffer (4X Bolt™ LDS Sample Buffer, Invitrogen™, Novex™, ThermoFisher Scientific) was added to the final concentration of 1X and final volume 20 µl, followed by incubation 5 min at 95°C and high-speed centrifugation. Proteins were separated by Tris-Glycine SDS-polyacrylamide gel eletrophoresis (SDS-PAGE). Electrophoresis was carried out on 10% acrylamide gels, for BIN1-Myc detection, and 15% or 4-12% gels (Bolt™ 4-12% Bis-Tris Plus Gels, Invitrogen™, ThermoFisher Scientific), for APP processing analysis (Table 2.3). SDS-PAGE was done at 100-120V for, approximately, 1h, using the Mini-PROTEAN Tetra cell (BioRad), with 25 mM Tris base; 192 mM Glycine (NZYTech); 0.1% SDS or with Blot™ MES SDS Running buffer ((20X) Blot™ MES SDS Running buffer, Invitrogen™, ThermoFisher Scientific) for 4-12% gels. The protein marker PageRuler™ Plus (PageRuler™ Plus Prestained 10-250kDa Protein Ladder, ThermoFisher Scientific) or Precision Plus Protein™ (Precision Plus Protein™ Unstained Standards, BioRad) were used.

Proteins separated were transferred to 0.45 µm nitrocellulose membranes (8.5×6 cm) (Amersham Protran 0.45 NC membranes, GE Healthcare), using the transfer system XCELL II™ Blot Module at 40V or Mini Blot Module at 10V (Invitrogen™, ThermoFisher Scientific), for 1h with 20 mM Tris base, 150 mM Glycine (NZYTech), 0.04% SDS and 20% (v/v) ethanol or for 4-12% gels, with Blot™ Transfer buffer (Blot™ Transfer buffer (20X), Invitrogen™, ThermoFisher Scientific).

Ponceau S solution (0,5% Ponceau S (Ponceau S for electrophoresis, Merck), 1% HoAC (Acetic glacial, 100%, anhydrous for analysis, Merck) was used to control protein transfer by detecting all proteins (Ausubel et al., 2003). After washing the dye, the membrane was block in 5% dry milk (Dry light milk, Molico, Nestlé) in PBS-T (PBS with 0,01% of Tween 20 (Tween 20 for synthesis, Sigma-Aldrich)) for 1h at RT. Primary antibodies (Table 2.2) diluted in 1% dry milk in PBS-T were incubated for 1h at RT or 16h at 4°C with constant agitation. Membranes were washed 4 times 5 min in PBS-T, before incubation with secondary antibodies, conjugated with Horseradish peroxidase (HRP), in 1% dry milk in PBS-T 1h at RT with agitation. Membranes were washed again, 4x 5 min, with PBS-T and processed using ECL (enhanced chemiluminescence) Prime kit (Amersham ECL Prime Detenction Reagent, GE Healthcare), consisting in a luminol solution and a peroxide solution (1:1). Detection of proteins is possible by the use of luminol, that when oxidized by HRP using hydrogen peroxide as the oxidizing agent, produces chemiluminescence (Burtis and Bruns, 2015). Images of immunoblots were captured using ChemiDoc imager (BioRad) within the linear range.

Table 2.3: SDS-PAGE Gels recipe

	Stacking gel	Resolving gel	
	6% Acrylamide (2ml)	10% Acrylamide (5ml)	15% Acrylamide (5ml)
dH_20	2.54 ml	2.40 ml	1.8 ml
Tris 1.5M pH 8.8	-	1.25 ml	1.25 ml
Tris 0.5M pH 6.8	1 ml	-	-
Acrylamide-Bis[1]	500	1.25	1.875 ml
SDS 10%	40	50	50
APS[2] 10%	40	50	50
TEMED[3]	4	4	4

[1] Acrylamide/Bis-acrylamide (29:1 solution), NZYTech
[2] Ammonium Persulphate (APS), NZYTech
[3] N, N, N′, N′-tetramethylethylenediamine, TEMED, NZYTech

Quantification of densitometry was done using ImageJ (https://imagej.nih.gov/ij/). First, images were inverted (Edit – invert) and, then, gel lanes were outlined by a vertical rectangular selection (ctrl+1 or Analyze – Gels – Select First Lane) that includes full-length APP and APP-CTFs in APP processing analysis. For the following lanes a selection with the same size was used (ctrl+2) and lane profile plots were generated (ctrl+3). After drawing lines to enclose peaks of interest, the area of these peaks was measure using the "Wand Tool". Housekeeping protein, α-Tubulin was used as a loading control to normalize the amount of the protein of interest. In APP processing analysis, APP-CTFs were normalized with APP full-length.

2.5 Co-immunoprecipitation (co-IP)

On ice, N2a cells were washed once with ice-cold PBS and incubated 5min with 600 µl of modified RIPA lysis buffer. Cells were scrap off and diluted until 2ml of lysis buffer. The resulted cell suspension was rotated 30 min at 4°C. After, cell suspension was centrifuged 10.000xg, 10min, 4°C. Supernatants were stored at -80°C for posterior immunoprecipitation (IP), illustrated in Figure 2.2.

Before capturing the bait protein with 2 µg of antibody, 16h at 4°C in a rotator, 30 µl of supernatant was saved for immunoblot analysis (input). As a negative control, half of the supernatant was incubated with 2 µg of a non-specific IgG antibody or cells without overexpression of bait or target proteins were used. Protein G-coupled Sepharose beads (Protein G Sepharose 4 Fast Flow, GE Healtcare) in PBS (50:50), previously washed 3x with PBS, were added (30 µl) to the lysate-antibody mix and incubated at 4°C in a rotator for 2h30. After, the mix was centrifuged 1 min, 100x g at 4°C and supernatant saved for immunoblot analysis (flow-through). Beads were washed 3x by adding 100 µl of lysis buffer A with 1% glycerol, mixing gently and centrifuging 1 min, 100x g at 4°C (3min in last wash). Beads were dried with a syringe before adding 26 µl of 2x LDS sample buffer. To elute immunoprecipitated proteins, the mix was boiled 5min at 95°C. SDS-PAGE was performed with the supernatant (7,5% acrylamide gels), and posterior immunoblotted against tags fused in bait and target proteins. Input and flow-trough were prepared for SDS-PAGE as indicated in "Immunoblotting" section.

When Myc-traps® (Myc-Trap® Agarose, Chromotek) were applied, the suggested protocol by Chromotek was followed. N2a cells were scrap off with 1 ml of ice-cold PBS and centrifuged at 500x g, 3 min at 4°C. Cell pellet was resuspended in 200 µl of the lysis buffer, 10 mM Tris-Cl pH 7.5, 150 mM NaCl, 0.5 mM EDTA (disodium salt dihydrate, 99.0-101.0%, VWR Chemicals), 0.5% NP-40 and PIC (1X) added fresh. This mild lysis buffer is probably least likely to interfere with protein-protein interactions. After being rotated for 30 min at 4°C, cell lysate was centrifuged at 20 000x g for 10 min, 4°C. Cell lysates were diluted with 300 µl of 10 mM Tris-Cl pH 7.5, 150 mM

NaCl, 0.5 mM EDTA (dilution buffer) and an aliquot was saved for immunoblotting analysis (input). Diluted lysates were added to the beads (20 µl), prepared by pipetting the necessary volume of the bead slurry after vortex, into 500 µl of dilution buffer with 1% glycerol, and centrifuged at 2 500x g, 2 min, 4°C. After discarding the supernatant, the beads were resuspended again and the washing was repeated two more times. Lysates-beads mix were rotated for 1h, as recommended, or 16h, 4°C. Next, the mix was centrifuged at 2 500x g, 2 min, 4°C and supernatant was saved (flow-through). Beads were resuspended in 500 µl of dilution buffer with 1% glycerol and washed 3x by centrifugation at 2.500x g for 2 min, 4°C. Beads were dried with a syringe before adding 27 µl of 2x LDS sample buffer. To elute immunoprecipitated proteins, the mix was boiled 5-10 min at 95°C. SDS-PAGE was carried out in 7.5% acrylamide gels. For immunoblotting against bait protein, 5 µl of supernatant was used and against target protein 20 µl was used (74% of final volume).

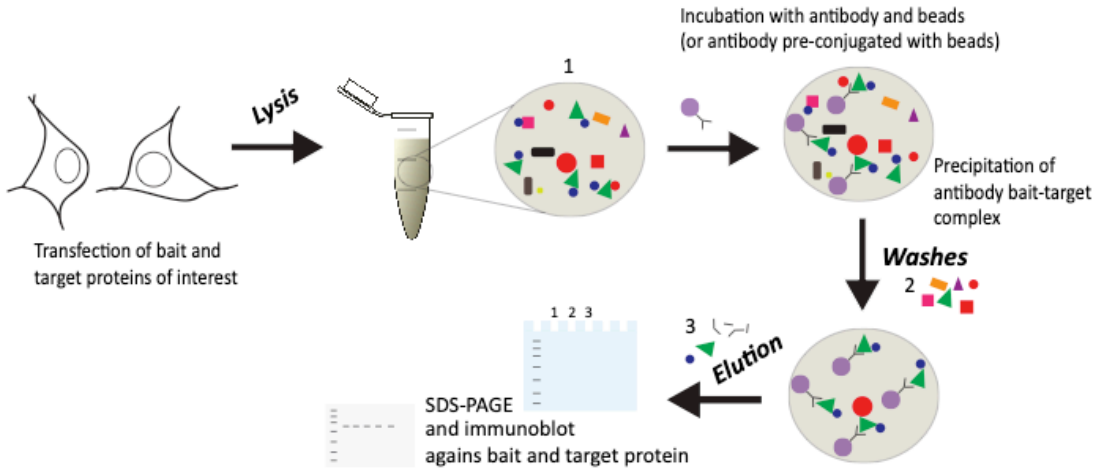

Figure 2.2: **Co-immunoprecipitation assay.** N2a cells transfected with bait and target proteins of interest, were lysed with modified RIPA lysis buffer. An aliquot of the total cell lysate (1) was saved and bait protein was captured by the incubation with antibody followed by beads or antibody pre-conjugated with beads. Non-bound proteins were washed (2) and immunoprecipitated proteins (3) were eluted. Fractions 1, 2 and 3 were analysed by SDS-PAGE and immunoblot against bait and target proteins.

2.6 IP-mass spectrometry sample preparation

Coomassie staining was used to check the total pool of proteins co-immunoprecipitated using Myc-traps® and N2a cells only overexpressing the bait protein fused with Myc. At RT with constant agitation, SDS-PAGE gels were pre-fixed 30 min in 50% MeOH (Methanol, HPLC grade, Fisher scientific), 10% HoAC, 40% H_20. Next, the gels were stained with 0.25% Coomassie Blue R-250 in the same solution for 1 h and destained in 5% MeOH, 7.5% HoAC, 87.5% H_20 until background was clear.

The CO-IP protocol was scaled up to perform mass spectrometry, as well as, quick confirmation by Coomassie staining after SDS-PAGE. Sodium orthovanadate Na_3VO_4 (gift from D. C. Barral, CEDOC), a phosphatase inhibitor, was added (1 µM) to the lysis buffer in two of three experiments done. Elution of co-immunoprecipitated proteins was done by glycine elution. Proteins are eluted by acidification that weakens the interaction between antibody and bound proteins. In this case, the beads were resuspended, after being dried, in 65 µl of 100 mM Glycine-HCl pH 2.8 and incubated 1 min with 14000 rpm in RT. Supernatant was saved (eluate 1) and elution was repeated to increase elution efficiency (eluate 2). Eluates were neutralized with equal

volume of NaOH and pH was checked with pH strips (pH Indicator Strips, 0-14 pH, Machery-Nagel). Before, 74% of eluted proteins were used for immunoblotting analysis against target protein, as such the same proportion was used. Half of the 74% was used in SDS-PAGE and the other half was stored at -80°C for mass spectrometry. For SDS-PAGE, 6X sample buffer was used before boiling 5 min at 95°C.

Mass spectrometry, a technique that measures the ratio between mass and charge of ionized molecules, will be performed it the eluted proteins. This method can extract the elemental composition of a sample and can be applied to proteomics by protein identification and quantification. After vaporization of solid or liquid samples, the ion source generates ions that are separated according to their mass-to-charge, m/z, ratio in the mass analyzer (Matthiesen and Bunkenborg, 2013). Electrospray Ionization (ESI) and Matrix-Assisted Laser Desorption-Ionization (MALDI) are two commonly used ionization methods applied in proteomics (Matthiesen and Mutenda, 2007). In the mass analyzer, several approaches can also be used. The output is a mass spectrum, intensities/abundance as a function of m/z values. Molecules can, then, be identified using a database of mass spectrums (Matthiesen and Bunkenborg, 2013).

The LC-MS/MS, liquid chromatography-tandem mass spectrometry, method will be implemented to allow the prior sample separation by reverse phase liquid chromatography and analysis by tandem mass spectrometry. In tandem MS, after ionization by nanoeletrospray, a form of ESI, a first mass analyzer, the Quadrupole mass filter, will separate the ions, called precursor ions, and these isolated ions are fragmented again by High Energy Collision Dissociation (HCD) (Michalski et al., 2011). In a second mass analyzer, the Orbitrap, m/z values are measured by the frequency of the oscillation of the trapped product ions along an electric field that is transformed to m/z values by Fourier Transformation (Hu et al., 2005; Michalski et al., 2011). Using this method, the identification of proteins in complex mixtures can be achieved (Michalski et al., 2011).

2.7 Statistics

Graphs were generated using GraphPad Prism 7 (https://www.graphpad.com). Data were expressed as mean ± SEM (standard error of mean). Statistical analysis was conducted with at least three independent experiments. Data was tested with D'Agostino-Pearson omnibus normality test. For parametric and unpaired data, two-tailed Student's t-test was used and for multiple comparisons, one-way ANOVA with Tukey's test was applied. For non-parametric and unpaired data, Mann-Whitney test was used or, for multiple comparison, Kruskal-Wallis test, followed by Dunn's multiple comparison test, was performed.

Chapter 3

Results

3.1 Intracellular Aβ accumulation

3.1.1 BIN1 domains contribution to Aβ accumulation

It is currently understood that trafficking events in the secretory and endocytic pathways regulate Aβ production and accumulation (J. Z. Tan and Gleeson, 2018), thought to be the initial trigger of the disease (Tampellini and Gouras, 2010). Several regulators of trafficking have been identified as putative risk factors of LOAD, being variants in BIN1 found the most frequent in LOAD. Previously, in the lab, it was observed that loss of BIN1 increases $A\beta_{42}$ levels in N2a cells and murine primary neurons (Burrinha, 2014; Marques, 2018; Ubelmann, Burrinha, Salavessa et al., 2017). BIN1 has, also, been implicated in intracellular endosome trafficking, specifically clathrin-mediated endocytosis, through membrane remodeling and ability to interact with endocytic and cytoskeleton proteins (reviwed by Prokic et al., 2014). To further uncover the mechanism involved in $A\beta_{42}$ accumulation, the contribution of each BIN1 domain was investigated in N2a cells. Specifically, I focused on BIN1 BAR, CLAP and SH3 domains due to their involvement in the intracellular trafficking, such as clathrin-mediated endocytosis. Indeed, the neuronal isoform CLAP domain mediates the interaction with the endocytic proteins clathrin and AP2 (Ramjaun and McPherson, 1998), the BAR and SH3 domain interact with dynamin (Ellis et al., 2012; Owen et al., 1998), and the SH3 domain, also, intracts with synaptojanin (Ramjaun et al., 1997).

With this aim, a rescue experiment upon BIN1 loss of function mediated by siRNA treatment of N2a cells was performed. RNA interference, RNAi, is a biological process in which RNA molecules inhibit protein synthesis by targeting mRNA molecules with small and specific interfering RNA, siRNA (Valencia-Sanchez et al., 2006). By using siRNA, BIN1 gene expression can be silenced or knockdown (KD) making it possible to study the rescue of BIN1 loss effects by different BIN1 domains. N2a cells were, first, treated with non-targeting siRNA, siControl cells, or siRNA specific against exon 3, commun to all isoforms of BIN1, siBIN1 cells. After 48h, cells were subsequently transiently transfected with plasmids enconding BIN1 full-length or the indicated domains described in Figure 3.1 O. After 24h of cDNA transfection, cells were fixed and immunostained against the Myc tag present in all transfected constructs and against $A\beta_{42}$ (Figure 3.2).

Myc immunostaining was found uniformly distributed in N2a cells (Figure 3.1 A-G), as seen before (Burrinha, 2014), and a characteristic punctate pattern of $A\beta_{42}$ immunofluorescence

was observed as previously (Almeida et al., 2006) (Figure 3.1 H-N). BIN1 knockdown expression by siRNA treatment was confirmed before in the lab (Ubelmann, Burrinha, Salavessa et al., 2017) by western blot for endogenous BIN1.

The mean $A\beta_{42}$ fluorescence was found increased in BIN1 knockdown cells by 65% in in comparison to control cells, as previously seen (Burrinha, 2004; Marques, 2018; Ubelmann, Burrinha, Salavessa et al., 2017) (Figure 3.1 Q). Choosing cells with similar re-expression levels (Figure 3.1 P), endogenous $A\beta_{42}$ levels were found to be decreased by re-expression of neuronal BIN1 isoform, nBIN1, as previously by Ubelmann, Burrinha, Salavessa et al. (2017), with a 75% decrease relative to siBIN1 treated cells and no significant difference relative to siControl treated cells. In contrast, the ubiquitous isoform, uBIN1, does not completely rescue the increase of intracellular $A\beta_{42}$, with a lower decrease, only 31%, in $A\beta_{42}$ levels. In Ubelmann, Burrinha, Salavessa et al. (2017), re-expression of the ubiquitous isoform was shown to not rescue the increase of $A\beta_{42}$ levels, so this validates that the neuronal BIN1 isoform is the most important in the control of Aβ accumulation. Ubiquitous isoform overexpression might have partially accounted for neuronal isoform function that resulted in a partial rescue of Aβ accumulation.

Interestingly, SH3 domain alone, as well as, neuronal isoform without BAR domain, nΔBAR, did not rescue $A\beta_{42}$ levels, with an 70% and 81% increase, respectively, similar to siBIN1 when compared to control cells. This data indicates that the BAR domain is necessary to control $A\beta_{42}$ levels. Indeed, expression of BAR domain of ubiquitous isoform, uΔSH3, rescues $A\beta_{42}$ levels similar to full-length neuronal isoform, inducing a mere 19% increase $A\beta_{42}$ levels in comparison to control cells. So, the BAR domain is necessary and sufficient to control $A\beta_{42}$ levels. Next, we will test the neuronal isofom BAR domain, which is nearly identical to ubiquitous isoform, when we prepare the plasmid. In addition, endogenous and overexpression levels could be compared by immunoblot against BIN1, in siControl cells, and Myc in the conditions with BIN1 re-expression.

The presence of the SH3 domain represents the only difference between uBIN1 and uΔSH3 and indicates that SH3 domain is involved in the resulted Aβ accumulation. As explained before, overexpression might have accounted for the partial neuronal isoform function, however this isoform does not appear to be regulated by an intramolecular interaction involving the SH3 domain, in contrast to neuronal isoform, by CLAP and SH3 intramolecular interaction (Malki et al., 2017). Like so, the SH3 domain of the ubiquitous isoform, equal to the neuronal isoform, would interact with dynamin and prevent its self-assembly (Owen et al., 1998), that in the neuronal isoform, however, is regulated by CLAP and SH3 interaction. Similarly, the ubiquitous BAR domain overexpression might have led to partial neuronal isoform function, but in absence of the SH3 domain it would not prevent dynamin self-assembly. This, probably, leads to greater BACE1 recycling to the plasma membrane and the restored Aβ levels observed.

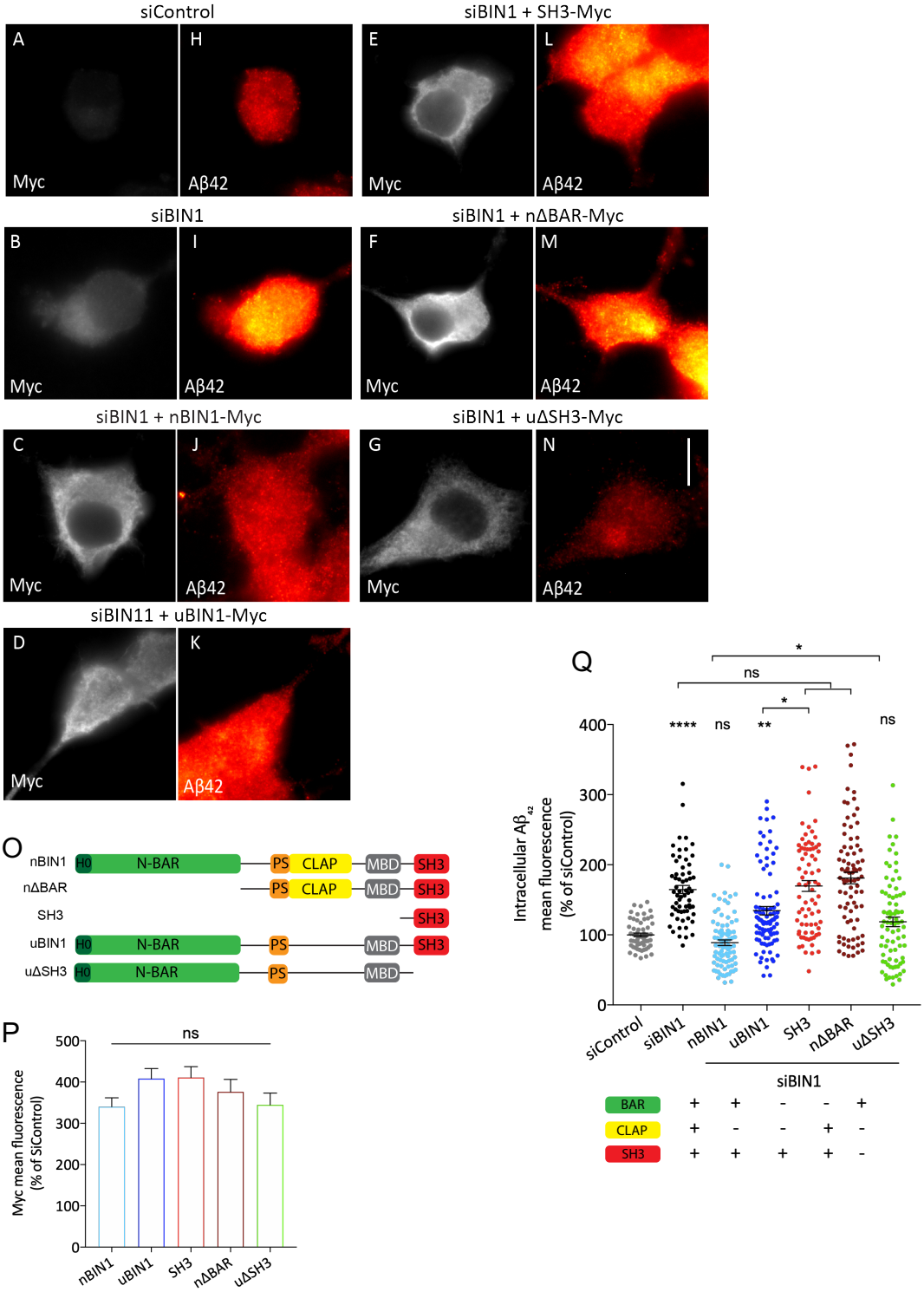

Figure 3.1: **BAR domain is sufficient to rescue Aβ production.** A-N. Representative images of N2a cells after BIN1 knockdown by siRNA treatment followed by transient transfection of mouse neuronal BIN1 isoform (nBIN1-Myc), ubiquitous BIN1 (uBIN1-Myc), BIN1 SH3 domain (SH3-Myc), neuronal BIN1 C-terminal (nΔBAR-Myc) and ubiquitous without SH3 domain (uΔSH3-Myc). Cells were immunostained for Myc (A-G) and for $A\beta_{42}$ (H-N). Bar=10 µm. O. Illustration of BIN1 constructs used. P. Myc mean fluorescence intensity, shown as percentage of Myc fluorescence in non-targeting siRNA cells (siControl; not shown). ns. p>0.9999, ns. p=0.5700 uBIN1 vs. uΔSH3, ns. p=0.2415 SH3 vs. uΔSH3, Kruskal-Wallis test. Q. Quantification of intracellular $A\beta_{42}$ mean fluorescence intensity. The presence or absence of each BIN1 domain is described. Results are shown as percentage of $A\beta_{42}$ mean fluorescence in siControl cells. ****p<0.0001 vs. siControl, **p=0.0082 vs. siControl, ns. p>0.9999 vs. siControl, ns. p>0.9999 siBIN1 vs. SH3, nΔBAR, *p=0.0307 uBIN1 vs. SH3, *p=0.0115 nBIN1-Myc vs. uΔSH3, Kruskal-Wallis test. P, Q. $N_{SiControl}$ =59, N_{siBIN1} =63, N_{nBIN1} =86, N_{uBIN1} =94, N_{SH3} =77, $N_{n\Delta BAR}$ =84 and $N_{u\Delta SH3}$ =81, n=2. Data is expressed as mean±SEM; ns, not significant.

3.1.2 Impact of BIN1 variants in Aβ accumulation

Two rare coding variants in BIN1, rs754834233 (PL) and rs138047593 (KR), were found significantly enriched in LOAD cases by Genome Wide Association Studies. Accordingly, to better understand the impact of BIN1 in sporadic Alzheimer these two variants have been investigated (Marques, 2018). The PL mutation localizes to the proline-serine rich domain and the KR mutation to the RT loop of SH3 domain, and both mutants are predicted to be harmful for BIN1 protein structure and function (M. S. Tan et al., 2014; Vardarajan et al., 2015).

Thus, using the same strategy as in 3.1.1, the impact of two BIN1 variants on rescuing $A\beta_{42}$ accumulation induced by BIN1 KD was studied. After BIN1 knockdown, through siRNA treatment, BIN1 constructs harbouring the PL and KR mutations were transfected in N2a cells. Cells were immunostained against Myc and $A\beta_{42}$ (Figure 3.2).

Myc immunostaining was again uniformly distributed, without a specific subcellular localization (Figure 3.2 A-E). Control cells, siControl, and siBin1 treated cells mock transfected and exhibited only a background fluorescence. The characteristic punctate pattern of Aβ42 immunofluorescence wasobserved (Figure 3.2 F-J).

In BIN1 knockdown cells, siBIN1, the mean intracellular $A\beta_{42}$ fluorescence was found increased by 66% in comparison to control cells (Figure 3.2 K), as previously observed (Burrinha, 2004; Marques, 2018; Ubelmann, Burrinha, Salavessa et al., 2017). The augmented $A\beta_{42}$ levels were rescued by the re-expression of neuronal isoform BIN1 wild-type (WT), as previous results, with a 60% decrease regarding siBIN1 cells. BIN1 PL and KR mutants did not rescue $A\beta_{42}$ elevated levels. These two mutants exhibit an 87% and 88% increase in $A\beta_{42}$ levels, respectively, regarding BIN1 WT expressing cells (Figure 3.2 K).

The two BIN1 rare coding variants studied, unlike BIN1 wild-type, did not rescue $A\beta_{42}$ levels, suggesting a loss of function of both BIN1 mutants. The two mutations localize to different sites within BIN1 sequence, however, both similarly affect $A\beta_{42}$ accumulation. This result supports the predicted impact that both mutants may have in BIN1 structure or stability (M. S. Tan et al., 2014; Vardarajan et al., 2015). If the two mutations affect Aβ accumulation through different mechanisms needs to be investigated.

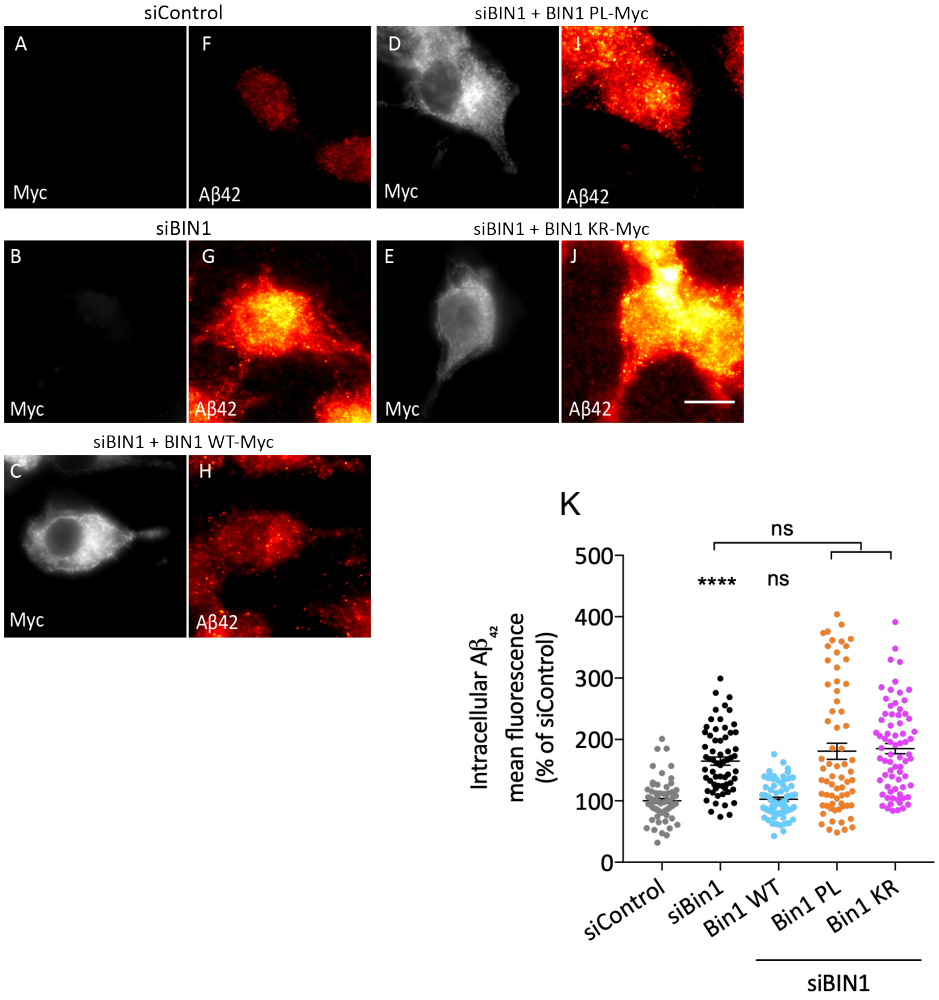

Figure 3.2: **BIN1 mutants do not rescue Aβ$_{42}$ accumulation.** A-J. Representative images of N2a cells after BIN1 knockdown by siRNA treatment followed by transient transfection of wild-type BIN1 (BIN1 WT-Myc), BIN1 PL mutant (BIN1 PL-Myc), BIN1 KR mutant (BIN1 KR-Myc). Cells were immunostained for Myc (A-E) and for Aβ$_{42}$ (F-J). Bar=10 μm. K. Quantification of intracellular Aβ$_{42}$ mean fluorescence intensity. $N_{SiControl}$=64, N_{siBIN1}=63, $N_{BIN1\ WT}$=73, $N_{BIN1\ PL}$ =67, $N_{BIN1\ KR}$ =72, n=3. Results are shown as percentage of Aβ$_{42}$ mean fluorescence in non-targeting siRNA cells (siControl). Data is expressed as mean±SEM; ns, not significant; ****p<0.0001 vs. siControl, ns. p>0.9999 vs. siControl, ns. p>0.9999 siBIN1 vs. BIN1 PL, BIN1 KR, ns p=0.45259 BIN1 PL vs. BIN1 KR, Kruskal-Wallis test.

3.2 APP processing

3.2.1 Impact of BIN1 variants in APP processing

Following the observation that the two BIN1 mutants in study do not rescue increased $A\beta_{42}$ levels by BIN1 knockdown, probably due to loss of function, it was necessary to investigate if this was a result of increased Aβ production. Aβ is generated through the processing of the transmembrane protein APP, by BACE1 and γ-secretase (Citron et al., 1996; U. C. Müller and Zheng, 2012; Serrano-Pozo et al., 2011). Thus, to answer our question, APP processing was analysed by western blot using the antibody Y188 against the intracellular C-terminal domain of APP, specifically the YENPTY motif, detecting APP full-length, as well as the APP C-terminal fragments, APP-CTFS (Figure 3.3 A). These fragments might include βCTF or αCTF, whereas γCTF is rapidly degraded (Cupers et al., 2001).

N2a cells were transiently transfected with BIN1 wild-type and the two mutants, BIN1 PL and BIN1 KR mutants. As a control, vector (Myc) transfected cells were used. After 24h of treatment, cells were lysed and immunoblotted against APP full-length and APP-CTFs (Figure 3.3; for full blot see Appendix).

Y188 antibody detected primarily two proteins (Figure 3.3 B). Between 130 and 100 kDa, it is possible to distinguish two higher molecular weight proteins that probably correspond to the mature and, immature and smaller forms of the full-length APP, as APP suffers post-transcriptional modifications (J. Z. Tan and Gleeson, 2018; Tomita et al., 1998), thus migrating between 110 and 120 kDa (Buxbaum, 1998). The lower molecular weight protein, with 15 to 10 kDa, corresponds to APP-CTFs, in agreement with the literature (Buxbaum, 1998). Technically, it is not possible to discern between the different C-terminal fragments. Nevertheless, considering the expected sizes of ~9 kDa for αCTF (C83) and ~11 kDa for βCTF (C89) (Delvaux et al., 2014), the inferior band will, probably, correspond to the latter. A faint band can also be observed, nearby 15 kDa that corresponds to the longer amyloidogenecic βCTF (C99) (Esposito, 2010).

App processing was analysed by the ratio between APP-CTFs and APP total levels (APP full lenght and APP-CTFs) (Figure 3.3 C). An increase in APP processing, was observed in all conditions, in comparison to control Myc expressing cells, however due to variability of the assay, only the KR mutant, with a 39% augment, seems to be statistically significant. This increase was also observed, previously, in BIN1 knockdown cells (Ubelmann, Burrinha, Salavessa et al., 2017) agreeing with the hypothesis that the mutantions lead to BIN1 loss of function. Having this in mind, the difference between control and mutant cells could be explained by the impact of the overexpression or due to dimerization between the expressed mutants and the endogenous BIN1 that results in a dominant negative effect.

APP levels were also quantified, after normalization with the loading control tubulin (Figure 3.5 D), and did not suffer a significant change.

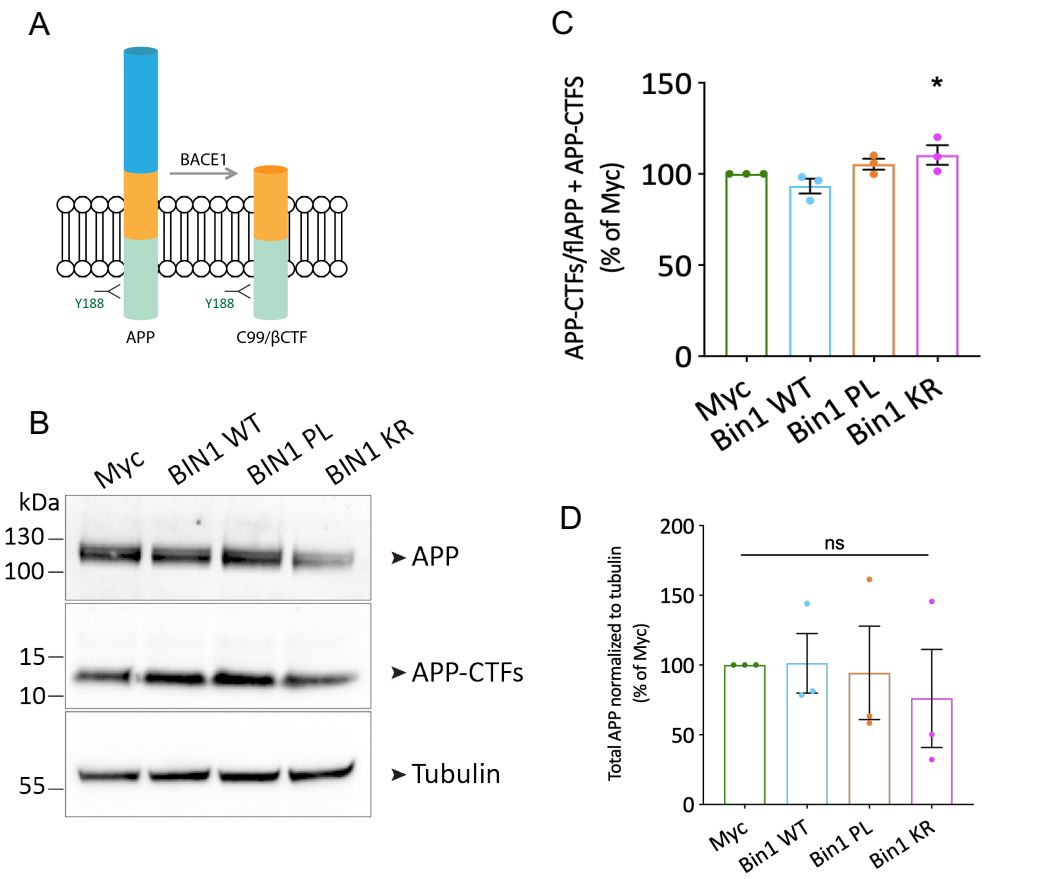

Figure 3.3: **BIN1 mutants impact in APP processing.** A. Y188 antibody recognizes the YENPTY motif (residues 682-687) in the C-terminal intracellular domain of the APP protein. Cleavage by BACE1 generates βCTF/C99 that is also recognize by the Y188 antibody. B. Western Blot analysis of N2a cells overexpressing Myc, BIN1 wild-type, BIN1 PL mutant or BIN1 KR mutant. For the representative immunoblot presented, proteins were sonified and separated on a 4-12% SDS-PAGE gel. Protein marker: PageRuler™ Plus. Endogenous full-length APP (flAPP; 130-100 kDa) and APP CTFs (15-10 kDa) levels by western blot with anti-APP anibody Y188 and tubulin (~55 kDa) using the anti-α-tubulin antibody. C. Densitometry quantification of APP-CTFs levels normalized to APP total levels (flAPP and APP-CTFs). Data is expressed as mean±SEM. n=3, *p=0.0372 Myc vs. BIN1 KR, Kruskal-Wallis test. D. Quantification of total APP levels normalized to the loading control, tubulin. n=3; Data is expressed as mean±SEM; ns, not significant; ns p>0.9999, Kruskal-Wallis test.

3.3 Intracellular traffic in AD

3.3.1 BIN1 variants effect in endosomes

The internalization of BACE1 and APP and their encounter in the early endosome allows the processing of APP that leads to Aβ generation. The segregation of these two proteins, by the recycling of BACE1 to the plasma membrane and the APP degradation in lysosomes or recycling to the TGN, works to limit Aβ production. In Alzheimer's disease, changes in endosomal trafficking have been reported, and indeed, enlargement of early endosomes were found to be an early event in sporadic AD (Cataldo et al., 1997; Cataldo et al., 2000).

Interestingly, BIN1 function in intracellular trafficking has been largely demonstrated in non-neuronal cells. Indeed, the interaction with several endocytic proteins has been demonstrated. In neurons, BIN1 KD was shown to increase early endosomes size and density (Calafate et al., 2016), proposing a causal role for BIN1 in the endosomal trafficking changes perceived in AD.

To investigate if the BIN1 mutants can rescue the increase early endosomes size induced by BIN1 KD, a rescue experiment was performed by the re-expression of neuronal BIN1 wild-type and mutants upon siRNA treatment. To identify the early endosomes, we expressed a GFP-tagged Rab5, a small GTPase that assembles on early endosomes, where it regulates the fusion with endocytic vesicles (Gorvel et al., 1991). After the treatment, cells were fixed and immunostained for the Myc-tag. Rab5-positive endosomes size and density were analyzed.

Rab5-GFP localized to punctate vesicles, especially abundant in the perinuclear region (Figure 3.4 A-E), as previously described (Chavrier et al., 1990; Kajiho et al., 2003). Regarding, Rab5-positive early endosomes density (Rab5 puncta per 100 μm^2 of cell area), presented as the number of Rab5-postive vesicles per 100 μm^2, no significant differences were observed (Figure 3.4 F), as seen by Marques (2018) using another early endosome marker, EEA1. This is also consistent with Cataldo et al. (1997), where the number of early endosomes in neurons from AD brains was found similar to those in control brains. Rab5-endosomes size, however, showed an increase in BIN1 KD cells (Figure 3.4 A1-E1, G) reproducing previous published data (Calafate et al., 2016; Ubelmann, Burrinha, Salavessa et al., 2017). This raise in endosome size was rescued by neuronal BIN1 wild-type expression, but also by BIN1 mutants. Early endosomes size frequency distribution is presented in Figure 3.4 H. We noticed, in siBIN1 treated cells, a decreased frequency of the smaller endosomes (<0.05 μm^2) and increased frequency of larger endosomes (>0.1 μm^2). The size distribuition of Rab5-endosomes was rescued by re-expression of BIN1 WT and PL and KR mutants. In addition, BIN1 WT expression induced a small decreased in the size distribuition of intermediate endosomes (0.05-0.1 μm^2) could be indicative of an effect of overexpression as it was described by Calafate et al., (2016).

As such, the loss of function of BIN1 mutants PL and KR impact on Aβ levels and APP processing does not seem to be mediated by an enlargement of early endosomes.

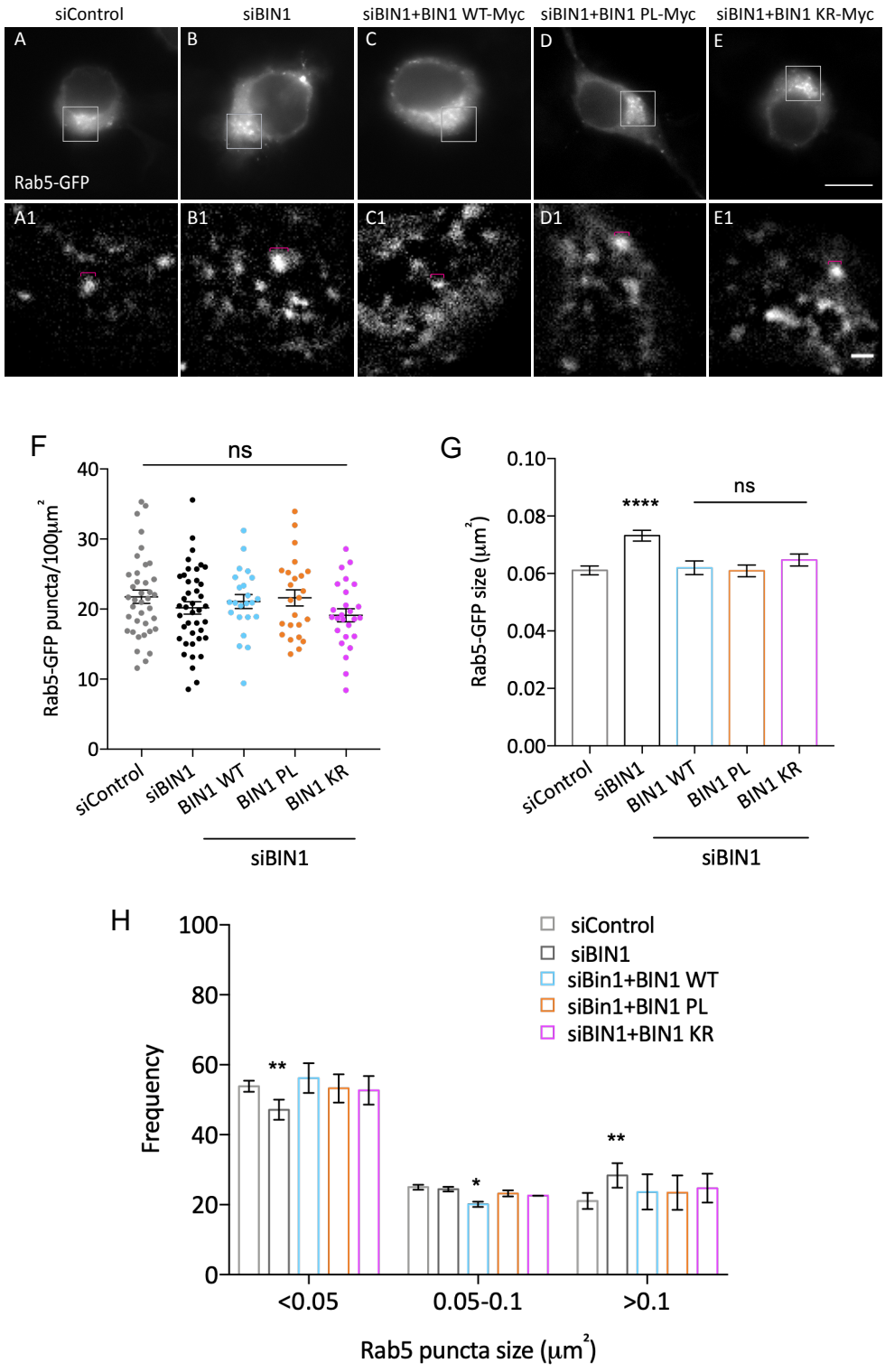

Figure 3.4: **BIN1 mutants do not induce early endosomes changes.** A-E. Representative images of N2a cells after siBIN1 treatment followed by transient transfection of Rab5-GFP, and wild-type BIN1 (BIN1 WT-Myc), BIN1 PL mutant (BIN1 PL-Myc) or BIN1 KR mutant (BIN1 KR-Myc). Bar=10 µm. A1-E1. Insets of A-E. after background substraction. Pink brackets highlight endosome size. Bar=1 µm. F. Rab5-positive endosomes density. Number of Rab5-GFP puncta per 100 µm^2. ns p>0.9999, ns p=0.9172 siControl vs. BIN1 KR, Kruskal-Wallis test. G. Rab5-positive endosomes size. Area of Rab5-GFP puncta (µm^2). ****p<0,0001 vs. siControl, ns p>0,9999 vs. siControl, ns p= 0,6663 BIN1 WT vs siControl, Kruskal-Wallis test. H. Distribuition of Rab5 endosomes size. **p=0,0021 BIN1 WT (<0.05) vs. siControl (<0.05), *p=0,0223 vs. siControl (0.05-0.1), **p=0,0011 vs siControl (>0.1), two-away ANOVA, Tukey's multiple comparisons test F-H. $N_{SiControl}$=38, N_{siBIN1}=42, $N_{BIN1\ WT}$=23, $N_{BIN1\ PL}$=25, $N_{BIN1\ KR}$=27, n=2. Data is expressed as mean±SEM. ns, not significant.

3.4 Interactome of BIN1 mutations

3.4.1 Impact of BIN1 mutants in BACE1 interaction

We have understood that both BIN1 PL and KR mutants appear to provoke BIN1 loss of function that leads to the increased Aβ accumulation. BIN1 loss was demonstrated to inhibit BACE1 exit from early endosomes and, consequently, increase APP processing (Ubelmann, Burrinha, Salavessa et al., 2017). However, the mechanism whereby the PL and KR mutations in BIN1 may affect Aβ production is still unclear. It is, therefore, necessary to investigate further BIN1 mutants' involvement in BACE1 traffic events abnormalities.

Previously, the interaction between BIN1 and BACE1 was observed, by a GST pulldown assay, and BIN1 BAR domain was proven essential for this interaction (Miyagawa et al., 2016). Now, by using a co-immunoprecipitation (co-IP) assay BIN1 mutations interaction with BACE1 will be investigated. The co-IP assay relies on the ability of immobilization of a protein complex by an antibody against a bait protein. Proteins that interact with the bait protein can be identified by immunoblotting (Berg, 2005).

Firstly, BIN1 wild-type interaction with BACE1 was verified. N2a cells were transiently transfected with Myc tagged neuronal BIN1 wild-type and BACE1 with a GFP tag, and, after 24h, cells were lysed. Immunoprecipitation of BACE1 was performed by the incubation with a GFP antibody for 16h and with protein G-coupled Sepharose beads for another 2h30 at 4°C. After washing the non-bound fraction, the immunoprecipited proteins were immunoblotted against GFP and Myc (Figure 3.5 A). If there is an interaction between these two proteins, BIN1 should be co-immunoprecipitated with BACE1. As a control, a non-target antibody IgG was used, as it should do not bind specific proteins.

Total cell lysate or input, and the fraction of not bond proteins or flow-through (FT) were immunoblotted in addition to immunoprecipitated proteins. The input, as it is taken before incubation with the antibodies, allows us to assess the expression of bait and target protein. Indeed, the good detection of BACE1-GFP and BIN1-Myc indicates good expression levels. BIN1-Myc was detected between 100 kDa and 75 kDa, in agreement with previous observations (Burrinha, 2014). BACE1-GFP was found at 150 kDa, a higher molecular weight than the expected ~70 kDa (Haniu et al., 2000) in addition to the GFP tag (26,9 kDa), possibly on account of dimer formation with the endogenous BACE1, observed by Schmechel et al. (2004) and Westmeyer et al. (2004), between 140 kDa and 160 kDa (Figure 3.5 A).

Immunoprecipitation of BACE1-GFP was confirmed by GFP blotting, although the use of capture and primary antibodies of the same species led to a high background signal as the co-eluted capture antibody is, also, recognized by the HRP- conjugated secondary antibody. Non-target antibody IgG showed high non-specific binding, but Myc staining did not indicated direct or indirect binding to BIN1. To eliminate non-specific binding, a step of pre-clearing could be done by the pre-incubation of the lysates with the beads that are discarded afterwards to remove the proteins that directly bind them.

In contrast, with BACE1-GFP immunoprecipitation BIN1 was co-eluted as shown by the faint band in Myc immunoblot (Figure 3.5 A).

Since the faint band in the IP was suggestive of BIN1 interaction with BACE1, the reciprocal immunoprecipitation was investigated next, using Myc-Traps® (Chromotek). Myc-Trap® comprises an anti-Myc Tag nanobody, a recombinant single variable domain, V_HH, from an alpaca heavy chain antibody, covalently coupled to the surface of agarose beads. As such, there is no need for a pre-incubation with the capture antibodies and the antibody is not co-eluted with immunoprecipitated proteins giving a lower background signal.

After 24h of transfection with BIN1-Myc and BACE1-GFP, N2a cells were lysed.

Immunoprecipitation of BIN1 was achieved by the incubation with Myc-Trap® for 1h and immunoprecipitated proteins, as well as, non-bound fraction and total cell lysate, were immunoblotted against Myc- and GFP-tag (Figure 3.5 B). As a negative control, N2a cells were transiently transfected with BIN1-Myc and GFP alone.

In total cell lysate (input), BIN1 expression was verified, and although it is less that the previous experiment, we obtained a good BIN1-Myc immunoprecipitation. Without antibody co-elution a cleaner background signal was possible. Regarding BACE1-GFP, in input, we obtained non-specific proteins, probably due to GFP antibody specificity issues, that are washed in the flow-through. Still, a GFP signal was well detected in BIN1-Myc and GFP transfected cells. This GFP signal was not present in the IP Myc. Instead, a faint band, around 100 kDa, can be observed in the IP Myc, corresponding to the co-immunoprecipitation of BACE1-GFP. In control cells, a hint of a band is also noticeable likely due to cross-contamination from the next well or non-specific antibody binding (Figure 3.5 B).

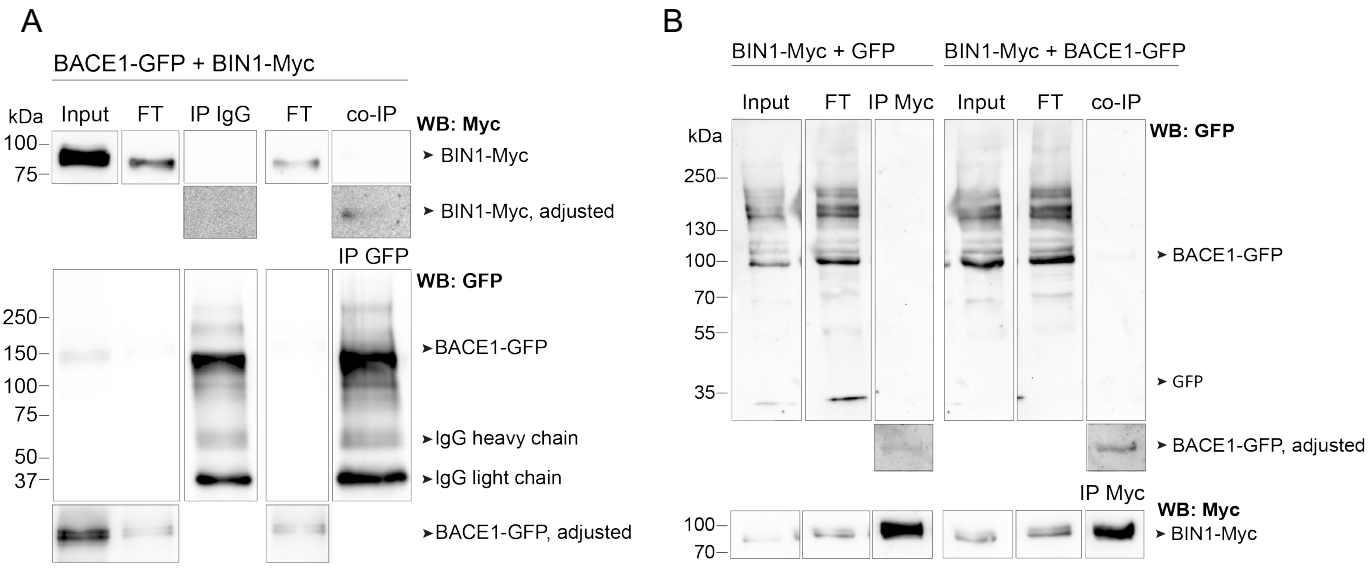

Figure 3.5: **BIN1 wild-type interaction with BACE1.** A. Co-immunoprecipitation assay of N2a cells lysates transfected with BIN1-Myc and BACE1-GFP. Immunoprecipitation of BACE1 was performed using anti-GFP antibody. As control, a non-target antibody (IgG) was used. Total cell lysate (input), fraction non-bound (flow-through, FT) and immunoprecipitated proteins (IP IgG or GFP) were separated by SDS-PAGE and immunoblotted against GFP and Myc. Protein marker: Precision Plus Protein™. To visualize BIN1-Myc in IP and BACE1-GFP in input a longer exposure time is presented. B. Reciprocal co-immunoprecipitation assay of N2a cells lysates transfected with BIN1-Myc and BACE1-GFP and BIN1-Myc and GFP. Immunoprecipitation of BIN1 was performed using using Myc-Trap®. As control, transfection with BIN1-Myc and empty plasmid with a GFP tag was carryed out. Total cell lysate (input), fraction non-bound (flow-through, FT) and immunoprecipitated proteins (IP IgG or Myc) were separated by SDS-PAGE and immunoblotted against GFP and Myc. Protein marker: PageRuler™ Plus. To visualize BACE1-GFP in IP a longer exposure time is presented.

Next, the interaction of BIN1 mutants with BACE1 was assessed. This time, N2a cells, transiently transfected with BACE1 and, BIN1 WT or the two mutants BIN1 PL or BIN1 KR, were lysed. After, cell lysates were immunoprecipitated with Myc-Trap® and the time of incubation was increased to 16h, in a tempt to increase the co-IP. Total cell lysate, fraction non-bound and immunoprecipitated proteins were resolved by SDS-PAGE and immunoblotted with anti-Myc

antibody and anti-BACE1, to control for previous non-specific binding of anti-GFP antibody (Figure 3.6).

BIN1 and BACE1 expression was confirmed in the input of N2a cell lysates transfected with only BACE1, our negative control, BACE1 and BIN1 wild-type and BACE1 and BIN1 PL or KR mutants. Additionally, the similar BIN1 expression levels of WT and BIN1 mutants validates our previous findings. In control cells, BACE1 expression was visibly greater than when BACE1-GFP is co-transfected with BIN1-Myc. This might have happened due to an impact of the co-transfection with BIN1 in BACE1 expression levels in the other conditions. Immunoprecipitation of BIN1 was nicely achieved as observed in IP Myc. Immunoblot against BACE1 confirms the co-immunoprecipitation of BACE1 with BIN1 WT and mutants. Unexpectadly, in control cells a band for BACE1 was also detected. This might be a consequence of the greater expression levels that might have led to aggregation and precipitation or to non-specific binding to the beads or, even, not sufficient washing. To discard non-specific binding agarose beads could be blocked in 1-3% BSA and in addition lysates could be pre-cleared by incubation with identical beads not coupled to an antibody.

By the ratio between BACE1 co-IP and BACE1 total levels (Figure 3.6 A), we controled that BACE1 co-IP in control cells is comparable to other conditions and was greater with BIN1 KR mutant expression.

The ratio between BACE1 co-IP and BIN1 immunoprecipitation (Figure 3.6 C), that controls for the different BIN1 IP levels, confirmed that BACE1 interacted more with BIN1 KR mutant than with BIN1 WT and PL.

It will be important to repeat the experiment using cells with similar levels of BACE1 expression to confirm the interaction with a working negative control. Nevertheless, our results are indicative of, at least, some interaction between BIN1 mutants and BACE1.

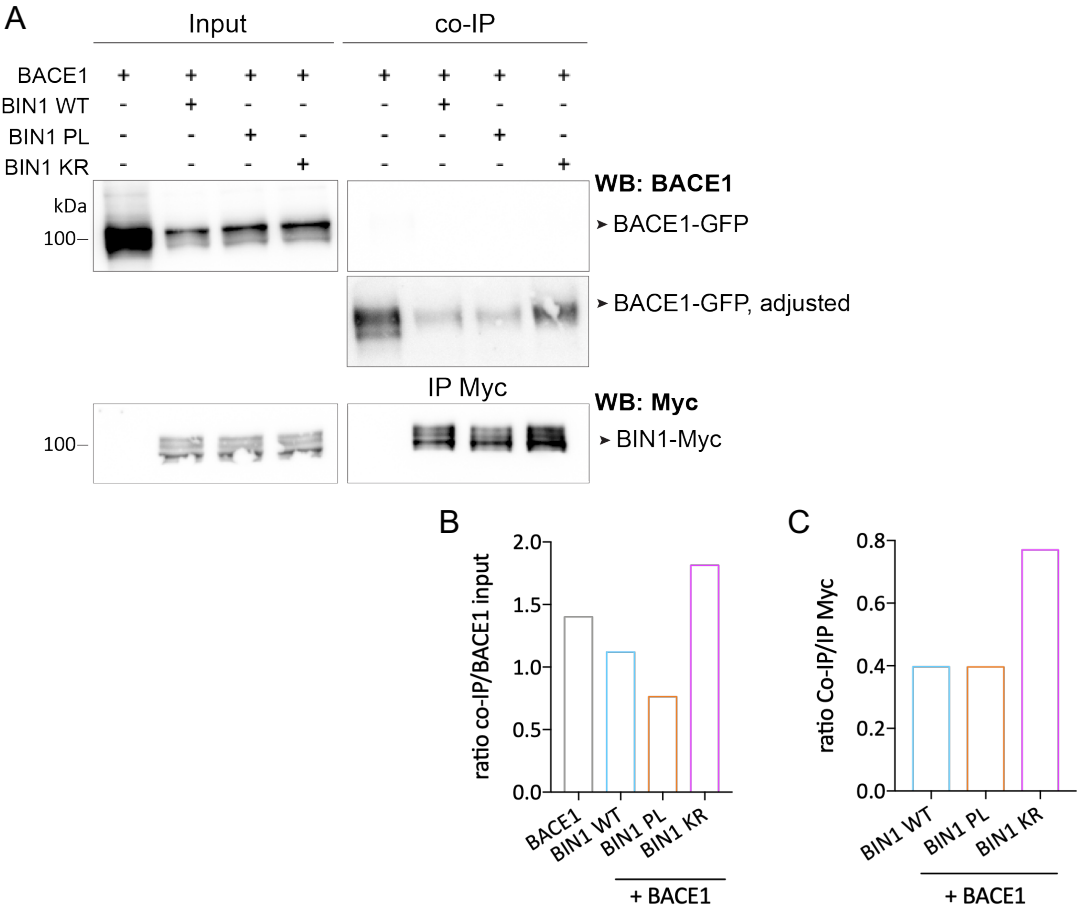

Figure 3.6: **BIN1 PL and KR mutants interaction with BACE1.** A. Co-immunoprecipitation assay of N2a cells lysates transfected with BACE1-GFP or BACE-GFP with BIN1-Myc WT, PL or KR mutants. Cell lysates were immunoprecipitated (IP) with Myc-Trap®. Total cell lysate (input) and immunoprecipitated proteins (IP Myc) were resolved by SDS-PAGE and visualized with anti-BACE1 and anti-Myc antibodies. Protein marker: PageRuler™ Plus. To visualize BACE1 in IP Myc a longer exposure time is presented. BACE1 co-IP to BACE1 input ratio is included (B), as well as, ratio between BACE1 co-IP and BIN1 immunoprecipitated (C).

3.4.2 Mass spectrometry: Interactome of BIN1 mutants

To go beyond BIN1 and BACE1 interaction, we next took a more unbiased approach to characterize better the interactome of neuronal BIN1 and how it is altered by the LOAD mutations. To do this we used the previous approach of the co-immunoprecipitation assay, followed by the identification of the whole BIN1 wild-type and mutants interactome by mass spectrometry. Differential interactors, if discovered, will be, next, investigated according to the biological process they are involved in and will give important clues to the mechanism whereby PL and KR mutants work to raise $A\beta_{42}$ levels.

Foremost, N2a cells were transfected with BIN1 wild-type, PL or KR mutants. These cells and a mock control, consisting of not transfected cells, were subjected to immunoprecipitation with Myc-Trap® for 16h, as previously. Immunoprecipitated proteins and total cell lysate were resolved by SDS-PAGE and detected using coomassie blue staining and immnoblotted against Myc. Like this, the total fraction of co-immunoprecipitated proteins with BIN1 was, first, checked by coomassie staining (Figure 3.7 A).

Uniform BIN1 contructs expression was confirmed by Myc immunoblot in transfected N2a cells in input, as well as, efficient immunoprecipitation of Myc-tagged BIN1 (IP Myc) (Figure 3.7 A). Mock control, without BIN1 exogenous expression, was used as a negative control of the assay. Through coomassie staining that detects as little as 0.1 μg protein, the complete fraction of immunoprecipitated proteins by BIN1 could be detected (Figure 3.7 A and B). A strong band at 100 kDa likely corresponds to BIN1, as it is easily deteted in transfected cells but not in mock cells. In IP Myc, we observed only a fraction of proteins all proteins of the total cell lysate (input), consistent with a specific co-immunoprecipitation of possible BIN1 interactors. And, although, the detection of several fainter bands in mock control indicates that there is a fraction of non-specific binding, this fraction can be subtracted upon analysis by mass spectrometry analysis. In transfected cells, we observed two main distinct regions between BIN1 WT and mutants (Figure 3.7 A), that gives rise to the distinct density band profile in Figure 3.7 B, suggesting differential quantitative and qualitative interactions. Having detected the total immunoprecipitated proteins by coomassie staining we can assure an easy detection by the more sensitive tool, mass spectrometry.

To proceed with the mass spectrometry analysis, the co-immunoprecipitation assay was scaled up to double the previous conditions. This time, however, Myc-Tag bound proteins were eluted with glycine buffer for in-solution analysis. Half of eluted proteins, in the same proportion as before, were, also, resolved in 4-12% SDS-PAGE gel and detected by coomassie staining (Figure 3.7 C).

Once more, a band likely corresponding to BIN1 can be easily detected by the absence in mock cells and strong presence in BIN1-Myc wild-type and PL or KR mutants immunoprecipitated cell lysates. And, as in Figure 3.7 B, two strong non-specific binding proteins are observed above 250 kDa and bellow 55 kDa that are, probably, a consequence of high expression that led to inefficient removal in the washing step. However, the efficiency of the elution seems to decrease by the new elution method. To improve the overall detection of proteins silver-staining, that detects as little as 5 ng, could be used.

Again, two distinct regions between conditions are apparent confirming the reproducibility of the assay. In BIN1 PL mutants transfected cells, however, fewer proteins are observed. To overpass the possibility of false results, two more experiments were performed, so three eluates for each condition will be analysed by mass spectrometry. Elution was, always, performed twice, giving rise to eluate 1 (EL1) and eluate 2 (EL2) to increase efficiency, and will be combined in mass spectrometry analysis.

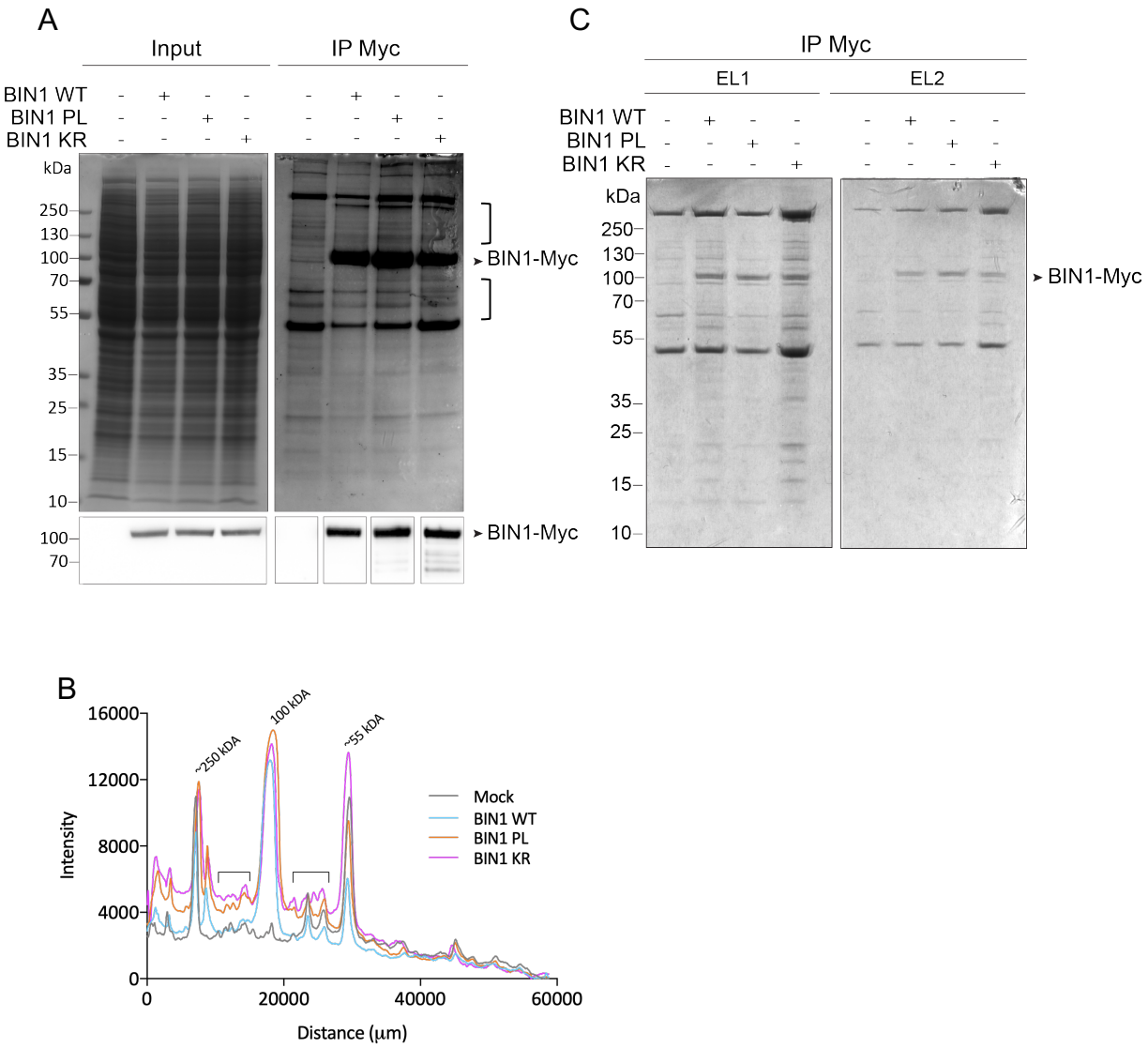

Figure 3.7: **Differential BIN1 WT and PL and KR mutant co-immunoprecipitation.** A,C. Co-immunoprecipitation assay of N2a cells lysates transfected with BIN1-Myc WT, PL or KR mutants (and a mock control). Cell lysates were immunoprecipitated (IP) with Myc-Trap®. Immunoprecipitated proteins (IP Myc) and, in A, total cell lysate (input) were resolved by SDS-PAGE (4-12% gel). Protein marker: PageRuler™ Plus. A. Immunoblot against Myc and, input and total fraction of immunoprecipitated proteins are visualized by Coomassie staining. Two distinct regions with different band patterns among the conditions are identified. B. Plot profile of A. The same distinct regions are identified. Molecular weights of the most intense bands were added for guidance. C. Immunoprecipitated proteins (IP Myc) detected by Coomassie staining after glycine elution. n=3. EL1, eluate 1; EL2, eluate 2.

Chapter 4

Discussion

In this study, we dissected the molecular mechanisms whereby BIN1 controls Aβ accumulation. Moreover, we investigated the impact of two rare coding BIN1 variants, found associated with LOAD, in BIN1 cellular functions and contribution to AD development.

First, we studied the contribution of BIN1 BAR, CLAP and SH3 domains to Aβ accumulation. These domains are especially involved in intracellular trafficking events, which are fundamental in the regulation of Aβ production and accumulation (J. Z. Tan and Gleeson, 2018). In N2a cells, we observed that BIN1 loss by siRNA treatment led to augmented intracellular $A\beta_{42}$ levels, explained in previous work to be due to the failed BACE1 recycling from early endosomes (Ubelmann, Burrinha, Salavessa et al., 2017), where Aβ production occurs. While the neuronal BIN1 isoform rescued this effect, the ubiquitous isoform did not completely rescued $A\beta_{42}$ increased levels. This difference might be explained by the presence, solely in the neuronal isoform, of the CLAP domain or an alternatively spliced exon, in the BAR domain, that promotes interaction with dynamin II (Ellis et al., 2012). These additional domains might regulate the recruitment of the neuronal BIN1 to a specific site, where it is likely to participate in clathrin-mediated processes.

SH3 and CLAP domains, in absence of the BAR domain, had the same outcome as BIN1 knockdown, suggesting a lack of function in Aβ production. These results are consistent with those by Miyagawa et al. (2016), where the absence of BIN1 BAR domain increased extracellular Aβ secretion in N2a cells. In this case, a dominant negative effect was observed that might be a result of the dimerization between the expressed mutant and the endogenous BIN1.

The BAR domain is important for membrane curvature induction and stabilization of the formed vesicle (Löw et al., 2008; Peter et al., 2004). Besides the inclusion of a site for the interaction with dynamin II in the neuronal isoform, this domain was observed to be essential for BIN1 interaction with BACE1 (Miyagawa et al. 2016). Expression of ubiquitous BAR domain resulted in a complete rescue of $A\beta_{42}$ increased levels. In a next experiment, the rescue will be assayed using the neuronal BAR domain, since there is an alternatively spliced exon within the BAR domain of the neuronal isoform that may impact its function. Thus far, our results suggest, that the BAR domain is pivotal for BIN1 function in regulating Aβ accumulation.

The impact of PL and KR mutants in neuronal BIN1 in Aβ accumulation was, next, investigated. In N2a cells, we observed that these mutants did not rescue increased $A\beta_{42}$ levels induced by BIN1 knockdown, suggesting a loss of function (Figure 4.1). Having the same effect as BIN1 constructs deprived of the BAR domain, is feasible that both mutants have an impact in BAR function. Since, PL and KR mutants localize to proline-serine rich domain and the SH3 domain, respectively, an impact in the BAR domain through the perturbation of BIN1 self-regulation is possible. In addition, both mutations are predicted to affect BIN1 structure or stability (M. S. Tan et al., 2014; Vardarajan et al., 2015). To understand if $A\beta_{42}$ augment levels was due to increased Aβ production, the role of the mutants in APP processing was investigated. APP processing was analysed by immunoblot against the intracellular C-terminal of APP, detecting APP full-length and APP-βCTF. The rate between APP-CTFs and APP showed a significant

increase only in KR mutant transfected cells. The mutants appear to induce loss of function and, when in overexpression studies, to have a dominant negative effect.

To further understand the mechanism, whereby BIN1 mutants lead to an increase in $A\beta_{42}$ levels, the impact in intracellular trafficking was considered. Since, enlargement of early endosomes were found in AD and BIN1 knockdown in rat primary neurons was shown to increase early endosomes size (Calafate et al., 2016) the mutants' impact in endosomes size and density was observed. No differences were observed regarding endosomes density, similar to Marques (2018) and Cataldo et al. (1997). Endosomes were found to be enlarged with BIN1 loss (Figure 4.1) and a decrease frequency of the smaller endosomes and increase in the larger endosomes was observed. This further confirms BIN1 involvement in intracellular trafficking pathways that result in Aβ accumulation. BIN1 mutants, however, rescued this effect, similar to neuronal BIN1 wild-type (Figure 4.1). Interestingly, Toh et al., (2018) investigated the role of sortin nexin 4, SNX4, in BACE1 transport. SNX4 has been identified as an essential component for sorting transferrin receptor form early endosomes to recycling endosomes (Traer et al., 2007). It was demonstrated that SNX4 depletion redirects BACE1 to late endosomes, leading to be co-transported with APP. This extension of BACE1 and APP colocalization was shown to increase Aβ production (Toh et al., 2018). Bearing in mind, that BIN1 interaction with SNX4 was observed before through a co-immunoprecipitation assay (Leprince et al., 2003) is it plausible that PL and KR mutants sequester SNX4 in a non-functional complex or in an abnormal localization that leads to the same effect as SNX4 depletion. This could explain the increase in Aβ accumulation with PL and KR mutants and the absence of early endosomal abnormalities. To prove this, we could investigate if BACE1 colocalization with a late endosome marker, Rab7, would increase with the BIN1 PL and KR mutants rescue. In addition, this would lead to an increase in BACE1 clearance that could be assessed by biotinylation degradation assay.

Having in mind, BIN1 function in BACE1 recycling and how both mutants appear to induce loss of function, the impact of the mutations in BIN1 interaction with BACE1 was explored. Firstly, a reciprocal co-immunoprecipitation assay was performed in N2a cells transiently transfected with BIN1-Myc and GFP tagged BACE1, using with a capture antibody against GFP to bait BACE1 or Myc-Traps® to capture BIN1-Myc. Next, the mutants' interaction with BACE1 was assessed and found to be visibly greater with BIN1 KR mutant. As the BAR domain is the domain responsible for this interaction, this implies that the mutations do not affect BAR domain interaction with BACE1 (Figure 4.1). We can speculate that the mutants raise $A\beta_{42}$ levels independently of their interaction with BACE1. The mutations could instead alter the interaction with other players in BACE1 recycling, like SNX4. As such, SNX4 could be the next target to be investigated by co-immunoprecipitation.

Our previous results indicate that BIN1 PL and KR mutants lead to a loss of function and our hypothesis suggests that the mechanism behind involves BIN1 function in BACE1 recycling to the plasma membrane. One hypothesis is that the two mutants, without affecting BIN1 interaction with BACE1, might result in loss of function by affecting BIN1 self-regulation, considering their location in the BIN1 protein. The mutations may increase or decrease BIN1 auto-inhibition by altering the binding between the CLAP domain and the SH3 domain. This may occur through changes in stability and structure of BIN1 protein or changes in the ability to be phosphorylated or dephosphorylated, as it is thought to be a necessary step in BIN1 self-inhibition (Sartori et al., 2018). The increased auto-inhibition could affect BAR domain function in membrane curvature generation and reduce BIN1 binding to endosomes, whereas if decreased BIN1 would be bound to dynamin preventing dynamin self-assembly required for scission and recycling. The appropriate regulation is, thus, important for BIN1 functions and a dysfunctional regulation would lead to decreased BACE1 recycling from the early endosomes and increased Aβ.

As such, in future work, it will be important to understand how the mutations affect neuronal BIN1 conformation, for example, through nuclear magnetic resonance (NMR), with purified proteins, as the different environment of the amino acid residues in an open or close

conformation will give differential spectrums. Also, the ability to be phosphorylated/dephosphorylated could be assessed through immunoblotting using a phosphor-specific antibody against a BIN1 phosphorylation site near CLAP domain, T348, observed to promote BIN1 open conformation. Importantly, the phosphorylation at T348 site was seen to increase in the brains of AD cases (Sartori et al., 2018). Mass spectrometry will also allow the mapping and analysis of phosphorylation sites (Dephoure et al., 2013).

Next, a more sensitive technique was applied to identify all BIN1 interactome. Using mass spectrometry following BIN1 immunoprecipitation, the qualitative and quantitative comparison between BIN1 wild-type and BIN1 mutants' protein-protein interactions is possible. The differential interactors will, next be investigated to allow us to further understand the mutants' mechanism of action. Foremost, by Coomassie staining, the total fraction of co-immunoprecipitated proteins with BIN1 was detected and two main distinct regions between conditions are observed. After this confirmation, immunoprecipitated proteins were eluted by glycine buffer to be digested in-solution, and, subsequently, these proteins will be separated and analysed by LC-MS/MS.

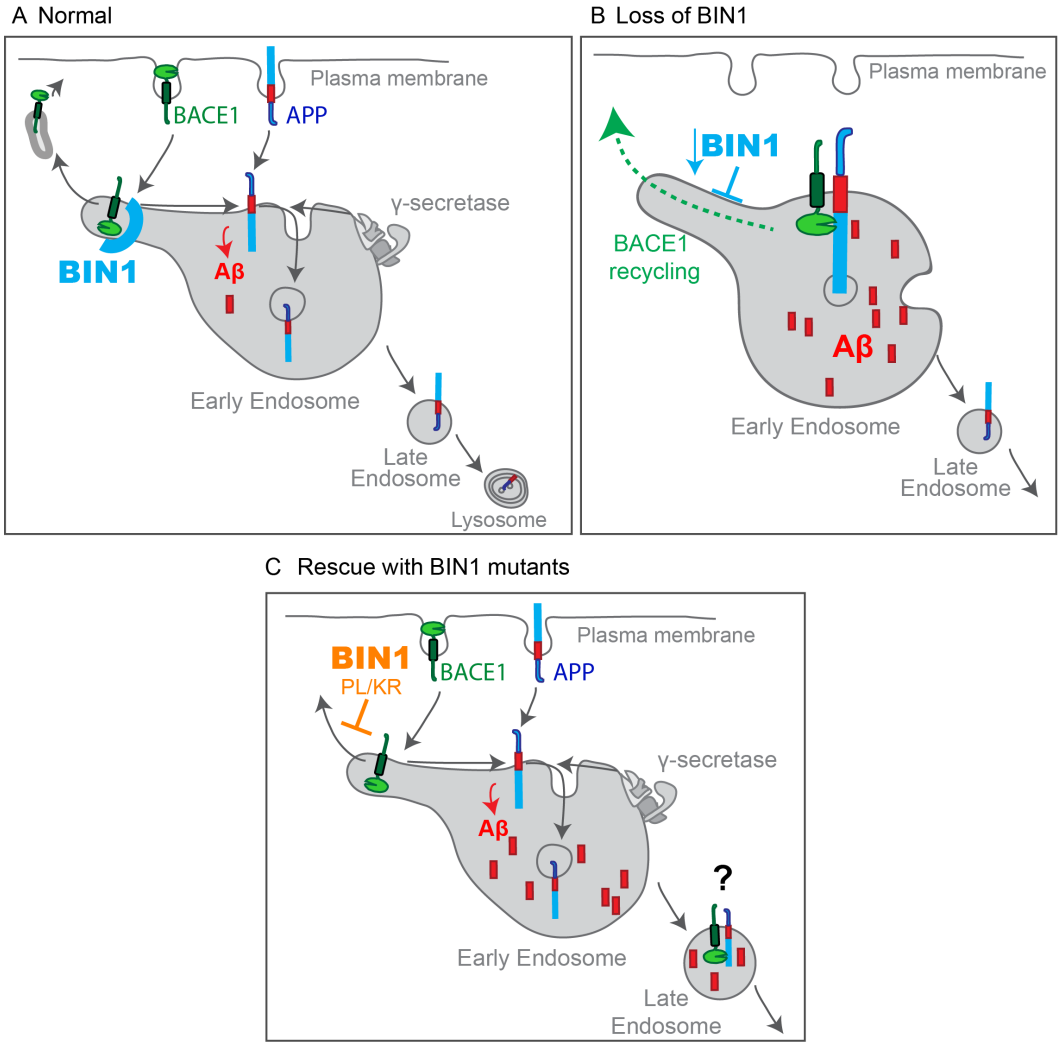

Figure 4.1: **Schematic representation of BIN1 mutants' rescue impact in endocytic trafficking and $A\beta_{42}$ accumulation.** (Adapted from Ubelmann, Burrinha, Salavessa et al., 2017) A. In normal conditions, BIN1 is involved in tubule scission for BACE1 exit from early endosomes. This regulation leads to less BACE1 and APP encounter in the early endosomes and controls Aβ production. B. The loss of BIN1 inhibits tubule scission leading to BACE1 accumulation in early endosomes increasing Aβ production and early endosomes size. C. BIN1 PL and KR mutants did not rescue $A\beta_{42}$ accumulation induced by BIN1 loss, indicating a loss of BIN1 function. BIN1 mutants, however, did not affect the interaction with BACE. Rescue with the mutants did not lead to an enlargment of early endosomes, as such, we suggest that the mutants lead to Aβ accumulation in late endosomes.

Chapter 5

Conclusion and future perspectives

In conclusion, our main findings are that the two BIN1 mutants in study did not rescued the increase in intracellular $A\beta_{42}$ levels induced by BIN1 loss (Figure 4.1). Thus far, we only confirmed an increase in APP processing regarding the BIN1 KR mutant. Together these findings indicate that the mutations lead to BIN1 loss of function. The impact of PL and KR mutants in the BAR domain function is suggested as the deletion of the BIN1 BAR domain leads, also, to an increase in $A\beta_{42}$ levels. Considering BAR domain function in membrane curvature generation and BACE1 interaction, it goes in agreement with loss of BIN1 function in BACE1 recycling that results in augmented Aβ accumulation. The mechanism whereby the mutants work is still not well understood. However, PL and KR mutants localize to proline-serine rich domain and the SH3 domain, respectively, so an impact in the BAR domain through the perturbation of BIN1 self-regulation is possible. Both mutants rescued the enlargement in early endosomes caused by BIN1 knockdown, however there is a possibility that the inhibition of BACE1 recycling directs BACE1 to late endosomes to prolong co-localization with APP (Figure 4.1). Interaction of BIN1 wild-type and BACE1 was observed by a co-immunoprecipitation. In addition, both mutants are found to interact with BACE1, and so the mutants raise $A\beta_{42}$ levels without affecting BACE1 interaction (Figure 4.1). Next, by co-immunoprecipitation-mass spectrometry, BIN1 interactome started to be investigated.

Further research is still necessary to uncover the impact of PL and KR mutants in BIN1 functions and how it could contribute to AD development. Since, our experimental model used is a mouse neuroblastoma cell line, N2a cells, the results achieved in this study need to be confirmed. First, mouse primary neuronal cultures will be used and later, induced human neurons differentiated from healthy iPSC, and genetically edited with our mutations by CRISP/Cas9 strategy, could be used.

Following the previous paper by Ubelmann, Burrinha, Salavessa et al. (2017), BIN1 mutants' effect in tubule scission for BACE1 recycling from early endosomes and also if the mutants increase the encounter of APP and BACE1 could be assessed.

To understand how the mutants do not appear to affect early endosomes size, we will investigate if BACE1 colocalization with a late endosome marker, Rab7, increases by BIN1 PL and KR mutants' overexpression upon BIN1 knockdown.

Also, the BIN1 mutants' possible impact in BIN1 self-regulation needs to be understood. It will be important to understand, for example, through nuclear magnetic resonance (NMR), if the mutations affect neuronal BIN1 conformation by inducing changes in stability and structure or changes in the ability to be phosphorylated/dephosphorylated. This ability will be assessed through immunoblotting of N2a cells transfected with BIN1 mutants against a BIN1 phosphorylation site near the CLAP domain, observed to be involved in the regulation of BIN1 intramolecular interaction (Sartori et al., 2018).

The differential interactors identified by mass spectrometry will be investigated according to the biological process they are involved to further understand the mutants' mechanism of action.

Importantly, the impact of BIN1 mutants on synapses can be uncovered, using primary neurons. The implication of BIN1 in synaptic vesicle recycling is supported by several lines of evidence, so we could determine if our mutants in BIN1 lead to endosomal trafficking deregulation that mediates synapse dysfunction, an early event in AD pathogenesis.

Bibliography

Adzhubei, I. A., et al. (2010). A method and server for predicting damaging missense mutations. Nature methods, 7(4), 248.

Alberts, Bruce; Johnson, Alexander; Lewis, Julian; Raff, Martin; Roberts, Keith; Walter, Peter (2015) Molecular Biology of The Cell. New York, NY: Garlan Science

Almeida, C. G., Sadat Mirfakhar, F., Perdigão, C., & Burrinha, T. (2018). Impact of late-onset Alzheimer's genetic risk factors on beta-amyloid endocytic production. Cellular and Molecular Life Sciences, 75, 2577-2589.

Almeida, C. G., Takahashi, R. H., & Gouras, G. K. (2006). β-Amyloid accumulation impairs multivesicular body sorting by inhibiting the ubiquitin-proteasome system. Journal of Neuroscience, 26(16), 4277-4288.

Almeida, C. G., Tampellini, D., Takahashi, R. H., Greengard, P., Lin, M. T., Snyder, E. M., & Gouras, G. K. (2005). Beta-amyloid accumulation in APP mutant neurons reduces PSD-95 and GluR1 in synapses. Neurobiology of disease, 20(2), 187-198.

Altschul, S.F., Gish, W., Miller, W., Myers, E.W. & Lipman, D.J. (1990) Basic local alignment search tool. Journal Molecular Biology 215:403-410.

Alzheimer, A. (1911). Über eigenartige Krankheitsfälle des späteren Alters. Zeitschrift für die gesamte Neurologie und Psychiatrie, 4(1), 356.

Alzheimer's Association. (2017). 10 Warning signs of Alzheimer's disease. Chicago. Retrieved from https://www.alz.org/media/Documents/alzheimers-dementia-memory-loss-alzheimers-10-warning-signs-b.pdf

Alzheimer's Association. (2019). Alzheimer's Disease Facts and Figures.Alzheimers Dement 15(3):321-87.

Alzheimer's Disease International. (2018). World Alzheimer Report 2018, The state of the art of dementia research: New frontiers.

Antonny, B., et al. (2016). Membrane fission by dynamin: what we know and what we need to know. The EMBO journal, 35(21), 2270-2284.

Atri, A. (2019). The Alzheimer's Disease Clinical Spectrum: Diagnosis and Management. Medical Clinics, 103(2), 263-293.

Ausubel, F. M., Brent, R., Kingston, R. E., Moore, D. D., Seidman, J. G., Smith, J. A., & Struhl, K. (2003). Current protocols in molecular biology, vol. 1 John Wiley & Sons. Inc., Brooklyn, New York, 3(1), 1994-2005.

Bales, K. R. (2000). Neuroinflammation and Alzheimer's disease: critical roles for cytokine/A beta-induced glial activation, NF-kappaB, and apolipoprotein E. Neurobiol Aging, 21, 427-432.

Ballard, C., Gauthier, S., Corbett, A., Brayne, C., & Aarsland, D. (2011). Jones e. Alzheimer's disease. Lancet, 377, 1019-1031.

Barnes, M. R., & Gray, I. C. (Eds.). (2003). Bioinformatics for geneticists. John Wiley & Sons.

Bendl, J., Stourac, et al. (2014). PredictSNP: robust and accurate consensus classifier for prediction of disease-related mutations. PLoS computational biology, 10(1), e1003440.

Berg, T. (2005). Methods in Molecular Biology Vol. 261: Protein–Protein Interactions: Methods and Applications. Edited by Haian Fu. *ChemBioChem*, *6*(2), 446-447.

Bertram, L., McQueen, M. B., Mullin, K., Blacker, D., & Tanzi, R. E. (2007). Systematic meta-analyses of Alzheimer disease genetic association studies: the AlzGene database. Nature genetics, 39(1), 17.

Best, B. P. (2015). Cryoprotectant toxicity: facts, issues, and questions. Rejuvenation research, 18(5), 422-436.

Boehm, M., & Bonifacino, J. S. (2001). Adaptins: the final recount. Molecular biology of the cell, 12(10), 2907-2920.

Braak, H., & Braak, E. V. A. (1995). Staging of Alzheimer's disease-related neurofibrillary changes. Neurobiology of aging, 16(3), 271-278.

Brunden, K. R., Trojanowski, J. Q., & Lee, V. M. Y. (2009). Advances in tau-focused drug discovery for Alzheimer's disease and related tauopathies. Nature reviews Drug discovery, 8(10), 783.

Burns, A. & Lliffe, S. (2009). Alzheimer's disease. BMJ, 338, b158.

Burrinha, T. M. A. (2014). Bridging integrator 1 (BIN1) controls beta-amyloid accumulation in Alzheimers desease (Master dissertation).

Burtis, C. A., & Bruns, D. E. (2015). Tietz fundamentals of clinical chemistry and molecular diagnostics. Elsevier Health Sciences.

Bush, W. S., & Moore, J. H. (2012). Genome-wide association studies. PLoS computational biology, 8(12), e1002822.

Butler, M. H., et al. (1997). Amphiphysin II (SH3P9; BIN1), a member of the amphiphysin/Rvs family, is concentrated in the cortical cytomatrix of axon initial segments and nodes of ranvier in brain and around T tubules in skeletal muscle. The Journal of cell biology, 137(6), 1355-1367.

Buxbaum, J. D., Thinakaran, G., Koliatsos, V., O'Callahan, J., Slunt, H. H., Price, D. L., & Sisodia, S. S. (1998). Alzheimer amyloid protein precursor in the rat hippocampus: transport and processing through the perforant path. *Journal of Neuroscience*, *18*(23), 9629-9637.
Calafate, S., Flavin, W., Verstreken, P., & Moechars, D. (2016). Loss of Bin1 promotes the propagation of tau pathology. Cell reports, 17(4), 931-940.
Cao, J., Hou, J., Ping, J., & Cai, D. (2018). Advances in developing novel therapeutic strategies for Alzheimer's disease. Molecular neurodegeneration, 13(1), 64.
Casal, E., et al. (2006). The crystal structure of the BAR domain from human Bin1/amphiphysin II and its implications for molecular recognition. Biochemistry, 45(43), 12917-12928.
Caselli, R. J., Beach, T. G., Knopman, D. S., & Graff-Radford, N. R. (2017). Alzheimer disease: scientific breakthroughs and translational challenges. Mayo Clinic Proceedings, 92(6), 978-994.
Castellano, J. M., et al. (2011). Human apoE isoforms differentially regulate brain amyloid-β peptide clearance. Science translational medicine, 3(89), 89ra57-89ra57
Cataldo, A. M., Barnett, J. L., Pieroni, C., & Nixon, R. A. (1997). Increased neuronal endocytosis and protease delivery to early endosomes in sporadic Alzheimer's disease: neuropathologic evidence for a mechanism of increased β-amyloidogenesis. *Journal of Neuroscience*, *17*(16), 6142-6151.
Cataldo, A. M., Peterhoff, C. M., Troncoso, J. C., Gomez-Isla, T., Hyman, B. T., & Nixon, R. A. (2000). Endocytic pathway abnormalities precede amyloid β deposition in sporadic Alzheimer's disease and Down syndrome: differential effects of APOE genotype and presenilin mutations. *The American journal of pathology*, *157*(1), 277-286.
Chapuis, J., et al. (2013). Increased expression of BIN1 mediates Alzheimer genetic risk by modulating tau pathology. Molecular psychiatry, 18(11), 1225.
Chasseigneaux, S., & Allinquant, B. (2012). Functions of Aβ, sAPPα and sAPPβ: similarities and differences. Journal of neurochemistry, 120, 99-108.
Chavrier, P., Parton, R. G., Hauri, H. P., Simons, K., & Zerial, M. (1990). Localization of low molecular weight GTP binding proteins to exocytic and endocytic compartments. *Cell*, *62*(2), 317-329.
Chia, P. Z. C., Toh, W. H., Sharples, R., Gasnereau, I., Hill, A. F., & Gleeson, P. A. (2013). Intracellular itinerary of internalised β-Secretase, BACE1, and its potential impact on β-Amyloid peptide biogenesis. Traffic, 14(9), 997-1013.
Choi, S. H., et al. (2014). A three-dimensional human neural cell culture model of Alzheimer's disease. *Nature*, *515*(7526), 274.
Christensen, D. Z., Schneider-Axmann, T., Lucassen, P. J., Bayer, T. A., & Wirths, O. (2010). Accumulation of intraneuronal Aβ correlates with ApoE4 genotype. Acta neuropathologica, 119(5), 555-566.
Cipriani, G., Dolciotti, C., Picchi, L., & Bonuccelli, U. (2011). Alzheimer and his disease: a brief history. Neurological Sciences, 32(2), 275-279.
Cirrito, J. R., et al. (2008). Endocytosis is required for synaptic activity-dependent release of amyloid-β in vivo. Neuron, 58(1), 42-51.
Citron, M., Diehl, T. S., Gordon, G., Biere, A. L., Seubert, P., & Selkoe, D. J. (1996). Evidence that the 42-and 40-amino acid forms of amyloid β protein are generated from the β-amyloid precursor protein by different protease activities. Proceedings of the National Academy of Sciences, 93(23), 13170-13175.
Corder, E. H., et al. (1994). Protective effect of apolipoprotein E type 2 allele for late onset Alzheimer disease. Nature genetics, 7(2), 180.
Cremona, O., & De Camilli, P. (1997). Synaptic vesicle endocytosis. *Current opinion in neurobiology*, *7*(3), 323-330.
Cremona, O., et al. (1999). Essential role of phosphoinositide metabolism in synaptic vesicle recycling. Cell, 99(2), 179-188.
Cupers, P., Orlans, I., Craessaerts, K., Annaert, W., & De Strooper, B. (2001). The amyloid precursor protein (APP)-cytoplasmic fragment generated by γ-secretase is rapidly degraded but distributes partially in a nuclear fraction of neurones in culture. *Journal of neurochemistry*, *78*(5), 1168-1178.
Das, U., Scott, D. A., Ganguly, A., Koo, E. H., Tang, Y., & Roy, S. (2013). Activity-induced convergence of APP and BACE-1 in acidic microdomains via an endocytosis-dependent pathway. Neuron, 79(3), 447-460.
Dawkins, E., & Small, D. H. (2014). Insights into the physiological function of the β-amyloid precuror protein: beyond Alzheimer's disease. Journal of neurochemistry, 129(5), 756-769.
Day, J. G., & Stacey, G. (Eds.). (2007). Cryopreservation and freeze-drying protocols (Vol. 368). Springer Science & Business Media.
De Rossi, P., et al. (2016). Predominant expression of Alzheimer's disease-associated BIN1 in mature oligodendrocytes and localization to white matter tracts. Molecular neurodegeneration, 11(1), 59.
De Rossi, P., et al. (2018). Aberrant accrual of BIN1 near Alzheimer's disease amyloid deposits in transgenic models. Brain Pathology.
De Strooper, B. (2003). Aph-1, Pen-2, and nicastrin with presenilin generate an active γ-secretase complex. Neuron, 38(1), 9-12.
Delvaux, E., Bentley, K., Stubbs, V., Sabbagh, M., & Coleman, P. D. (2013) Differential processing of amyloid precursor protein in brain an in peripheral blood leukocytes. *Neurobiology of aging*, 34 (6), 1680-1686.

Dephoure, N., Gould, K. L., Gygi, S. P., & Kellogg, D. R. (2013). Mapping and analysis of phosphorylation sites: a quick guide for cell biologists. *Molecular biology of the cell*, *24*(5), 535-542.
Di Paolo, G., & Kim, T. W. (2011). Linking lipids to Alzheimer's disease: cholesterol and beyond. Nature Reviews Neuroscience, 12(5), 284.
Di Paolo, G., et al. (2002). Decreased synaptic vesicle recycling efficiency and cognitive deficits in amphiphysin 1 knockout mice. *Neuron*, *33*(5), 789-804.
Dickson, D. W. (2004). Apoptotic mechanisms in Alzheimer neurofibrillary degeneration: cause or effect?. The Journal of clinical investigation, 114(1), 23-27.
Ehrlich, I., & Malinow, R. (2004). Postsynaptic density 95 controls AMPA receptor incorporation during long-term potentiation and experience-driven synaptic plasticity. Journal of Neuroscience, 24(4), 916-927.
Ellis, J. D., et al. (2012). Tissue-specific alternative splicing remodels protein-protein interaction networks. Molecular cell, 46(6), 884-892.
Esposito, L. A. (2010). Measuring APP carboxy-terminal fragments. In *Alzheimer's Disease and Frontotemporal Dementia*(pp. 71-84). Humana Press, Totowa, NJ.
Falcone, S., et al. (2014). N-WASP is required for Amphiphysin-2/BIN1-dependent nuclear positioning and triad organization in skeletal muscle and is involved in the pathophysiology of centronuclear myopathy. EMBO molecular medicine, 6(11), 1455-1475.
Falkenburger, B. H., Jensen, J. B., Dickson, E. J., Suh, B. C., & Hille, B. (2010). Symposium Review: Phosphoinositides: lipid regulators of membrane proteins. The Journal of physiology, 588(17), 3179-3185.
Farrer, L. A., et al. (1997). Effects of age, sex, and ethnicity on the association between apolipoprotein E genotype and Alzheimer disease: a meta-analysis. Jama, 278(16), 1349-1356.
Feany, M. B., Lee, S., Edwards, R. H., & Buckley, K. M. (1992). The synaptic vesicle protein SV2 is a novel type of transmembrane transporter. *Cell*, *70*(5), 861-867.
Fernando, P., et al. (2009). Bin1 SRC homology 3 domain acts as a scaffold for myofiber sarcomere assembly. Journal of Biological Chemistry, 284(40), 27674-27686.
Ferri, C. P., et al. (2005). Global prevalence of dementia: a Delphi consensus study. The lancet, 366(9503), 2112-2117.
Fjorback, A. W., & Andersen, O. M. (2012). SorLA is a molecular link for retromer-dependent sorting of the Amyloid precursor protein. Communicative & integrative biology, 5(6), 616-619.
Fjorback, A. W., et al. (2012). Retromer binds the FANSHY sorting motif in SorLA to regulate amyloid precursor protein sorting and processing. Journal of Neuroscience, 32(4), 1467-1480.
Förstl, H., & Kurz, A. (1999). Clinical features of Alzheimer's disease. European archives of psychiatry and clinical neuroscience, 249(6), 288-290.
Fugier, C., et al. (2011). Misregulated alternative splicing of BIN1 is associated with T tubule alterations and muscle weakness in myotonic dystrophy. Nature medicine, 17(6), 720.
Gauthier, N. C., et al. (2007). Early endosomes associated with dynamic F-actin structures are required for late trafficking of H. pylori VacA toxin. The Journal of cell biology, 177(2), 343-354.
Gene [Internet]. Bethesda (MD): National Library of Medicine (US), National Center for Biotechnology Information; 2004 – [cited 2019 Jun 9]. Available from: https://www.ncbi.nlm.nih.gov/gene/214
Glennon, E. B., et al. (2019). Loss of the Alzheimer's-linked bridging integrator 1 (BIN1) protein affects synaptic structure and disrupts tau localisation and release. *bioRxiv*, 646406.
Glennon, E. B., Whitehouse, I. J., Miners, J. S., Kehoe, P. G., Love, S., Kellett, K. A., & Hooper, N. M. (2013). BIN1 is decreased in sporadic but not familial Alzheimer's disease or in aging. PLoS One, 8(10), e78806.
Global Health Estimates 2016: Disease burden by Cause, Age, Sex, by Country and by Region, 2000-2016. Geneva, World Health Organization; 2018.
González-Reyes, R. E., Nava-Mesa, M. O., Vargas-Sánchez, K., Ariza-Salamanca, D., & Mora-Muñoz, L. (2017). Involvement of astrocytes in Alzheimer's disease from a neuroinflammatory and oxidative stress perspective. Frontiers in molecular neuroscience, 10, 427.
Gorvel, J. P., Chavrier, P., Zerial, M., & Gruenberg, J. (1991). rab5 controls early endosome fusion in vitro. *Cell*, *64*(5), 915-925.
Gouras, G. K., Tsai, J., Naslund, J., Vincent, B., Edgar, M., Checler, F., ... & Greengard, P. (2000). Intraneuronal Aβ42 accumulation in human brain. The American journal of pathology, 156(1), 15-20.
Graeber, M. B., & Mehraein, P. (1999). Reanalysis of the first case of Alzheimer's disease. European archives of psychiatry and clinical neuroscience, 249(3), S10-S13.
Guerreiro, R., et al. (2013). TREM2 variants in Alzheimer's disease. New England Journal of Medicine, 368(2), 117-127.
Haass, C., & Selkoe, D. J. (2007). Soluble protein oligomers in neurodegeneration: lessons from the Alzheimer's amyloid β-peptide. Nature reviews Molecular cell biology, 8(2), 101.
Hardy, J. (1997). Amyloid, the presenilins and Alzheimer's disease. Trends in neurosciences, 20(4), 154-159.
Hardy, J., & Selkoe, D. J. (2002). The amyloid hypothesis of Alzheimer's disease: progress and problems on the road to therapeutics. science, 297(5580), 353-356
Harold, D., et al. (2009). Genome-wide association study identifies variants at CLU and PICALM associated with Alzheimer's disease. Nature genetics, 41(10), 1088.

Hasegawa, J., Strunk, B. S., & Weisman, L. S. (2017). PI5P and PI (3, 5) P2: minor, but essential phosphoinositides. Cell structure and function, 17003.
Hippius, H., & Neundörfer, G. (2003). The discovery of Alzheimer's disease. Dialogues in clinical neuroscience, 5(1), 101
Hirano, A. (1994). Hirano bodies and related neuronal inclusions. Neuropathology and applied neurobiology, 20(1), 3-11.
Holler, C. J., Davis, P. R., Beckett, T. L., Platt, T. L., Webb, R. L., Head, E., & Murphy, M. P. (2014). Bridging integrator 1 (BIN1) protein expression increases in the Alzheimer's disease brain and correlates with neurofibrillary tangle pathology. Journal of Alzheimer's Disease, 42(4), 1221-1227.
Hollingworth, P., et al. (2011). Common variants at ABCA7, MS4A6A/MS4A4E, EPHA1, CD33 and CD2AP are associated with Alzheimer's disease. Nature genetics, 43(5), 429.
Holtzman, D. M., Morris, J. C., & Goate, A. M. (2011). Alzheimer's disease: the challenge of the second century. Science translational medicine, 3(77), 77sr1-77sr1.
Hu, Q., Noll, R. J., Li, H., Makarov, A., Hardman, M., & Graham Cooks, R. (2005). The Orbitrap: a new mass spectrometer. *Journal of mass spectrometry*, *40*(4), 430-443.
Huang, Y. W. A., Zhou, B., Wernig, M., & Südhof, T. C. (2017). ApoE2, ApoE3, and ApoE4 differentially stimulate APP transcription and Aβ secretion. Cell, 168(3), 427-441.
Hudry, E., et al. (2013). Gene transfer of human Apoe isoforms results in differential modulation of amyloid deposition and neurotoxicity in mouse brain. Science translational medicine, 5(212), 212ra161-212ra161.
Ibrahim, M. M., & Gabr, M. T. (2019). Multitarget therapeutic strategies for Alzheimer's disease. Neural regeneration research, 14(3), 437.
James, B. D., & Bennett, D. A. (2019). Causes and Patterns of Dementia: An Update in the Era of Redefining Alzheimer's Disease. Annual review of public health, 40.
Jellinger, K. A. (2004). Head injury and dementia. Current opinion in neurology, 17(6), 719-723.
Johnson, J. W., & Kotermanski, S. E. (2006). Mechanism of action of memantine. Current opinion in pharmacology, 6(1), 61-67.
Kadlec, L., & Pendergast, A. M. (1997). The amphiphysin-like protein 1 (ALP1) interacts functionally with the cABL tyrosine kinase and may play a role in cytoskeletal regulation. Proceedings of the National Academy of Sciences, 94(23), 12390-12395.
Kajiho, H., Saito, K., Tsujita, K., Kontani, K., Araki, Y., Kurosu, H., & Katada, T. (2003). RIN3: a novel Rab5 GEF interacting with amphiphysin II involved in the early endocytic pathway. *Journal of cell science*, *116*(20), 4159-4168.
Kaksonen, M., & Roux, A. (2018). Mechanisms of clathrin-mediated endocytosis. Nature Reviews Molecular Cell Biology, 19(5), 313.
Kallas-Kivi, A., Trei, A., Stepanjuk, A., Ruisu, K., Kask, K., Pooga, M., & Maimets, T. (2018). The role of integrin β1 in the heterogeneity of human embryonic stem cells culture. Biology open, 7(11), bio034355.
Kamal, A., Almenar-Queralt, A., LeBlanc, J. F., Roberts, E. A., & Goldstein, L. S. (2001). Kinesin-mediated axonal transport of a membrane compartment containing β-secretase and presenilin-1 requires APP. Nature, 414(6864), 643.
Kamenetz, F., et al. (2003). APP processing and synaptic function. Neuron, 37(6), 925-937.
Kandel, E. R., Schwartz, J. H., Jessell, T. M., Siegelbaum, S. A., & Hudspeth, A. J. (2000). Principles of neural science, 4, 1227-1246. New York: McGraw-Hill.
Katzung, B. G., Masters, S. B., & Trevor, A. J. (2012). Basic and clinical pharmacology (lange basic science). McGraw-Hill Education.
Kins, S., & Beyreuther, K. (2006). Teasing out the tangles. Nature medicine, 12(7), 764.
Klebe, RJ. and Ruddle, FH. (1969) Neuroblastoma: Cell culture analysis of a differentiating stem cell system. J Cell Biol 43: 69A.
Köhler, C. (2016). Granulovacuolar degeneration: a neurodegenerative change that accompanies tau pathology. Acta neuropathologica, 132(3), 339-359.
Kojima, C., et al. (2004). Regulation of Bin1 SH3 domain binding by phosphoinositides. The EMBO journal, 23(22), 4413-4422.
LaFerla, F. M., & Oddo, S. (2005). Alzheimer's disease: Aβ, tau and synaptic dysfunction. Trends in molecular medicine, 11(4), 170-176.
Lambert, J. C., et al. (2013). Meta-analysis of 74,046 individuals identifies 11 new susceptibility loci for Alzheimer's disease. Nature genetics, 45(12), 1452.
Lee, E., Marcucci, et al. (2002). Amphiphysin 2 (Bin1) and T-tubule biogenesis in muscle. Science, 297(5584), 1193-1196.
Lee, V. M., Goedert, M., & Trojanowski, J. Q. (2001). Neurodegenerative tauopathies. Annual review of neuroscience, 24(1), 1121-1159.
Lehtonen, S., Zhao, F., & Lehtonen, E. (2002). CD2-associated protein directly interacts with the actin cytoskeleton. American Journal of Physiology-Renal Physiology, 283(4), F734-F743.
Leprince, C., Le Scolan, E., Meunier, B., Fraisier, V., Brandon, N., De Gunzburg, J., & Camonis, J. (2003). Sorting nexin 4 and amphiphysin 2, a new partnership between endocytosis and intracellular trafficking. *Journal of cell science*, *116*(10), 1937-1948.

Leprince, C., Romero, F., Cussac, D., Vayssiere, B., Berger, R., Tavitian, A., & Camonis, J. H. (1997). A new member of the amphiphysin family connecting endocytosis and signal transduction pathways. Journal of Biological Chemistry, 272(24), 15101-15105.
Levy-Lahad, E., et al. (1995). A familial Alzheimer's disease locus on chromosome 1. Science, 269(5226), 970-973.
Lichte, B., Veh, R. W., Meyer, H. E., & Kilimann, M. W. (1992). Amphiphysin, a novel protein associated with synaptic vesicles. The EMBO journal, 11(7), 2521-2530.
Löw, C., et al. (2008). Structure and dynamics of helix-0 of the N-BAR domain in lipid micelles and bilayers. Biophysical journal, 95(9), 4315-4323.
Lynch, J. R., et al. (2003). APOE genotype and an ApoE-mimetic peptide modify the systemic and central nervous system inflammatory response. Journal of Biological Chemistry, 278(49), 48529-48533.
Malki, I., Cantrelle, F. X., Sottejeau, Y., Lippens, G., Lambert, J. C., & Landrieu, I. (2017). Regulation of the interaction between the neuronal BIN 1 isoform 1 and Tau proteins–role of the SH 3 domain. The FEBS journal, 284(19), 3218-3229.
Marks, B., & McMahon, H. T. (1998). Calcium triggers calcineurin-dependent synaptic vesicle recycling in mammalian nerve terminals. Current biology, 8(13), 740-749.
Marques, A. C. M. (2018). The impact of Bridging Integrator 1 (BIN1) rare coding mutations on the development of Late-Onset Alzheimer's Disease (Master dissertation).
Marquer, C., et al. (2011). Local cholesterol increase triggers amyloid precursor protein-Bace1 clustering in lipid rafts and rapid endocytosis. *The FASEB journal*, *25*(4), 1295-1305.
Matthiesen R., Mutenda K.E. (2007) Introduction to Proteomics. In: Matthiesen R. (eds) Mass Spectrometry Data Analysis in Proteomics. Methods in Molecular Biology, vol 367. Humana Press
Matthiesen, R., & Bunkenborg, J. (2013). Introduction to mass spectrometry-based proteomics. In *Mass spectrometry data analysis in proteomics* (pp. 1-45). Humana Press, Totowa, NJ.
Mattson, M. P. (2004). Pathways towards and away from Alzheimer's disease. Nature, 430(7000), 631.
McClure, S. J., & Robinson, P. J. (1996). Dynamin, endocytosis and intracellular signalling. Molecular membrane biology, 13(4), 189-215.
McKhann, G. M., et al. (2011). The diagnosis of dementia due to Alzheimer's disease: Recommendations from the National Institute on Aging-Alzheimer's Association workgroups on diagnostic guidelines for Alzheimer's disease. Alzheimer's & dementia, 7(3), 263-269.
McLean, C. A., et al. (1999). Soluble pool of Aβ amyloid as a determinant of severity of neurodegeneration in Alzheimer's disease. Annals of neurology, 46(6), 860-866.
Meyerholz, A., Hinrichsen, L., Groos, S., Esk, P. C., Brandes, G., & Ungewickell, E. J. (2005). Effect of clathrin assembly lymphoid myeloid leukemia protein depletion on clathrin coat formation. Traffic, 6(12), 1225-1234.
Michaelson, D. M. (2014). APOE ε4: The most prevalent yet understudied risk factor for Alzheimer's disease. Alzheimer's & Dementia, 10(6), 861-868.
Michalski, A., et al. (2011). Mass spectrometry-based proteomics using Q Exactive, a high-performance benchtop quadrupole Orbitrap mass spectrometer. *Molecular & Cellular Proteomics*, *10*(9), M111-011015.
Micheva, K. D., Ramjaun, A. R., Kay, B. K., & McPherson, P. S. (1997). SH3 domain-dependent interactions of endophilin with amphiphysin. FEBS letters, 414(2), 308-312.
Michikawa, M., Fan, Q. W., Isobe, I., & Yanagisawa, K. (2000). Apolipoprotein E exhibits isoform-specific promotion of lipid efflux from astrocytes and neurons in culture. Journal of neurochemistry, 74(3), 1008-1016.
Miyagawa, T., et al. (2016). BIN1 regulates BACE1 intracellular trafficking and amyloid-β production. Human molecular genetics, 25(14), 2948-2958.
Mochizuki, A., Tamaoka, A., Shimohata, A., Komatsuzaki, Y., & Shoji, S. I. (2000). Aβ42-positive non-pyramidal neurons around amyloid plaques in Alzheimer's disease. The Lancet, 355(9197), 42-43.
Moechars, D., et al. (1999). Early phenotypic changes in transgenic mice that overexpress different mutants of amyloid precursor protein in brain. Journal of Biological Chemistry, 274(10), 6483-6492.
Morishima-Kawashima, M. (2014). Molecular mechanism of the intramembrane cleavage of the β-carboxyl terminal fragment of amyloid precursor protein by γ-secretase. Frontiers in physiology, 5, 463.
Mueller, S. G., et al. (2005). Ways toward an early diagnosis in Alzheimer's disease: the Alzheimer's Disease Neuroimaging Initiative (ADNI). Alzheimer's & Dementia, 1(1), 55-66.
Müller, T., Meyer, H. E., Egensperger, R., & Marcus, K. (2008). The amyloid precursor protein intracellular domain (AICD) as modulator of gene expression, apoptosis, and cytoskeletal dynamics—relevance for Alzheimer's disease. Progress in neurobiology, 85(4), 393-406.
Müller, U. C., & Zheng, H. (2012). Physiological functions of APP family proteins. Cold Spring Harbor perspectives in medicine, 2(2), a006288.
Müller, U. C., Deller, T., & Korte, M. (2017). Not just amyloid: physiological functions of the amyloid precursor protein family. *Nature Reviews Neuroscience*, *18*(5), 281.
Naj, A. C., et al. (2011). Common variants at MS4A4/MS4A6E, CD2AP, CD33 and EPHA1 are associated with late-onset Alzheimer's disease. Nature genetics, 43(5), 436.
Namba, Y., Tomonaga, M., Kawasaki, H., Otomo, E., & Ikeda, K. (1991). Apolipoprotein E immunoreactivity in cerebral amyloid deposits and neurofibrillary tangles in Alzheimer's disease and kuru plaque amyloid in Creutzfeldt-Jakob disease. Brain research, 541(1), 163-166.

Negorev, D., Simon, D., & Riethman, H. (1996). The Bin1 gene localizes to human chromosome 2q14 by PCR analysis of somatic cell hybrids and fluorescence in situ hybridization. Genomics, 33(2).
Owen, D. J., Wigge, P., Vallis, Y., Moore, J. D. A., Evans, P. R., & McMahon, H. T. (1998). Crystal structure of the amphiphysin-2 SH3 domain and its role in the prevention of dynamin ring formation. The EMBO journal, 17(18), 5273-5285.
Pandurangan, A. P., Ochoa-Montaño, B., Ascher, D. B., & Blundell, T. L. (2017). SDM: a server for predicting effects of mutations on protein stability. Nucleic acids research, 45(W1), W229-W235.
Peter, B. J., Kent, H. M., Mills, I. G., Vallis, Y., Butler, P. J. G., Evans, P. R., & McMahon, H. T. (2004). BAR domains as sensors of membrane curvature: the amphiphysin BAR structure. Science, 303(5657), 495-499.
Piper, R. C., Dikic, I., & Lukacs, G. L. (2014). Ubiquitin-dependent sorting in endocytosis. Cold Spring Harbor Perspectives in Biology, 6(1), a016808.
Praticò, D., Uryu, K., Leight, S., Trojanoswki, J. Q., & Lee, V. M. Y. (2001). Increased lipid peroxidation precedes amyloid plaque formation in an animal model of Alzheimer amyloidosis. Journal of Neuroscience, 21(12), 4183-4187.
Prokic, I., Cowling, B. S., & Laporte, J. (2014). Amphiphysin 2 (BIN1) in physiology and diseases. Journal of molecular medicine, 92(5), 453-463.
Rahimzadeh, M., Sadeghizadeh, M., Najafi, F., Arab, S., & Mobasheri, H. (2016). Impact of heat shock step on bacterial transformation efficiency. Molecular biology research communications, 5(4), 257.
Rajendran, L., & Annaert, W. (2012). Membrane trafficking pathways in Alzheimer's disease. Traffic, 13(6), 759-770.
Ramjaun, A. R., & McPherson, P. S. (1998). Multiple amphiphysin II splice variants display differential clathrin binding: identification of two distinct clathrin-binding sites. Journal of neurochemistry, 70(6), 2369-2376.
Ramjaun, A. R., Micheva, K. D., Bouchelet, I., & McPherson, P. S. (1997). Identification and characterization of a nerve terminal-enriched amphiphysin isoform. Journal of Biological Chemistry, 272(26), 16700-16706.
Rao, Y., & Haucke, V. (2011). Membrane shaping by the Bin/amphiphysin/Rvs (BAR) domain protein superfamily. Cellular and Molecular Life Sciences, 68(24), 3983-3993.
Rapp, A., Gmeiner, B., & Hüttinger, M. (2006). Implication of apoE isoforms in cholesterol metabolism by primary rat hippocampal neurons and astrocytes. Biochimie, 88(5), 473-483.
Razzaq, A., et al. (2001). Amphiphysin is necessary for organization of the excitation–contraction coupling machinery of muscles, but not for synaptic vesicle endocytosis in Drosophila. Genes & development, 15(22), 2967-2979.
Rebeck, G. W., Reiter, J. S., Strickland, D. K., & Hyman, B. T. (1993). Apolipoprotein E in sporadic Alzheimer's disease: allelic variation and receptor interactions. Neuron, 11(4), 575-580.
Ren, G., Vajjhala, P., Lee, J. S., Winsor, B., & Munn, A. L. (2006). The BAR domain proteins: molding membranes in fission, fusion, and phagy. Microbiol. Mol. Biol. Rev., 70(1), 37-120.
Riddell, D. R., et al. (2008). Impact of apolipoprotein E (ApoE) polymorphism on brain ApoE levels. Journal of Neuroscience, 28(45), 11445-11453.
Ringman, J. M., et al. (2012). Plasma signaling proteins in persons at genetic risk for Alzheimer disease: influence of APOE genotype. Archives of neurology, 69(6), 757-764.
Rovelet-Lecrux, A., et al. (2006). APP locus duplication causes autosomal dominant early-onset Alzheimer disease with cerebral amyloid angiopathy. Nature genetics, 38(1), 24.
Sakamuro, D., Elliott, K. J., Wechsler-Reya, R., & Prendergast, G. C. (1996). BIN1 is a novel MYC–interacting protein with features of a tumour suppressor. Nature genetics, 14(1), 69.
Salto, R., et al. (2015). β-Hydroxy-β-methylbutyrate (HMB) promotes neurite outgrowth in Neuro2a cells. PloS one, 10(8), e0135614.
Sannerud, R., et al. (2011). ADP ribosylation factor 6 (ARF6) controls amyloid precursor protein (APP) processing by mediating the endosomal sorting of BACE1. Proceedings of the National Academy of Sciences, 108(34), E559-E568.
Sartori, M., et al. (2018). BIN1 recovers tauopathy-induced long-term memory deficits in mice and interacts with Tau through Thr348 phosphorylation. bioRxiv, 462317.
Saunders, A. M., et al. (1993). Association of apolipoprotein E allele ϵ4 with late-onset familial and sporadic Alzheimer's disease. Neurology, 43(8), 1467-1467.
Schellenberg, G. D., et al. (1992). Genetic linkage evidence for a familial Alzheimer's disease locus on chromosome 14. Science, 258(5082), 668-671.
Schmechel, A., Strauss, M., Schlicksupp, A., Pipkorn, R., Haass, C., Bayer, T. A., & Multhaup, G. (2004). Human BACE forms dimers and colocalizes with APP. *Journal of Biological Chemistry*, *279*(38), 39710-39717.
Schürmann, B., et al. (2019). A novel role for the late-onset Alzheimer's disease (LOAD)-associated protein Bin1 in regulating postsynaptic trafficking and glutamatergic signaling. *Molecular psychiatry*, 1.
Serrano-Pozo, A., Frosch, M. P., Masliah, E., & Hyman, B. T. (2011). Neuropathological alterations in Alzheimer disease. Cold Spring Harbor perspectives in medicine, 1(1), a006189.
Seshadri, S., et al. (2010). Genome-wide analysis of genetic loci associated with Alzheimer disease. Jama, 303(18), 1832-1840.

Shao, W., Peng, D., & Wang, X. (2017). Genetics of Alzheimer's disease: From pathogenesis to clinical usage. Journal of Clinical Neuroscience, 45, 1-8.
Shen, L., & Jia, J. (2016). An overview of genome-wide association studies in Alzheimer's disease. Neuroscience bulletin, 32(2), 183-190.
Shinohara, M., et al. (2016). APOE2 eases cognitive decline during aging: clinical and preclinical evaluations. Annals of neurology, 79(5), 758-774.
Sisodia, S. S., & St George-Hyslop, P. H. (2002). γ-secretase, Notch, Aβ and Alzheimer's disease: where do the presenilins fit in?. Nature Reviews Neuroscience, 3(4), 281.
Small, S. A., & Gandy, S. (2006). Sorting through the cell biology of Alzheimer's disease: intracellular pathways to pathogenesis. Neuron, 52(1), 15-31.
Sokalingam, S., Raghunathan, G., Soundrarajan, N., & Lee, S. G. (2012). A study on the effect of surface lysine to arginine mutagenesis on protein stability and structure using green fluorescent protein. PloS one, 7(7), e40410.
Sontag, J. M., Fykse, E. M., Ushkaryov, Y., Liu, J. P., Robinson, P. J., & Südhof, T. C. (1994). Differential expression and regulation of multiple dynamins. Journal of Biological Chemistry, 269(6), 4547-4554.
St George-Hyslop, P. H., et al. (1987). The genetic defect causing familial Alzheimer's disease maps on chromosome 21. Science, 235(4791), 885-890.
Stamenova, S. D., French, M. E., He, Y., Francis, S. A., Kramer, Z. B., & Hicke, L. (2007). Ubiquitin binds to and regulates a subset of SH3 domains. Molecular cell, 25(2), 273-284.
Stern, Y., Gurland, B., Tatemichi, T. K., Tang, M. X., Wilder, D., & Mayeux, R. (1994). Influence of education and occupation on the incidence of Alzheimer's disease. Jama, 271(13), 1004-1010.
Stocker, H., Möllers, T., Perna, L., & Brenner, H. (2018). The genetic risk of Alzheimer's disease beyond APOE ε4: systematic review of Alzheimer's genetic risk scores. Translational psychiatry, 8(1), 166.
Strittmatter, W. J., et al. (1993). Binding of human apolipoprotein E to synthetic amyloid beta peptide: isoform-specific effects and implications for late-onset Alzheimer disease. Proceedings of the National Academy of Sciences, 90(17), 8098-8102.
Strober, W. (1997). Trypan blue exclusion test of cell viability. Current protocols in immunology, 21(1), A-3B.
Takahashi, R. H., Almeida, C. G., Kearney, P. F., Yu, F., Lin, M. T., Milner, T. A., & Gouras, G. K. (2004). Oligomerization of Alzheimer's β-amyloid within processes and synapses of cultured neurons and brain. Journal of Neuroscience, 24(14), 3592-3599.
Takahashi, R. H., Milner, T. A., Li, F., Nam, E. E., Edgar, M. A., Yamaguchi, H., ... & Gouras, G. K. (2002). Intraneuronal Alzheimer Aβ42 accumulates in multivesicular bodies and is associated with synaptic pathology. The American journal of pathology, 161(5), 1869-1879.
Tam, J. H. K., & Pasternak, S. H. (2017). Clinical Manifestations. The Cerebral Cortex in Neurodegenerative and Neuropsychiatric Disorders: Experimental Approaches to Clinical Issues, 83.
Tampellini, D., & Gouras, G. K. (2010). Synapses, synaptic activity and intraneuronal Aβ in Alzheimer's disease. Frontiers in aging neuroscience, 2, 13.
Tan, J. Z. A., & Gleeson, P. A. (2019). The role of membrane trafficking in the processing of amyloid precursor protein and production of amyloid peptides in Alzheimer's disease. Biochimica et Biophysica Acta (BBA)-Biomembranes.
Tan, M. S., Yu, J. T., & Tan, L. (2013). Bridging integrator 1 (BIN1): form, function, and Alzheimer's disease. Trends in molecular medicine, 19(10), 594-603.
Tan, M. S., Yu, J. T., Jiang, T., Zhu, X. C., Guan, H. S., & Tan, L. (2014). Genetic variation in BIN1 gene and Alzheimer's disease risk in Han Chinese individuals. Neurobiology of aging, 35(7), 1781-e1.
Tebar, F., Bohlander, S. K., & Sorkin, A. (1999). Clathrin assembly lymphoid myeloid leukemia (CALM) protein: localization in endocytic-coated pits, interactions with clathrin, and the impact of overexpression on clathrin-mediated traffic. Molecular biology of the cell, 10(8), 2687-2702.
Thal, D. R., Rüb, U., Orantes, M., & Braak, H. (2002). Phases of Aβ-deposition in the human brain and its relevance for the development of AD. Neurology, 58(12), 1791-1800.
Toh, W. H., Chia, P. Z. C., Hossain, M. I., & Gleeson, P. A. (2018). GGA1 regulates signal-dependent sorting of BACE1 to recycling endosomes, which moderates Aβ production. *Molecular biology of the cell*, *29*(2), 191-208.
Tomita, S., Kirino, Y., & Suzuki, T. (1998). Cleavage of Alzheimer's amyloid precursor protein (APP) by secretases occurs after O-glycosylation of APP in the protein secretory pathway Identification of intracellular compartments in which APP cleavage occurs without using toxic agents that interfere with protein metabolism. *Journal of Biological Chemistry*, *273*(11), 6277-6284.
Tosto, G., & Reitz, C. (2013). Genome-wide association studies in Alzheimer's disease: a review. Current neurology and neuroscience reports, 13(10), 381.
Traer, C. J., et al. (2007). SNX4 coordinates endosomal sorting of TfnR with dynein-mediated transport into the endocytic recycling compartment. *Nature cell biology*, *9*(12), 1370.
Tremblay, R. G., Sikorska, M., Sandhu, J. K., Lanthier, P., Ribecco-Lutkiewicz, M., & Bani-Yaghoub, M. (2010). Differentiation of mouse Neuro 2A cells into dopamine neurons. Journal of neuroscience methods, 186(1), 60-67.

Tsutsui, K., Maeda, Y., Tsutsui, K., Seki, S., & Tokunaga, A. (1997). cDNA cloning of a novel amphiphysin isoform and tissue-specific expression of its multiple splice variants. Biochemical and biophysical research communications, 236(1), 178-183.
Ubelmann, F., Burrinha, T., & Almeida, C. G. (2017). Measuring the Endocytic Recycling of Amyloid Precursor Protein (APP) in Neuro2a Cells. EMBO Reports.
Ubelmann, F., Burrinha, T., Salavessa, L., Gomes, R., Ferreira, C., Moreno, N., & Almeida, C. G. (2017). Bin1 and CD2AP polarise the endocytic generation of beta-amyloid. EMBO reports, 18(1), 102-122.
Urrutia, R., Henley, J. R., Cook, T., & McNiven, M. A. (1997). The dynamins: Redundant or distinct functions for an expanding family of related GTPases?. Proceedings of the National Academy of Sciences, 94(2), 377-384.
Valencia-Sanchez, M. A., Liu, J., Hannon, G. J., & Parker, R. (2006). Control of translation and mRNA degradation by miRNAs and siRNAs. *Genes & development*, *20*(5), 515-524.
Vardarajan, B. N., et al. (2015). Rare coding mutations identified by sequencing of A lzheimer disease genome-wide association studies loci. Annals of neurology, 78(3), 487-498.
Verghese, P. B., et al. (2013). ApoE influences amyloid-β (Aβ) clearance despite minimal apoE/Aβ association in physiological conditions. Proceedings of the National Academy of Sciences, 110(19), E1807-E1816.
Ward, A., Crean, S., Mercaldi, C. J., Collins, J. M., Boyd, D., Cook, M. N., & Arrighi, H. M. (2012). Prevalence of apolipoprotein E4 genotype and homozygotes (APOE e4/4) among patients diagnosed with Alzheimer's disease: a systematic review and meta-analysis. Neuroepidemiology, 38(1), 1-17.
Wechsler-Reya, R., Sakamuro, D., Zhang, J., Duhadaway, J., & Prendergast, G. C. (1997). Structural Analysis of the Human BIN1 Gene Evidence For Tissue-Specific Transcriptional Regulation And Alternate Rna Splicing. Journal of Biological Chemistry, 272(50), 31453-31458.
Weggen, S., & Beher, D. (2012). Molecular consequences of amyloid precursor protein and presenilin mutations causing autosomal-dominant Alzheimer's disease. Alzheimer's research & therapy, 4(2), 9.
West, H. L., Rebeck, G. W., & Hyman, B. T. (1994). Frequency of the apolipoprotein E ε2 allele is diminished in sporadic Alzheimer disease. Neuroscience letters, 175(1-2), 46-48.
Wigge, P., Kohler, K., Vallis, Y., Doyle, C. A., Owen, D., Hunt, S. P., & McMahon, H. T. (1997). Amphiphysin heterodimers: potential role in clathrin-mediated endocytosis. Molecular biology of the cell, 8(10), 2003-2015.
Willnow, T. E., & Andersen, O. M. (2013). Sorting receptor SORLA–a trafficking path to avoid Alzheimer disease. J Cell Sci, 126(13), 2751-2760.
Wolfe, M. S. (2007). When loss is gain: reduced presenilin proteolytic function leads to increased Aβ42/Aβ40. EMBO reports, 8(2), 136-140.
World Health Organization. (2017). Dementia. Retrieved from https://www.who.int/en/news-room/fact-sheets/detail/dementia
Wu, T., & Baumgart, T. (2014). BIN1 membrane curvature sensing and generation show autoinhibition regulated by downstream ligands and PI (4, 5) P2. Biochemistry, 53(46), 7297-7309.
Xiao, Q., et al. (2012). Role of phosphatidylinositol clathrin assembly lymphoid-myeloid leukemia (PICALM) in intracellular amyloid precursor protein (APP) processing and amyloid plaque pathogenesis. Journal of Biological Chemistry, 287(25), 21279-21289.
Yamazaki, Y., Painter, M. M., Bu, G., & Kanekiyo, T. (2016). Apolipoprotein E as a therapeutic target in Alzheimer's Disease: A review of basic research and clinical evidence. CNS drugs, 30(9), 773-789.
Yao, J., Nowack, A., Kensel-Hammes, P., Gardner, R. G., & Bajjalieh, S. M. (2010). Cotrafficking of SV2 and synaptotagmin at the synapse. *Journal of Neuroscience*, *30*(16), 5569-5578.
Zhao, G., Cui, M. Z., Mao, G., Dong, Y., Tan, J., Sun, L., & Xu, X. (2005). γ-Cleavage is dependent on ζ-cleavage during the proteolytic processing of amyloid precursor protein within its transmembrane domain. Journal of Biological Chemistry, 280(45), 37689-37697.
Ziegler-Graham, K., Brookmeyer, R., Johnson, E., & Arrighi, H. M. (2008). Worldwide variation in the doubling time of Alzheimer's disease incidence rates. Alzheimer's & Dementia, 4(5), 316-323.

Appendix

APP processing analysis of BIN1 variants transfected cells

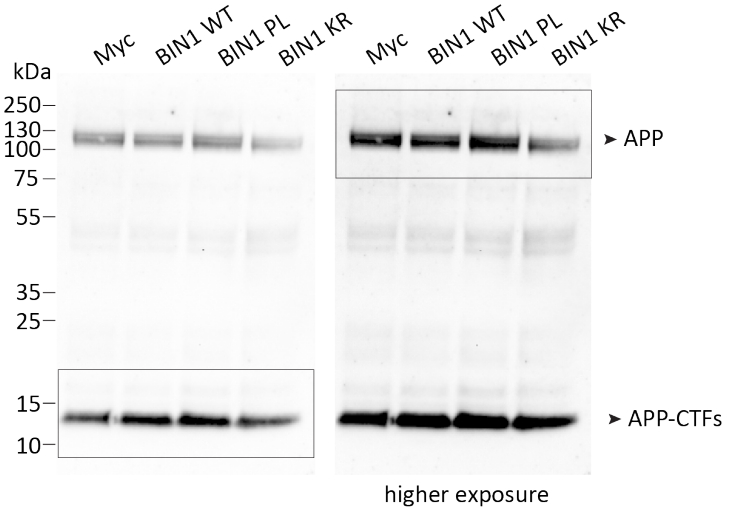

Figure 1: **APP processing analysis of BIN1 variants transfected cells.** APP processsing analysis of N2a cells transfected with Myc, BIN1 wild-type, BIN1 PL or KR mutant. For the representative immunoblot presented, proteins were sonified and separated on a 4-12% SDS-PAGE gel. Endogenous full-length APP (130-100 kDa) (with higher exposure) and APP-CTFs (15-10 kDa) levels by western blot with anti-APP anibody Y188. Protein marker: PageRuler^{TM} Plus.

Annex

Sequence alignment of mouse and human BIN1 isoform 1

```
Mouse   1  MAEMGSKGVTAGKIASNVQKKLTRAQEKVLQKLGKADETKDEQFEQCVQNFNKQLTEGTR  60
           MAEMGSKGVTAGKIASNVQKKLTRAQEKVLQKLGKADETKDEQFEQCVQNFNKQLTEGTR
Human   1  MAEMGSKGVTAGKIASNVQKKLTRAQEKVLQKLGKADETKDEQFEQCVQNFNKQLTEGTR  60

Mouse  61  LQKDLRTYLASVKAMHEASKKLSECLQEVYEPEWPGRDEANKIAENNDLLWMDYHQKLVD  120
           LQKDLRTYLASVKAMHEASKKL+ECLQEVYEP+WPGRDEANKIAENNDLLWMDYHQKLVD
Human  61  LQKDLRTYLASVKAMHEASKKLNECLQEVYEPDWPGRDEANKIAENNDLLWMDYHQKLVD  120

Mouse 121  QALLTMDTYLGQFPDIKSRIAKRGRKLVDYDSARHHYESLQTAKKKDEAKIAKPVSLLEK  180
           QALLTMDTYLGQFPDIKSRIAKRGRKLVDYDSARHHYESLQTAKKKDEAKIAKPVSLLEK
Human 121  QALLTMDTYLGQFPDIKSRIAKRGRKLVDYDSARHHYESLQTAKKKDEAKIAKPVSLLEK  180

Mouse 181  AAPQWCQGKLQAHLVAQTNLLRNQAEEELIKAQKVFEEMNVDLQEELPSLWNSRVGFYVN  240
           AAPQWCQGKLQAHLVAQTNLLRNQAEEELIKAQKVFEEMNVDLQEELPSLWNSRVGFYVN
Human 181  AAPQWCQGKLQAHLVAQTNLLRNQAEEELIKAQKVFEEMNVDLQEELPSLWNSRVGFYVN  240

Mouse 241  TFQSIAGLEENFHKEMSKLNQNLNDVLVSLEKQHGSNTFTVKAQPSDNAPEKGNKSPSPP  300
           TFQSIAGLEENFHKEMSKLNQNLNDVLV LEKQHGSNTFTVKAQPSDNAP KGNKSPS P
Human 241  TFQSIAGLEENFHKEMSKLNQNLNDVLVGLEKQHGSNTFTVKAQPSDNAPAKGNKSPS-P  299

Mouse 301  PDGSPAATPEIRVNHEPEPASGASPGATIPKSPSQLRKGPPVPPPPKHTPSKEMKQEQIL  360
           PDGSPAATPEIRVNHEPEPA GA+PGAT+PKSPSQLRKGPPVPPPPKHTPSKE+KQEQIL
Human 300  PDGSPAATPEIRVNHEPEPAGGATPGATLPKSPSQLRKGPPVPPPPKHTPSKEVKQEQIL  359

Mouse 361  SLFDDAFVPEISVTTPSQFEAPGPFSEQASLLDLDFEPLPPVASPVKAPTPSGQSIPWDL  420
           SLF+D FVPEISVTTPSQFEAPGPFSEQASLLDLDF+PLPPV SPVKAPTPSGQSIPWDL
Human 360  SLFEDTFVPEISVTTPSQFEAPGPFSEQASLLDLDFDPLPPVTSPVKAPTPSGQSIPWDL  419

Mouse 421  WEPTESQAGILPSGEPSSAEGSFAVAWPSQTAEPGPAQPAEASEVVG------GAQEPGE  474
           WEPTES AG LPSGEPS+AEG+FAV+WPSQTAEPGPAQPAEASEV G      GAQEPGE
Human 420  WEPTESPAGSLPSGEPSAAEGTFAVSWPSQTAEPGPAQPAEASEVAGGTQPAAGAQEPGE  479

Mouse 475  TAASEATSSSLPAVVVETFSATVNGAVEGSAGTGRLDLPPGFMFKVQAQHDYTATDTDEL  534
           TAASEA SSSLPAVVVETF ATVNG VEG +G GRLDLPPGFMFKVQAQHDYTATDTDEL
Human 480  TAASEAASSSLPAVVVETFPATVNGTVEGGSGAGRLDLPPGFMFKVQAQHDYTATDTDEL  539

Mouse 535  QLKAGDVVLVIPFQNPEEQDEGWLMGVKESDWNQHKELEKCRGVFPENFTERVQ  588
           QLKAGDVVLVIPFQNPEEQDEGWLMGVKESDWNQHKELEKCRGVFPENFTERVQ
Human 540  QLKAGDVVLVIPFQNPEEQDEGWLMGVKESDWNQHKELEKCRGVFPENFTERVQ  593
```

Figure 1: **Sequence alignment of mouse and human BIN1 isoform 1.** Mouse (NP_033798.1) and human (NP_647593.1) BIN1 brain isoform 1 primary sequences have 95% identity. Using the BLAST tool in NCBI database (Altschul et al., 1990).